
Electronic Thesis and Dissertation Repository

12-8-2017 10:00 AM

Stable Cu, Fe, and Ni Isotopic Systematics of the Sudbury Offset Dikes and Associated Rocks

Peter Christoffersen, *The University of Western Ontario*

Supervisor: Bouvier, Audrey, *The University of Western Ontario*

Co-Supervisor: Osinski, Gordon, *The University of Western Ontario*

A thesis submitted in partial fulfillment of the requirements for the Master of Science degree in Geology

© Peter Christoffersen 2017

Follow this and additional works at: <https://ir.lib.uwo.ca/etd>



Part of the [Geochemistry Commons](#)

Recommended Citation

Christoffersen, Peter, "Stable Cu, Fe, and Ni Isotopic Systematics of the Sudbury Offset Dikes and Associated Rocks" (2017). *Electronic Thesis and Dissertation Repository*. 5179.
<https://ir.lib.uwo.ca/etd/5179>

This Dissertation/Thesis is brought to you for free and open access by Scholarship@Western. It has been accepted for inclusion in Electronic Thesis and Dissertation Repository by an authorized administrator of Scholarship@Western. For more information, please contact wlsadmin@uwo.ca.

Abstract

The stable isotope ratio compositions of Fe, Ni, and Cu ($\delta^{56}\text{Fe}$, $\delta^{60}\text{Ni}$, and $\delta^{65}\text{Cu}$) are reported for the first time in rocks from the Sudbury Igneous Complex (SIC). Massive sulfide ores, Quartz Diorite (QD), Inclusion bearing Quartz Diorite (IQD), and rocks from members of the Main Mass of the SIC were analyzed. The objective was to better understand the origin(s) and source(s) of the Offset Dikes and the associated sulfide mineralization. Based on stable isotope ratios and petrographic observations, two distinct types of sulfide mineralization hosted within the Offset Dikes are identified. Massive sulfide mineralization hosted within the Offset Dikes was identified to be different than the disseminated blebby sulfide mineralization found within the QD and IQD, based on coordinated isotopic and petrographic analyses. Comparisons of the stable isotope ratios of Fe, Ni, and Cu between rock samples from different Offset Dikes established a homogeneity in Fe, Ni, and Cu compositions. Including between the QD and IQD, and their disseminated sulfides. A correlation between $\delta^{60}\text{Ni}$, and $\delta^{65}\text{Cu}$ values, with lighter compositions for the massive sulfides compared to the residual main mass, indicates an early magmatic origin for the massive sulfides compared to the disseminated sulfides contained in the Offset Dikes.

Keywords

Sudbury Igneous Complex, Fe isotopes, Ni isotopes, Cu isotopes, Sulfides, Economic Geology, Impact Cratering, Quartz Diorite, Offset Dikes

Co-Authorship Statement (where applicable)

The collaborative nature of project analyses resulted in co-authorship on the integrated articles presented. Specifically, Dr. Bastian Georg and Dr. Karla Newman are staff scientists at the Trent Water Quality Centre who aided in the measurement of Cu and Fe isotopic ratios presented in this project and the two manuscripts herein. Dr. Laura Wasylenki is an associate professor, and Dr. Shui-jiong Wang a post-doctoral researcher under her supervision at Indiana University. Both aided in the measurement of Ni isotopic ratios presented in this project and the two manuscripts herein. Drs. Audrey Bouvier and Gordon Osinski supervised the project and contributed to the writing and editing of all the included articles.

Acknowledgments

First and foremost, I would like to thank my advisors Dr. Audrey Bouvier and Dr. Gordon “Oz” Osinski for giving me the amazing opportunity to study the best impact crater on Earth with the greatest isotopes.

This project was made possible thanks to Wallbridge Mining Company Limited, and its personnel are thanked for their cooperation, interest in the study and providing core samples, information, and access to their property.

I would like to thank Dr. Bastian Georg and Dr. Karla Newman for their assistance with the mass spectrometers at the Trent University Water Quality Centre. On the same note, I would like to thank Dr. Laura Wasylenki and Dr. Shui-jiong Wang at the Indiana University SESAME Lab for their assistance and provision of the double spike. Additional thanks goes to Dr. Blair Gibson for assistance in the GEOMETRIC Lab at Western.

Dad, Mom, and Anna, Thank You for your love and support during the highs and lows of grad school and life.

I would like to thank my geology friends during this journey whether late nights in the lab, late nights running a rover in “Martah”, or late nights at the pub. Jon O’, Jess, Matt, Lindsay, Sarah, Zach, Andrea, Kienan, everyone I’m forgetting, and the SpaceRocks, and GEOMETRIC groups, Thank You for making the curveballs of grad school hittable.

I would like to thank the Saint Lawrence University Geology department. First, for giving me a solid foundation in Geology, and for putting up with my questions. Jeff Chiarenzelli, Mark Erickson, and David Kratzmann, Thank You.

I’d like to thank my defense committee Elizabeth Webb, Peter Brown, and Peter Lightfoot

Finally, and most importantly I would like to acknowledge Levi Keszey, Tom Callahan, James Wrigley, Dave Kruger, Whitney Brown, Grace Pezzella, Erica Lehner, and the rest of my AMC Hut Croo family. You helped me pick myself after failure in life, and taught me the value of hard work. Without you I would not be here, Solvitur Crumpus.

Table of Contents

Abstract.....	i
Co-Authorship Statement (where applicable).....	ii
Acknowledgments.....	iii
List of Tables	vii
List of Figures	viii
Chapter 1.....	1
1 Introduction.....	1
1.1 Stable Isotope Geochemistry	1
1.1.1 Stable Cu Isotopes and their Fractionation Processes.....	5
1.1.2 Stable Fe Isotopes and their Fractionation Processes	8
1.1.3 Stable Ni Isotopes and their Fractionation Processes	11
1.2 A Multi-Isotopic Approach to Sulfide Petrogenesis at Sudbury	14
1.3 Impact Cratering	15
1.3.1 Impact melting and impact melt rocks.....	18
1.4 Sudbury Geology	19
1.4.1 Sudbury Igneous Complex.....	22
1.4.2 Offset Dikes	22
1.5 Introduction to the Thesis	25
1.6 References.....	25
Chapter 2.....	38
2 Chemical Extraction and Measurement of Stable Fe, Cu, and Ni isotopes	38
2.1 Introduction.....	38
2.2 Evaluation of Analytical Methods	38
2.2.1 Sample Dissolution.....	39
2.2.2 Cu and Fe Purification and Measurement.....	39

2.2.3	Cu Mass Spectrometry	41
2.2.4	Fe Mass Spectrometry.....	42
2.2.5	Ni Purification.....	43
2.2.6	Ni Mass Spectrometry.....	46
2.2.7	Double Spiking	46
2.3	Conclusions.....	47
2.4	References.....	48
Chapter 3.....		50
3	Stable Cu, Fe, and Ni Isotopic Systematics of the Sudbury Offset Dikes and Associated Rocks	50
3.1	Introduction.....	50
3.2	Geologic Background	51
3.3	Samples	55
3.4	Analytical Methods.....	57
3.4.1	Mass Spectroscopy.....	58
3.4.2	Optical and Electron Microscopy Methods	61
3.5	Results.....	61
3.5.1	Petrographic, EDS, and WDS Data	62
3.5.2	Isotopic Results.....	66
3.6	Discussion.....	73
3.6.1	Isotopic Variations in Offset Dikes, Main Mass, and Country Rocks.....	73
3.6.2	Isotopic Variations in Massive Sulfide Mineralization	75
3.6.3	Origin of Sulfide Mineralization within the Offset Dikes	78
3.7	Conclusions.....	79
3.8	References.....	80
Chapter 4.....		91

4	Conclusions and Future work	91
4.1	Fe, Ni, and Cu Method Improvements.....	91
4.2	Significance.....	92
4.3	Recommendations for future measurement	93
4.4	References.....	94
	Appendices.....	96
	Curriculum Vitae	100

List of Tables

Table 3-1: Column chemistry procedure for the separation of Cu and Fe from sample matrices on 2ml of AG-MP1 100-200 mesh in Biorad® poly-prep columns.....	60
Table 3-2: Column chemistry procedure for the separation of Ni from sample matrices on 2ml of AG50W-X8, 200-400 mesh in Biorad® poly-prep columns.	61
Table 3-3: Table of $\delta^{65}\text{Cu}$ values, Cu concentrations, and number of analyses of Offset Dikes, Sulfide Ores, SIC Main Mass, and Target Rocks from the Sudbury impact structure.	67
Table 3-4: Table of $\delta^{54}\text{Fe}$ values, Fe concentrations, and number of analyses of Offset Dikes, Sulfide Ores, SIC Main Mass, and Target Rocks from the Sudbury impact structure.	68
Table 3-5: Table of $\delta^{60}\text{Ni}$ values, Ni concentrations, and number of analyses of Offset Dikes, Sulfide Ores, SIC Main Mass, and Target Rocks from the Sudbury impact structure.	69
Table 3-6: Table of R^2 and P-values obtained from performing a simple linear regression of the listed elements abundance against the isotopic ratio of a given sample (e.g. $\delta^{54}\text{Fe}$ against Fe elemental abundance). The given P-values indicate that the only statistically significant results are the moderate correlations between the concentration of Fe and Cu within the sulfides and their corresponding isotopic compositions. All simple linear regressions performed in ioGAS.....	70

List of Figures

Figure 1-1: Conceptual diagram of crater formation. The right hand side displays simple crater formation, while complex crater formation is displayed on the left. Modified from Osinski and Pierazzo, 2013..... 16

Figure 1-2: Geologic map of the Sudbury impact structure and the surrounding region with schematic diagram of the stratigraphy of the Sudbury Igneous Complex, Whitewater Group, and some Footwall units. Based on data from OGS bedrock regional 1:250,000 scale and internal Wallbridge Mining Company Limited maps. Stratigraphic column after Ames et al. (2008), with unit thickness approximated relative to one another..... 21

Figure 2-1: Elution Curve for SUDPAC 017, a sulfide containing QD sample from the intersection of the Foy and Hess offsets. 40

Figure 2-2: A) $\delta^{65}\text{Cu}$ of ICP Cu solution at twice concentration and half concentration relative to the bracketing standard. B) $\delta^{65}\text{Cu}$ of ICP Cu solution doped with common matrix elements K (28%), Mg (7%), Co (65%), 50ppb Zn and variable amounts of Cu. A shift can be seen from 0‰ (A) to ~0.15‰ (B) $\delta^{65}\text{Cu}$ likely due to the presence of Zn. Zn doping was tested as an internal standard, but failed to yield reproducible standard values. 42

Figure 2-3: Elution curves for the first column of the Ni separation protocol separating metals such as Fe and Cu (top), and the second column protocol separating Ni from cations such as Ca, Al, Ti, and Mg (bottom). 45

Figure 3-1: Geologic map of the Sudbury Igneous Complex and surrounding Superior Province and Huronian footwall rocks along with the post-impact Whitewater Group. From OGS bedrock regional 1:250,000 scale and internal Wallbridge Mining Company Limited maps. Sample numbers and locations are displayed as yellow dots. Also displayed is a schematic cross section of the rock units associated with the Sudbury impact structure after Ames et al. (2008)..... 54

Figure 3-2: A) Outcrop of IQD from the Foy Offset containing clasts of felsic and mafic gneiss hammer for scale. B) Outcrop of IQD from the Foy Offset containing felsic and mafic gneiss along with disseminated blebs of sulfide mineralization hammer for scale. C) Outcrop

of QD from the Hess Offset in contact with granite of the Cartier Batholith hammer for scale. D) Outcrop of QD from the Foy Offset with grease pencil for scale. Outcrops shown in A, B, and D are from a section of the Foy Offset north of the intersection between the Foy and Hess Offset Dikes. Outcrop shown in C is from the western section of the Hess Offset Dike where SUDPAC 020 was collected. 56

Figure 3-3: Photomicrographs showing the two styles of sulfide mineralization seen within the Offset Dikes. A,B, and C) massive sulfide mineralization consisting of pyrrhotite, pyrite, chalcopyrite, pentlandite, and magnetite from the Trill Offset (SUD 040 [A,B]) and Parkin Offset (WMM-015-W2 [C]). D) disseminated blebby sulfide mineralization from the intersection of the Foy and Hess Offsets (SUD 017). Abbreviations are as follows: Cpy – chalcopyrite, Mag – magnetite, Pn – pentlandite, Po – pyrrhotite, and Py – pyrite. 63

Figure 3-4: A) Composition maps of CoNiCu (RGB) of massive sulfide ore from the Trill Offset (WTR-028). Enlarged area highlighted in red. B) Enlargement displaying oscillatory zonation of Co within pyrite grains in red. 64

Figure 3-5: A,B) Composition map of CoNiCu (RGB) of a bleb of disseminated sulfide from sample SUD 017 displaying a lack of Co zonation or enrichment. Optical photomicrograph of the sample shown in Fig. 3-5D. C) Composition map of CoNiCu (RGB) of massive sulfide ore from the Trill Offset (SUD 040). Co enrichment is displayed within the pyrites in red. Optical photomicrograph of the sample shown in Fig. 3-5A,B..... 65

Figure 3-6: Graphs displaying the distribution of $\delta^{65}\text{Cu}$, $\delta^{56}\text{Fe}$, and $\delta^{60}\text{Ni}$ values measured for each lithology sampled. Error bars given as 2SD. 71

Figure 3-7: Plot of $\delta^{65}\text{Cu}$ values against $\delta^{56}\text{Fe}$ values (top) and $\delta^{65}\text{Cu}$ values against $\delta^{60}\text{Ni}$ values (bottom) measured for each sample along with basic sample description with some specific samples labelled. Gray bars correspond to Bulk Silicate Earth (BSE) values for $\delta^{65}\text{Cu}$ and $\delta^{60}\text{Ni}$, and MORB values for $\delta^{56}\text{Fe}$. The black line is a linear regression of Sublayer, QD, IQD, and massive sulfide isotopic compositions, and defined as $\delta^{65}\text{Cu} = 1.24*\delta^{60}\text{Ni} - 0.19$ with an R^2 of 0.93. Dashed lines represent a 95% confidence envelope. 72

List of Appendices

Appendix A: Silicate Geochemistry measured by ICP-MS, average error of 5-10% 96

Appendix B: Sulfide Geochemistry measured by ICP-MS, average error of 5-10% 99

Chapter 1

1 Introduction

Recent advances in stable isotope geochemistry have greatly improved the ability to accurately and precisely measure non-traditional stable “heavy” isotopes (e.g., Ca, Cr, Cu, Fe, Ni, Se, Sr, Zn, Hg, U) (Teng et al., 2017). This improvement in techniques and instrumentation has opened new doors of inquiry into geologic processes and the origins of enigmatic geologic bodies. These improved techniques and instrumentation will be leveraged to measure the Fe, Ni, and Cu stable isotopic composition of the Sudbury Igneous Complex (SIC) Offset Dikes, and their associated rocks. The objectives of these measurements and this research are: evaluate the origin(s) and source(s) of the Offset Dikes and the sulfides they contain; and investigate the evolution and differentiation of the SIC as the impact melt sheet of a large diameter crater. This chapter introduces concepts of stable isotope geochemistry, previous work on Cu, Fe, and Ni stable isotopes, and important questions posed by the Sudbury Igneous Complex.

1.1 Stable Isotope Geochemistry

Isotopic fractionation is a process whereby two or more isotopes become unevenly distributed between reservoirs. In the context of geology, includes rocks, magmas, fluid, and/or minerals. Isotopic fractionation effects can arise due to chemical and physical processes and fall under two main types, mass-dependent and mass-independent (Teng et al., 2017). Mass-dependent fractionation is any fractionation process whereby the mass of the isotopes being fractionated control the distribution (fractionation) of the isotopes between reservoirs. During mass-dependent fractionation, the larger the mass difference

between the isotopes being fractionated, the larger the fractionation which can occur. During mass-independent fractionation, the mass of the isotopes in question does not control the fractionation of those isotopes. Mass-independent fractionation is a relatively rare phenomenon, with only a few mass-independent fractionation processes identified. Mass independent fractionation naturally occurs mainly in O and S isotopes by photodissociation reactions, or are identified for many elements due to nucleosynthetic anomalies preserved in primitive meteoritic materials.

There are two main types of mass-dependent fractionation, equilibrium fractionation and kinetic fractionation. Equilibrium fractionation is dependent on the zero point energy of a molecule where heavier isotopes have lower zero-point energies and vibrational frequencies. Thus as a reaction goes to completion, isotopes are fractionated based on their mass. An example of equilibrium fractionation would be any physical and/or chemical reaction which reacts to completion e.g. vinegar and baking soda. In contrast, during kinetic fractionation it is the velocity of molecules and atoms which drives fractionation. Lighter molecules containing lighter isotopes are faster than molecules containing heavier isotopes in order to keep kinetic energy constant. Kinetic fractionation processes include evaporation, incomplete reactions, unidirectional processes, some biological processes, and reactions taking place at a very rapid rate.

Several concepts are essential to the measurement of stable isotopes, and understanding how they fractionate. These equations and principles are detailed below using the two isotopes of Cu, ^{65}Cu and ^{63}Cu as an example. Processes specific to stable Cu, Fe, and Ni isotopes at Sudbury will be covered in detail in subsequent sections.

Isotopic ratio (R): The ratio of the abundance of two isotopes,

$$R^{65/63} = \frac{{}^{65}\text{Cu}}{{}^{63}\text{Cu}} \quad \text{Eq. 1-1}$$

Fractionation factor (α): the ratio between two of the same isotopic ratios (R) from two different substances A and B,

$$\alpha_{A-B}^{65/63} = \frac{R_A^{65/63}}{R_B^{65/63}} \quad \text{Eq. 1-2}$$

Delta value (δ): The deviation of a measured isotopic ratio from an isotopic standard of known composition represents the isotopic offset of an unknown sample. This notation is used because of the difficulty in measuring the absolute abundance of isotopes by magnetic sector mass spectrometry. Also, fractionation effects are usually small in magnitude. The units used for Fe, Cu and Ni are usually given in per mil (‰), or parts per thousand, but could also be given in epsilon notation which corresponds to deviation per 10,000. All isotopic ratios reported in this thesis are expressed as delta values given in per mil (‰).

$$\delta^{65}\text{Cu} = \left[\frac{R_{\text{Unknown}}^{65/63} - R_{\text{Standard}}^{65/63}}{R_{\text{Standard}}^{65/63}} - 1 \right] \times 1000 \quad \text{Eq. 1-3}$$

Which expanded becomes:

$$\delta^{65}\text{Cu} = \left[\frac{\frac{{}^{65}\text{Cu}_{\text{Unknown}}}{{}^{63}\text{Cu}_{\text{Unknown}}} - \frac{{}^{65}\text{Cu}_{\text{Standard}}}{{}^{63}\text{Cu}_{\text{Standard}}}}{\frac{{}^{65}\text{Cu}_{\text{Standard}}}{{}^{63}\text{Cu}_{\text{Standard}}}} - 1 \right] \times 1000 \quad \text{Eq. 1-4}$$

Big delta (Δ): Big delta is the difference between the delta values (δ) measured in two materials A and B. This value can also be used to linearly approximate the fractionation factor between two reservoirs (Eq. 6). This approximation is accurate at high temperatures, but is much less accurate in lower temperature systems. If the difference between the sample and standard (Eq. 3) is too large however, the error from approximating exponential fractionation laws as a linear function becomes too great.

$$\Delta_{a-b} = \delta_a - \delta_b \quad \text{Eq. 1-5}$$

$$\Delta_{a-b} \approx 1000 \ln \alpha_{a-b} \quad \text{Eq. 1-6}$$

In addition to these equations, there are several important qualitative principles of isotopic research. 1) The magnitude of an isotopic fractionation, α , will decrease as temperature increases (Urey, 1947). This occurs as a result of the overall system becoming more energetic, as this happens, the relative difference in vibrational energy potential between two given isotopes decreases. 2) Heavy isotopes become enriched in materials where the bonds are stronger (i.e., solids over liquids, liquids over gases, and phases with the highest oxidation state). 3) Light isotopes are more reactive and during kinetic fractionation will become enriched in the product of that reaction. This is a result of the lower amount of energy required to move or react lighter molecules due to their lower mass. Because isotopic fractionations are dependent on physical and chemical conditions; isotopic fractionation can be used to evaluate the conditions and processes a given material experienced.

1.1.1 Stable Cu Isotopes and their Fractionation Processes

Cu is a first row transition metal with two stable isotopes ^{63}Cu and ^{65}Cu , with an abundance of 69.2% and 30.8% respectively. The mass difference between the two isotopes of Cu is 2 atomic mass units (amu), a 1.5% mass difference. This is a relatively low difference in mass compared to O, S, and C isotopes. As a result of the small relative difference in mass of Cu stable isotopes, during high temperature equilibrium fractionation processes it is expected that the resulting fractionations will be small. Cu can transition between two oxidation states Cu (I) and Cu (II) under temperature and pressure conditions commonly found on the Earth's surface and in geologic materials. The fractionation between these two oxidation states was first characterized by Zhu et al. (2002) who found $\Delta^{65}\text{Cu}_{\text{Cu(II)-Cu(I)}} = 4\text{‰}$ during the reduction of aqueous Cu(II) to Cu(I) during iodide precipitation at 20 °C. Subsequent studies concluded that the change in oxidation state, not the change in phase, caused the large fractionation observed between the redox states (Maréchal and Sheppard, 2002; Ehrlich et al., 2004; Mathur et al., 2005). Kinetic fractionation processes are more likely than equilibrium processes to create large observed fractionations. Such processes include phase transformations which do not achieve equilibrium such as evaporation, and reactions which occur rapidly such as the separation of immiscible melts like sulfide melt from silicate melt. Reactions which occur very rapidly are often unable to achieve equilibrium, which can result in unbalanced reactions and large fractionations. The process of sulfur segregation in a melt is potentially quite important for Cu given its abundance in magmatic sulfide ores. A terrestrial example of Cu fractionation due to kinetic processes is the relatively extreme enrichment in ^{65}Cu observed in tektites with $\delta^{65}\text{Cu}$ values as high as +7‰ (Moynier et

al., 2010). A process thought to form tektites is the rapid quenching of vapor and melt following hypervelocity meteorite impacts. As Cu is a moderately volatile element, loss of ^{63}Cu through evaporation of Cu likely causes this observed enrichment of ^{65}Cu in tektites.

1.1.1.1 Igneous processes

Due to the fact that most igneous processes on Earth take place at high temperature, the isotopic fractionations that occur in igneous settings are generally very low with a measured range of $\delta^{65}\text{Cu}$ in silicate igneous rocks falling between -0.3 to 0.5‰ (Othman et al., 2006; Kehata and Irata, 2013; Liu et al., 2014; Savage et al., 2015). This varies little from the composition of the Bulk Silicate Earth (BSE) measured by Savage et al. (2015) of $\delta^{65}\text{Cu}_{\text{BSE}} = 0.07 \pm 0.10\text{‰}$.

When a melt reaches sulfur saturation, the separation of sulfide melt from silicate melt is a process of interest due to the possibility of creating significant isotopic fractionations. Savage et al. (2015) carried out experiments to measure $\Delta^{65}\text{Cu}_{\text{sulfide-silicate}}$. Despite an inability to fully separate sulfide which was disseminated within the silicate fraction, Savage et al. (2015) performed mass-balance calculations to estimate $\Delta^{65}\text{Cu}_{\text{sulfide-silicate}}$ based on $\delta^{65}\text{Cu}_{\text{sulfide}}$. The authors found a wide range of values ($\sim -0.5\text{‰}$ to -20‰) which they attribute to error propagation from incomplete separation of silicate and sulfide phases from the sample capsules. However, some important conclusions can still be drawn from their experiments. First, their experiments suggest that the sign of $\Delta^{65}\text{Cu}_{\text{sulfide-silicate}}$ is negative, second despite their wide range of values; the magnitude of the values is much higher than that observed between suites of silicate lithologies generated by partial melting and differentiation processes. It could be concluded that partial melting

and differentiation processes of silicate melts, which generally occur at high temperatures, will have little effect on the $\delta^{65}\text{Cu}$ composition of their crystallized products. In fact, these processes are likely an order of magnitude lower than separating sulfides from siliceous melt.

1.1.1.2 Sulfide Ores

Larson et al. (2003) was the first study to note a wide range of $\delta^{65}\text{Cu}$ values (-3 to +2.5‰) in ore minerals. Additional studies have broadened the range of values observed for sulfide minerals considerably; with secondary sulfide minerals displaying values ranging from -16.5 to +12 ‰ (Mathur et al., 2005). In contrast to secondary sulfide ores, primary sulfide ores have been found to display a narrower range of values than secondary ore minerals ($0 \pm 0.5\%$). These observations have led to the systematic study of Cu isotopes within sulfide ores to evaluate the relative roles of hydrothermal processes (Graham et al., 2004; Maher and Larson, 2007; Li et al., 2010; Mathur et al., 2012), redox processes within ore deposits (Mathur et al., 2005; Markl, Lahaye, et al., 2006; Asael et al., 2007, 2009), and sources of metals (Graham et al., 2004; Malitch et al., 2014; Ripley et al., 2015). Mathur et al. (2009) also evaluated the use of Cu isotopes as exploration and vectoring tool for Cu porphyry deposits. This was achieved by comparing values from hypogene and supergene environments, and evaluating what conditions and processes caused the isotopic fractionations observed.

Redox changes were first invoked to explain the large variation in $\delta^{65}\text{Cu}$ values observed in secondary supergene ore deposits (Larson et al., 2003). Further studies agreed that redox changes were the primary explanation for isotopic fractionation (Larson et al., 2003; Ehrlich et al., 2004; Mathur et al., 2005). However, the experimentally measured

fractionation factors of redox changes cannot account for observed natural variability, as they are too low to create the observed fractionations on their own (Sherman, 2013).

Some possible mechanisms to explain the variability seen in natural systems are, multiple episodes of hydrothermal activity resulting in multiple episodes of fractionation. Or, that phase changes, Rayleigh distillation, and/or open system behavior mechanisms are working in concert with redox changes to create the large variations seen in natural systems (Moynier et al. 2017). Rayleigh distillation is an exponential relationship which would create much larger observed fractionations. While the removal or addition of material and energy via an open system; this might allow for the preferential removal of isotopes and the generation of large observed fractionations.

Although many of the studies summarized above focused on secondary sulfides, Ripley et al. (2015) studied the Cu isotopic composition of magmatic Ni-Cu-PGE sulfide ore deposits from the Midcontinent Rift System in North America. The authors were able to measure a difference in the Cu isotopic composition between the sheet and conduit style intrusions of the Midcontinent Rift. Along with host rock data, the authors investigated the source of Cu within the deposits, and whether crustal Cu was incorporated into the deposits. The authors concluded that the incorporation of crustal Cu could not fully explain the values measured at the Duluth Complex. While crustal contamination of sheet-style mineralization, was only likely if the mantle source of the magma had a light $\delta^{65}\text{Cu}$ value.

1.1.2 Stable Fe Isotopes and their Fractionation Processes

Iron is a first row transition metal with four stable isotopes, and the fourth most abundant element in the Earth's crust. It has a wide variety of chemical behavior and forms a wide

variety of minerals. Fe has four stable isotopes, ^{54}Fe , ^{56}Fe , ^{57}Fe , and ^{58}Fe with abundances of 5.845, 91.754, 2.1191, and 0.2919 atom% respectively (Berglund and Wieser 2011). The mass difference between the most commonly measured isotopes, ^{54}Fe and ^{56}Fe is 2 (amu) for a 1.8% mass difference. As a result, Fe commonly exhibits much smaller mass fractionations than lighter elements such as O, S, and C. Fe has three redox states which are commonly found in geologic settings as metallic iron (Fe^0), ferrous iron (Fe^{2+}), and ferric iron (Fe^{3+}). Metallic Fe^0 is not naturally found at the Earth's surface. However, as a result of the oxidation state of the crust and mantle; Fe^{2+} , and Fe^{3+} are commonly distributed in different geological systems. Redox changes between Fe^{2+} and Fe^{3+} are thought to be a mechanism that allows large fractionations of Fe isotopes to occur. This is a mechanism that has been invoked to explain an observed systematic increase in $\delta^{56}\text{Fe}$ values in igneous rocks with increasing SiO_2 content (Dauphas et al., 2014).

1.1.2.1 Igneous processes

Due to the relatively small difference in mass between the isotopes of Fe coupled with the high temperature that igneous processes operate at, it was initially thought that Fe isotopes in igneous rocks would display a small variation in their isotopic signatures. However, this has been proven to not always be the case. For instance, evolved igneous rocks such as granites have been observed to have a significantly heavier Fe isotopic composition than less evolved igneous rocks (Poitrasson and Freydier, 2005; Heimann et al., 2008; Dauphas et al., 2009; Schuessler et al., 2009; Sossi et al., 2012; Zambardi et al., 2014; Foden et al., 2015; He et al., 2017). In short, as SiO_2 content of silicic rocks increases, the Fe composition of the rock becomes heavier. Although exotic processes such as thermal diffusion (Zambardi et al., 2014), magma immiscibility (Zhu et al.,

2015), and fluid exsolution (Poitrasson and Freyrier, 2005) have been invoked to explain this phenomena, Dauphas et al. (2014) and Foden et al. (2015) argue that fractional crystallization alone can explain the variation. Additional support of this argument can be found in the observation that crystallization of olivine can produce a significant fractionation of Fe isotopes (Teng et al., 2008).

Another process producing significant fractionation of Fe isotopes is the interaction between sulfide and silicate melts. Schuessler et al. (2007) experimentally determined the average fractionation between pyrrhotite and silicate melt ($\Delta^{56}\text{Fe}_{\text{pyrrhotite-silicate melt}}$) for a temperature range of 840-1000 °C was $-0.35 \pm 0.04\%$, the pyrrhotite was found to preferentially incorporate the lighter isotope of Fe. In their experiments the silicate melt consisted of a hydrated peralkaline rhyolitic melt. The authors also suggested that for basaltic systems or systems with a higher amount of Fe^{2+} as part of the total amount of Fe the fractionation observed would be lower in magnitude.

1.1.2.2 Sulfide Ores

Within sulfide ore systems, there are several processes that can potentially fractionate Fe isotopes, making sulfide ore systems an attractive system to study. One of the key processes which affects Fe isotopic ratios in magmatic sulfide systems is the interaction of sulfide and silicate melt (Schuessler et al., 2007; Hiebert et al., 2013). Another important process is the deposition and interaction of sulfide minerals within hydrothermal systems (Rouxel et al., 2004; Rouxel et al., 2008; Polyakov and Soultanov, 2011). As a result, Fe isotopes in conjunction with petrographic and other isotopic techniques, have been investigated as a tool to distinguish between hydrothermal and magmatic systems (Hofmann et al., 2014), investigate hydrothermal ore systems (Horn et

al., 2006; Markl, von Blanckenburg, et al., 2006; Wang et al., 2015), different sources of mineralization (Zhu et al., 2016), contamination of mineral systems (Hiebert et al., 2013), and as a geo-thermometer (Wawryk and Foden, 2015).

Hiebert et al. (2013) used Fe isotopes along with S isotopes at the Voisey's Bay deposit to evaluate the level of crustal contamination and the specific crustal contaminants within the deposit. The authors reported a small range of $\delta^{56}\text{Fe}$ values for mineralized samples, but the measured values were centered on mantle values for $\delta^{56}\text{Fe}$ estimated from periodotites ($-0.02 \pm 0.026\%$) (Dauphas et al. 2017). Analysis of the $\delta^{56}\text{Fe}$ values revealed a sulfide and silicate melt in equilibrium with each other which the authors conclude was a result of the greater amount of Fe in the silicate melt in comparison to the sulfide melt.

Syverson et al. (2017) experimentally investigated the fractionation between chalcopyrite and Fe-bearing hydrothermal fluids at 350 °C and 500 bars to better understand Fe behavior at undersea vents. A $\Delta^{56}\text{Fe}_{\text{chalcopyrite-Fe}^{2+}(\text{aq})}$ of $0.09 \pm 0.17\%$ was measured and found consistent with theoretical predictions. They subsequently argue that $\delta^{56}\text{Fe}$ compositions of chalcopyrite can be used as a proxy for $\delta^{56}\text{Fe}$ content of hydrothermal fluids.

It has been noted that Komatiite Fe-Ni sulfide deposits display a small range of negative $\delta^{56}\text{Fe}$ values; this is consistent with high-temperature fractionations in melts with a high silicate magma to sulfide magma ratio (Dauphas et al., 2017).

1.1.3 Stable Ni Isotopes and their Fractionation Processes

Nickel is a first row transition metal with five stable isotopes ^{58}Ni , ^{60}Ni , ^{61}Ni , ^{62}Ni , and ^{64}Ni with abundances of 68.0769, 26.2231, 1.1399, 3.6345, and 0.9255 atom%

respectively (Gramlich et al. 1989). Commonly found in sulfide ores, as a minor component in most silicate minerals, and within the Earth's core based on geophysical evidence. Ni is an important industrial metal for the creation of metal alloys such as stainless steel, and high strength alloys used in jet engines. Compared to Cu and Fe, the study of the stable isotopes of Ni in terrestrial materials is a new field. Most studies of Ni isotopes have been conducted on meteoritic, peridotitic, and mantle derived materials. This is a result of the difficulty in measuring Ni stable isotopes and the complex column separation procedures required to separate Ni from geologic materials. Low yields during Ni extraction and purification can result in isotopic fractionation during extraction procedures, and inaccurate measurement of the isotopic ratio. Chemically, Ni can exist in multiple oxidation states, but in geological material Ni is most commonly found as Ni²⁺. As a result, redox changes thought to be a major driver of transition metal isotope fractionation (Dauphas et al., 2014), likely play little role in the fractionation of Ni isotopes in shallow geologic settings. However, Ni does change its redox state from +2 to 0 as it partitions into the metal fraction of a melt, an important process during planetary core formation. There have been attempts to measure Ni isotopic fractionation between metal and silicate material. Lazar et al. (2012) reported $\Delta^{62/58}\text{Ni}_{\text{metal-silicate}} = 0.25 \pm 0.02 \times 10^6 / T^2$ between metal and talc from isotope partitioning experiments; Chernonozhkin et al. (2016) also reported analyses of metal and silicate material from pallasites and mesosiderites. While yet to be measured, $\Delta^{62/58}\text{Ni}_{\text{sulfide-silicate}}$ is likely a large enough value to produce significant isotopic fractionations (Elliott and Steele, 2017). There is likely a significant isotopic fractionation due to the partitioning of Ni between silicate and sulfide as a result of the change in bonding environment (e.g. redox state).

1.1.3.1 Igneous processes

Investigations of Ni isotopic fractionation during igneous processes has not received much attention. The lack of Ni redox state changes between different common sulfide and silicate phases, eliminates redox changes as a possible driver of large fractionations of Ni isotopes. Most studies of igneous material have focused on defining the $\delta^{60}\text{Ni}$ values of the bulk silicate Earth, mostly by analyzing mantle and mantle derived material. With the $\delta^{60}\text{Ni}$ value of the bulk silicate Earth (BSE) having been measured as $0.18 \pm 0.04\text{‰}$ (Steele et al., 2011), $0.15 \pm 0.24\text{‰}$ (Cameron et al., 2009), $0.05 \pm 0.05\text{‰}$ (Gueguen et al., 2013), and $0.23 \pm 0.06\text{‰}$ (Gall et al., 2017). The Bulk Silicate Earth (BSE) is the original composition of the silicate part of the Earth prior to the differentiation of the first crustal material. Recently however, measurements of mantle rocks and their minerals (olivine, pyroxene and garnet) showed resolvable differences in $\delta^{60}\text{Ni}$ between mineral phases explaining small differences measured among ultramafic mantle rocks (Gall et al., 2017).

1.1.3.2 Sulfide Ores

Ni isotopes within sulfides display a wide range in values compared to silicate igneous rocks, and have begun to be studied in greater depth during the previous decade. This makes sulfide ores an exciting area of study, and likely to expand in scope in the coming years due to improved methods for extracting and purifying Ni from geologic materials (e.g. those detailed in Chapter 2). A wide range of $\delta^{60/58}\text{Ni}$ values (-1 to -0.3) have been measured in Ni-bearing sulfides from komatiites (Gueguen et al., 2013; Hofmann et al., 2014; Steele et al., 2011) and sulfide ore from the Thompson Ni belt (Tanimizu and Hirata, 2006). One exception to these series of isotopically light measurements is a

$\delta^{60/58}\text{Ni}$ value of $\sim 0.5\text{‰}$ measured from a Sudbury pentlandite sample (Tanimizu and Hirata, 2006).

Hofmann et al. (2014) used Ni isotopes along with Fe and S isotopes to examine the magmatic and hydrothermal history of the Trojan and Shangani nickel sulfide deposits in Zimbabwe. The authors were able to argue against a sedimentary source for Ni based on the isotopic composition measured at the deposit. Used in conjunction with petrographic analysis, Fe, and S isotopes; the authors determined that the generally low grade deposits had a magmatic origin with subsequent hydrothermal reworking. They further suggest that post-magmatic hydrothermal processes played an important role in the upgrading of what were initially, low grade deposits.

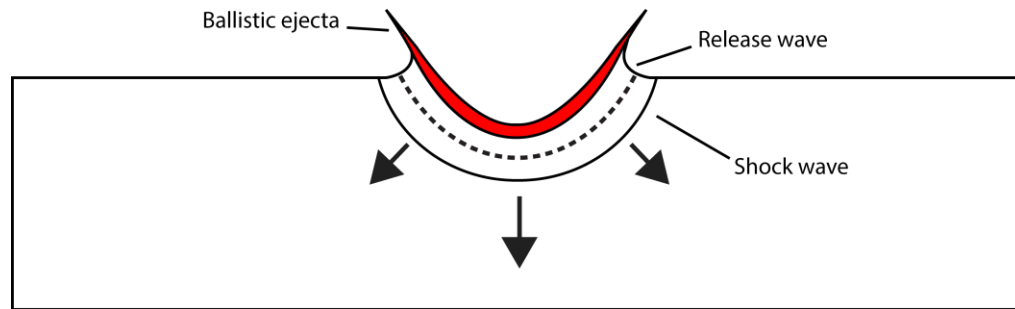
1.2 A Multi-Isotopic Approach to Sulfide Petrogenesis at Sudbury

This project aims to use the integrated analyses of stable Fe, Ni, and Cu isotopes to understand sulfide and host-rock petrogenesis at Sudbury. Based on the afore-mentioned knowledge of how Fe, Ni, and Cu isotopes behave during magmatic and hydrothermal processes, it is hoped that an analysis of stable Fe, Ni, and Cu isotopes will allow the evaluation of sulfide genesis and evolution. Such as, the hydrothermal history of the sulfides, metal sources of the sulfides, and the identification of sulfide segregation within magma(s). Coupled with petrographic analysis, stable Fe, Ni, and Cu isotopes offer powerful tools to identify and examine sulfide petrogenesis and development. The identification and refinement of sulfide petrogenesis and evolution models at Sudbury will provide valuable information towards improving Ni-Cu-PGE ore deposit exploration models.

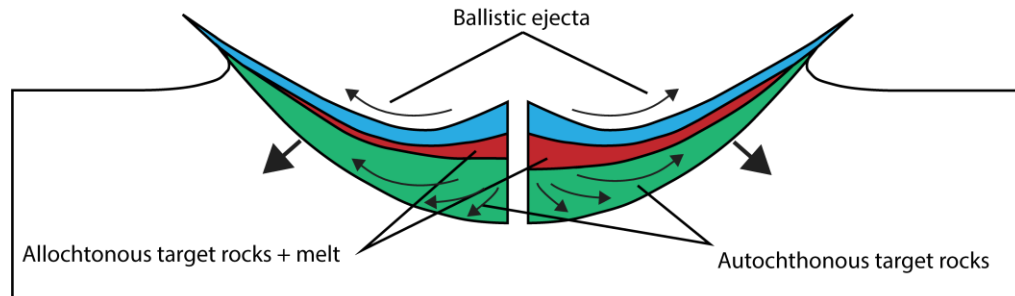
1.3 Impact Cratering

Impact cratering is a ubiquitous geologic process occurring on every solid body in the solar system. Driven by the physical processes arising from the collision of solid bodies; hypervelocity impacts, where the striking projectile is large enough to pass through the atmosphere with little deceleration and strike its target at its original cosmic velocity (French, 1998), form high-pressure shock waves that result in the creation of craters larger than several meters. While the impact cratering process is a continuum, in order to better evaluate the cratering process it has been divided into three stages, contact and compression, excavation, and modification (Fig. 1-1) (Gault et al., 1968).

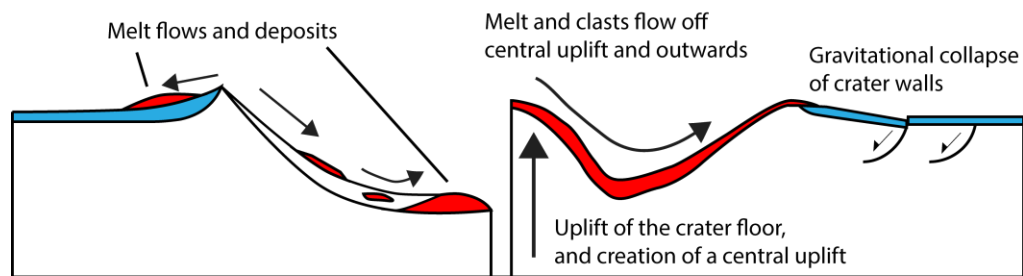
First, the contact and compression stage begins when the projectile first makes contact with the surface it is impacting and begins to compress the target material. The projectile penetrates the target material creating a shock wave; moves through and compresses the target material and the impactor. Eventually the shock wave moving through the impactor reaches the top of the impactor, and is reflected back down into the impactor and target as a rarefaction wave (Ahrens and O'Keefe, 1972). This unloads, or releases the pressure created by the initial shock wave, and causes the melting and vaporization of the projectile and target material (Gault et al., 1968; Melosh, 1989). When this rarefaction wave reaches the interface of the target and projectile, the contact and compression stage transitions into the excavation stage (Melosh, 1989).



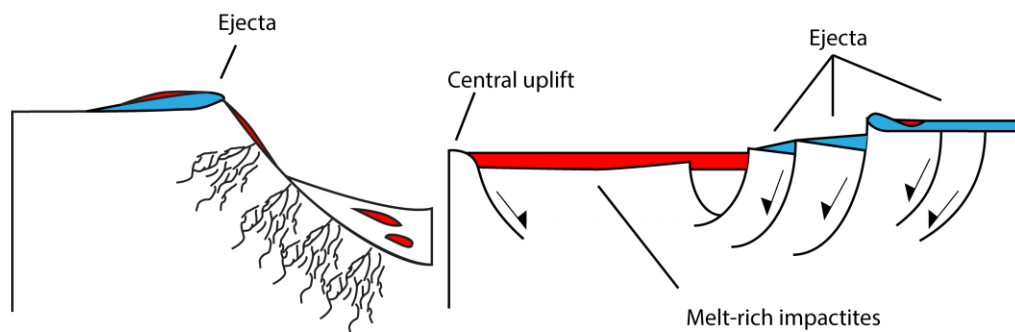
Contact and compression stage



Excavation stage



Modification stage



End modification stage

Figure 1-1: Conceptual diagram of crater formation. The right hand side displays simple crater formation, while complex crater formation is displayed on the left. Modified from Osinski and Pierazzo, 2013.

The excavation stage is characterized by the development of the transient cavity of the impact crater, it is during this phase the crater is opened (Melosh, 1989). It is important to note that by this point the projectile has unloaded, melted, and/or vaporized. As the initial shock wave moves through the target, it sets into motion the target material with an outward radial trajectory. This initial shock wave, combined with rarefaction waves from shock waves which initially travelled upward generates an excavation flow-field removing material; creating the transient cavity (Dence, 1968; Grieve and Cintala, 1982). The ejected material from the excavation flow field is ballistically ejected beyond the rim of the transient cavity, generating deposits of ejected material (Oberbeck, 1975). Once the transient cavity formed during the excavation stage reaches its maximum lateral extent, the modification stage begins.

The modification stage is considered the final stage of impact cratering, and ends once any major movement within the target material ends. The end result of the modification stage is dependent on the force of the impact, gravitational pull of the impacted body, and the strength of the impacted material (Melosh and Ivanov, 1999). There are several morphologies that can result from impact cratering formed during the modification stage, simple craters, complex craters, peak-ring craters, and multi-ring craters. Simple craters are craters that display only a bowl shaped depression in the target surface. Complex craters in addition to having a bowl-shaped depression, also contain a central uplifted area known as a central peak or central uplift in eroded structures. Multi-ring basins are very large craters that display multiple rings of uplifted and slumped material in concentric circles around the center of the impacted surface.

Central peaks and peak rings are formed when the target surface moves upward in response to its unloading after the downward force of the impactor is no longer pressing down on the surface during the excavation stage. The target surface moves upward, and produces a central uplift. Peak ring craters are a variation on this morphology whereby the central uplift grows so rapidly it “overshoots” its equilibrium height (Kenkmann et al., 2013). This causes the central uplift to be gravitationally unstable and collapses downward and outward to form a circular ring of uplifted material in the middle of the crater (Melosh and Ivanov, 1999).

1.3.1 Impact melting and impact melt rocks

During impact, a rarefaction, or release wave is generated when the initial shock wave is reflected downward after reaching the upper limit of the projectile (Ahrens and O’Keefe, 1972). This release wave move through and unloads both the impactor, and target rocks. This unloading causes shock melting as the pressure-volume work generated by the compression shock wave is not fully recovered and the remaining pressure-volume work becomes waste heat (Grieve et al., 1977).

This waste heat causes melting of the target material, a thermodynamically irreversible process. While dependent on several factors, the amount of melt generated by shock melting during hypervelocity impact is primarily driven by the size of the impactor, while variables such as composition and velocity are second order (Cintala and Grieve, 1998). It is important to note, that shock melting is a fundamentally different process than endogenic igneous systems. Shock melting is dependent on the shock pressure generated by the compressing shock wave, and compressibility of the target material. Impact melt products include impact-melt bearing breccias, impact melt rocks, and glasses. While

these are important impact melt products, the focus of this thesis are the melts generated from the impact melt sheet of the Sudbury Impact structure. These products fall outside that purview, and a focus is given to impact melt sheets and related processes and products.

As crater size increases eventually, impact melt will pond at the base of the crater and begin to form a coherent sheet of impact melt, also known as an impact melt sheet. Some large impact melt sheets have been noted to undergo igneous differentiation, the Main Mass of the Sudbury Igneous Complex (SIC) being a prime terrestrial example (Grieve et al., 1991b; Therriault et al., 2002). However, there are conflicting observations of the presence (Vaughan et al., 2013), or absence (Spudis et al., 2014) of a differentiated impact melt sheet at the lunar Orientale impact basin. Along with observations suggesting the South Pole Akin Basin contains a differentiated impact melt sheet (Vaughan and Head, 2014), have triggered debate as to whether large impact melt sheets always undergo igneous differentiation. Or, if igneous differentiation of impact melt sheet is the exception rather than the rule of large impact melt sheets.

1.4 Sudbury Geology

Located within central Ontario, Canada, along the boundary between the Southern and Superior Provinces, the Sudbury impact structure is recognized as the eroded remains of a 200-250 km wide multi-ring impact basin (Grieve et al., 1991). From U-Pb dating of zircon the age of the Sudbury impact has been identified as 1.85 Ga, during the Penokean orogeny (Davis, 2008). The resulting crater and impact melt sheet was subsequently modified by the Penokean (1.89-1.83 Ga) (Schulz and Cannon, 2007), Yavapai (1.744-1.704 Ga) (Raharimahefa et al., 2014), Mazatzal/ Labradorian (1.7-1.6 Ga) (Van Schmus,

1993; Rivers, 1997), and Grenville (1.235-0.945 Ga) Orogenies (Bethune and Ty, 1997).

As a result syn-orogenic timing of the Sudbury impact event, and the subsequent orogenic events the original impact structure was deformed into an elliptical shape.

The Sudbury impact structure consists of the Whitewater Group, the Sudbury Igneous Complex (SIC), and the shocked and brecciated target rocks of the crater floor (Fig. 1-2).

The Whitewater Group is a series post-impact breccias and sediments consisting of four formations, in ascending order, the Onaping, Vermilion, Onwatin, and Chelmsford Formations (Grieve et al., 2010). In contrast to the Vermilion, Onwatin, and Chelmsford Formations, the Onaping Formation is not sedimentary in origin, and has been the subject of vigorous debate as to its origin (Grieve et al., 2010).

Several attempts have been made to measure the diameter of the transient cavity of the Sudbury crater, with the diameter estimates range from 100-130 km (Grieve et al., 1991a; Deutsch et al., 1995; Spray et al., 2004). Estimates of the total amount of impact melt generated at Sudbury range from $\sim 30,000 \text{ km}^3$ (Zieg and Marsh, 2005) to $\sim 31,000 \text{ km}^3$ (Pope et al., 2004). These estimates are rather consistent with the scaling relationships of Grieve and Cintala, (1997). Considering the amount of melt and the size of the transient crater diameter, the initial crater formed at Sudbury was likely a peak-ring or possibly a multi-ring impact structure. There is also additional evidence to support this conclusion from a ring system identified by Spray et al. (2004).

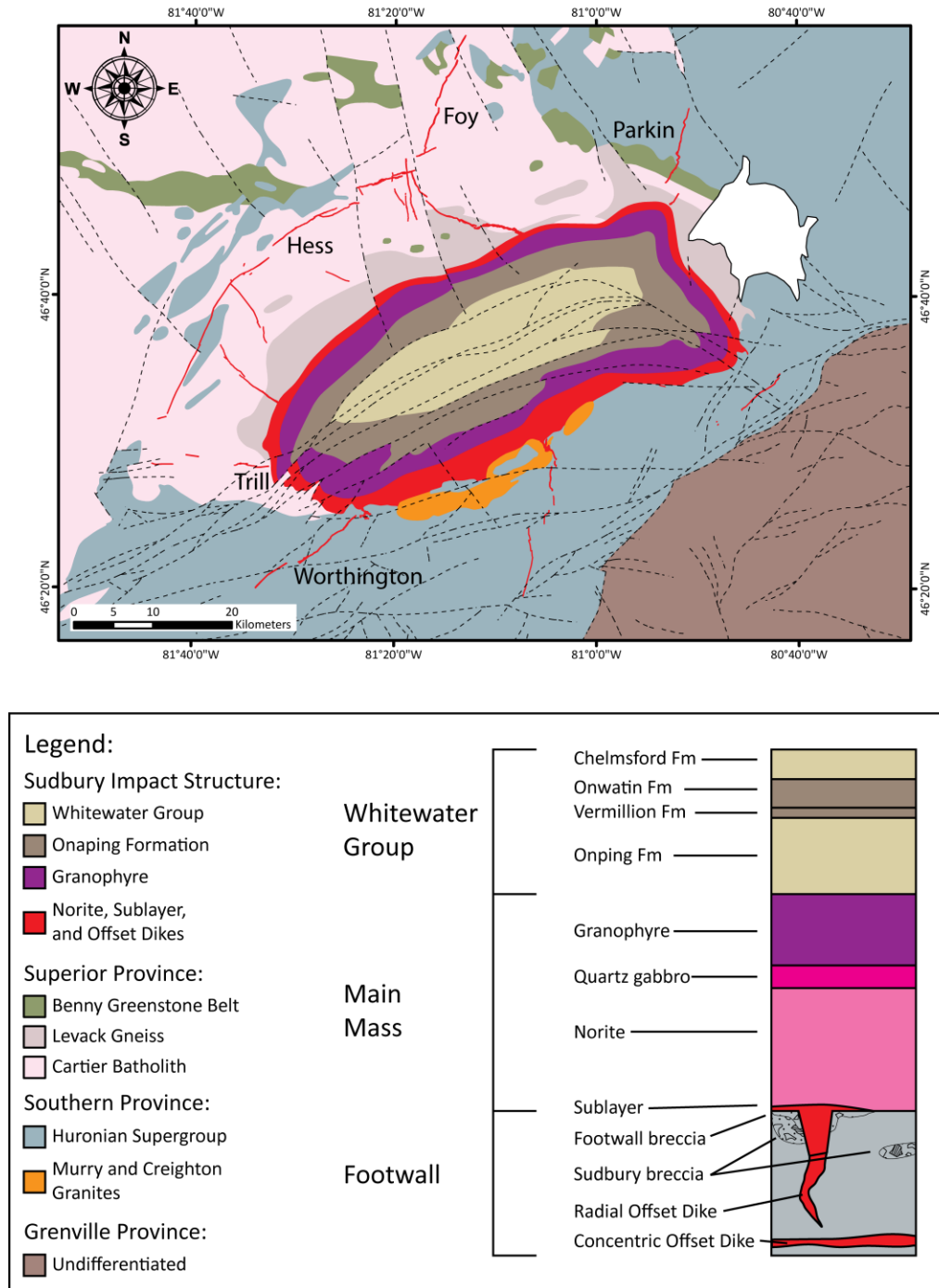


Figure 1-2: Geologic map of the Sudbury impact structure and the surrounding region with schematic diagram of the stratigraphy of the Sudbury Igneous Complex, Whitewater Group, and some Footwall units. Based on data from OGS bedrock regional 1:250,000 scale and internal Wallbridge Mining Company Limited maps. Stratigraphic column after Ames et al. (2008), with unit thickness approximated relative to one another.

1.4.1 Sudbury Igneous Complex

The Sudbury Igneous Complex (SIC) consists of the differentiated Main Mass, Sublayer, and Offset Dikes created from the melt sheet of the Sudbury impact crater. The Main Mass is the differentiated melt sheet generated from the impact event and is broadly divided from top to bottom into the Upper Contact Unit, Granophyre, Quartz Gabbro, Norite, and Sublayer units (Dickin et al., 1996; Lightfoot et al., 1997; Anders et al., 2015). Several mechanisms have historically been proposed for the differentiation of the Sudbury melt sheet. At the present however, there are three main models for the differentiation of the Sudbury melt sheet, with the first the most widely accepted:

- Crystal-liquid differentiation where the settling and accumulation of cumulus minerals created the Norite and Quartz Gabbro units (Lightfoot et al., 1997; Lightfoot et al., 2001; Therriault et al., 2002).
- Melting of the country rock generated felsic melt and mafic melt. As a result of density differences, the felsic melts rose and the mafic melts sank. This produced a density stratified magmatic system from which the melt sheet was differentiated (Golightly, 1994).
- In the initial melt sheet, two immiscible melts formed which then coalesced and separated due to immiscibility into two melts. These two separate melts crystallized to form the Norite and Granophyre (Zieg and Marsh, 2005).

1.4.2 Offset Dikes

The radial and concentric Offset Dikes of the SIC were derived from the melt sheet of the Sudbury impact structure, and emplaced below and adjacent to the target rock which

experienced syn- and post- emplacement faulting (Lightfoot et al., 1997). The name Offset Dike is derived from observed offsets in the dikes on the metre to kilometre scale perpendicular to strike. They are considered by some to be similar to the granophyre dikes seen at the Vredefort impact structure in South Africa (Dietz, 1961). Radiometric U-Pb zircon ages from the Hess Offset Dike of 1849.1 ± 0.9 Ma (Bleeker et al., 2014), Copper Cliff Offset Dike of 1849.8 ± 2 Ma (Corfu and Lightfoot, 1996), and zircon and baddeleyite ages from Foy of $1852 \pm 4/-3$ Ma (Osterman et al., 1996) are identical with the 1.85 Ga age of the impact event (Krogh et al., 1982; Davis, 2008). Geochemical analyses, such as major and trace element multivariate analyses from the offset dikes (Pilles et al., 2017) support emplacement shortly after impact (Tuchscherer and Spray, 2002).

Differing arguments have been made as to specifically when the Offset Dikes were emplaced, whether during the excavation stage of the Sudbury impact (Murphy and Spray, 2002), the modification stage (Wood and Spray, 1998; Murphy and Spray, 2002) or between 1-10 Ka post-impact (Hecht et al., 2008). Several mechanisms have been proposed for the emplacement of the Offset Dikes; broadly stated, multiple injections (Morris and Pay, 1981; Murphy and Spray, 2002; Klimesch et al., 2015) versus a single injection of material.

The Offset Dikes have historically been termed “quartz diorite”; although the rock types range from quartz monzodioritic through granodioritic and tonalitic, herein the Offset Dikes will be referred to as quartz diorite for historical consistency (Wood and Spray, 1998; Murphy and Spray, 2002; Lightfoot et al., 2001). Broadly, the offset dikes are divided into two main lithologies, an inclusion-rich quartz diorite phase (IQD), and an inclusion-poor quartz diorite phase (QD). Inclusions found within the IQD range from

footwall material of the Levack Gneiss Complex, Cartier Granitoid, Huronian Supergroup, to clasts of QD. The offset dikes are considered to have been derived from the undifferentiated impact melt sheet of the Sudbury Impact structure (Lightfoot et al., 1997a).

Discontinuous segmented bodies of QD enveloped in SUBX also exist, however their physical link to the SIC is not clear due to erosion, and their presence in SUBX raises questions about whether they were generated in situ, or emplaced. The nature of the contact between the Offset Dikes and the footwall varies with distance from the SIC, and composition of the host rock. In general, the greater the distance of the Offset Dike from the SIC, the sharper the contact will be between footwall and dike (Lightfoot, 2016). The radial offset dikes are usually connected to the Main Mass through embayments, and extend out through the footwall for hundreds of meters to tens of km from the base of the SIC. The concentric offset dikes run roughly parallel the structure of the Main Mass, and are found at surface up to ~20 km away from the present erosional base of the Main Mass. There is no known connection between the Main Mass and the concentric dikes; a prime example of this type of offset dike is the Hess Dike in the North Range (Wood and Spray, 1998). The 7km long Manchester Dike in the South Range is comparable.

Both the QD and IQD contain varying amounts of sulfide mineralization, ranging from barren to economic amounts of sulfide. Generally the QD has very low sulfide content, and the IQD very high sulfide content. However most known deposits are associated with IQD of the Frood-Stobie, Copper Cliff, and Worthington-Victoria Offset Dikes (Lightfoot, 2016). Sulfide mineralization within the Offset Dikes consists mainly of pyrite, chalcopyrite, pentlandite, and pyrrhotite. Of the Offset Dikes sampled in this

study, the Parkin, Foy, and Worthington Offsets have contained or contain deposits which have been mined (Lightfoot and Farrow, 2002; Murphy and Spray, 2002; Tuchscherer and Spray, 2002).

1.5 Introduction to the Thesis

The goal of this thesis is to use Cu, Fe, and Ni stable isotopes to investigate the SIC, its Offset Dikes, and sulfides contained therein. To this goal the thesis is organized as follows. In chapter 2 we evaluate the effectiveness of methods used for the separation of Fe, Cu, and Ni from geologic materials, and the measurement of Fe, Cu, and Ni stable isotopic ratios from those geologic materials. In chapter 3 we present and discuss $\delta^{56}\text{Fe}$, $\delta^{60}\text{Ni}$, and $\delta^{65}\text{Cu}$ values measured from the SIC, the Offset Dikes, and sulfides. Finally, chapter 4 is devoted to a discussion of improvements to the method used to extract Fe, Cu, and Ni from geologic materials, the significance of our conclusions, and avenues for future research.

1.6 References

- Ahrens, T.J., and O'Keefe, J.D., 1972, Shock melting and vaporization of lunar rocks and minerals: *The Moon*, v. 4, p. 214–249.
- Ames, D.E., Davidson, A., and Wodicka, N., 2008, Geology of the giant Sudbury polymetallic mining camp, Ontario, Canada: *Economic Geology*, v. 103, p. 1057–1077.
- Anders, D.A., Osinski, G.R., Grieve, R.A.F., and Brillinger, D.T.M., 2015, The Basal Onaping Intrusion in the North Range: Roof rocks of the Sudbury Igneous Complex: *Meteoritics & Planetary Science*, v. 50, p. 1577–1594.

- Asael, D., Matthews, A., Bar-Matthews, M., and Halicz, L., 2007, Copper isotope fractionation in sedimentary copper mineralization (Timna Valley, Israel): *Chemical Geology*, v. 243, p. 238–254.
- Asael, D., Matthews, A., Oszczepalski, S., Bar-Matthews, M., and Halicz, L., 2009, Fluid speciation controls of low temperature copper isotope fractionation applied to the Kupferschiefer and Timna ore deposits: *Chemical Geology*, v. 262, p. 147–158.
- Bethune, K.R., and Ty, A., 1997, Metamorphism of the Sudbury diabase dyke-swarm: From Protolith to two-pyroxene-garnet coronite: *Canadian Mineralogist*, v. 35, p. 1191–1220.
- Bleeker, W., Kamo, S.L., Ames, D.E., and Smith, D., 2014, New U-Pb ages for some key events in the Sudbury area, including the Creighton Granite and Joe Lake metagabbro, in Geological Association of Canada - Mineralogical Association of Canada Annual Meeting, Program with Abstracts, p. 33.
- Cameron, V., Vance, D., Archer, C., and House, C.H., 2009, A biomarker based on the stable isotopes of nickel: *Proceedings of the National Academy of Sciences*, v. 106, p. 10944–10948.
- Chernonozhkin, S.M., Goderis, S., Costas-Rodríguez, M., Claeys, P., and Vanhaecke, F., 2016, Effect of parent body evolution on equilibrium and kinetic isotope fractionation: A combined Ni and Fe isotope study of iron and stony-iron meteorites: *Geochimica et Cosmochimica Acta*, v. 186, p. 168–188.
- Cintala, M.J., and Grieve, R. a. F., 1998, Scaling impact melting and crater dimensions: Implications for the lunar cratering record: *Meteoritics & Planetary Science*, v. 33, p. 889–912.
- Corfu, F., and Lightfoot, P.C., 1996, U-Pb Geochronology of the Sublayer Environment, Sudbury Igneous Complex, Ontario: *Economic Geology*, v. 91, p. 1263–1269.
- Dauphas, N., Craddock, P.R., Asimow, P.D., Bennett, V.C., Nutman, A.P., and Ohnenstetter, D., 2009, Iron isotopes may reveal the redox conditions of mantle

melting from Archean to Present: *Earth and Planetary Science Letters*, v. 288, p. 255–267.

Dauphas, N., John, S.G., and Rouxel, O., 2017, Iron Isotope Systematics: Reviews in *Mineralogy and Geochemistry*, v. 82, p. 415–510.

Dauphas, N., Roskosz, M., Alp, E.E., Neuville, D.R., Hu, M.Y., Sio, C.K., Tissot, F.L.H., Zhao, J., Tissandier, L., Médard, E., and Cordier, C., 2014, Magma redox and structural controls on iron isotope variations in Earth ' s mantle and crust: v. 398, p. 127–140.

Davis, D.W., 2008, Sub-million-year age resolution of Precambrian igneous events by thermal extraction-thermal ionization mass spectrometer Pb dating of zircon: Application to crystallization of the Sudbury impact melt sheet: *Geology*, v. 36, p. 383–386.

Dence, M.R., 1968, Shock zoning at Canadian craters: Petrography and structural implications.: *Contributions from the Dominion Astrophysical Observatory in Victoria*, v. 8.

Deutsch, A., Grieve, R.A.F., Avermann, M.E., Bischoff, L., Brockmeyer, P., Buhl, D., Lakomy, R., Müller-Mohr, V., Ostermann, M., and Stoffler, D., 1995, The Sudbury Structure (Ontario, Canada): a tectonically deformed multi-ring impact basin: *Geologische Rundschau*, v. 84, p. 697–709.

Dickin, A.P., Artan, M.A., and Crocket, J.H., 1996, Isotopic evidence for distinct crustal sources of North and South Range ores, Sudbury Igneous Complex: *Geochimica et Cosmochimica Acta*, v. 60, p. 1605–1613.

Dietz, R.S., 1961, Vredefort Ring Structure : Meteorite Impact Scar ? *The Journal of Geology*, v. 69, p. 499–516.

Ehrlich, S., Butler, I., Halicz, L., Rickard, D., Oldroyd, A., and Matthews, A., 2004, Experimental study of the copper isotope fractionation between aqueous Cu(II) and covellite, CuS: *Chemical Geology*, v. 209, p. 259–269.

- Elliott, T., and Steele, R.C.J., 2017, The Isotope Geochemistry of Ni: Reviews in Mineralogy and Geochemistry, v. 82, p. 511–542.
- Foden, J., Sossi, P.A., and Wawryk, C.M., 2015, Lithos Fe isotopes and the contrasting petrogenesis of A-, I- and S-type granite: LITHOS, v. 212–215, p. 32–44.
- French, B.M., 1998, Traces of catastrophe: A handbook of shock-metamorphic effects in terrestrial meteorite impact structures, in LPI Contributions 954,.
- Gall, L., Williams, H.M., Halliday, A.N., and Kerr, A.C., 2017, Nickel isotopic composition of the mantle: Geochimica et Cosmochimica Acta, v. 199, p. 196–209.
- Gault, D. E., Quaide, W. L., and Oberbeck, V. R., 1968, Impact cratering mechanics and structures: Shock Metamorphism of Natural Materials, p. 87–99.
- Golightly, J.P., 1994, The Sudbury Igneous Complex as an impact melt; evolution and ore genesis: Proceedings of the Sudbury-Noril'sk Symposium, p. 105–117.
- Graham, S., Pearson, N., Jackson, S., Griffin, W., and O'Reilly, S.Y., 2004, Tracing Cu and Fe from source to porphyry: In situ determination of Cu and Fe isotope ratios in sulfides from the Grasberg Cu-Au deposit: Chemical Geology, v. 207, p. 147–169.
- Grieve, R.A.F., Ames, D.E., Morgan, J. V., and Artemieva, N., 2010, The evolution of the Onaping Formation at the Sudbury impact structure: Meteoritics and Planetary Science, v. 45, p. 759–782.
- Grieve, R.A.F., and Cintala, M.J., 1982, A method for estimating the initial impact conditions of terrestrial cratering events, exemplified by its application to Brent crater, Ontario, in Lunar and Planetary Science Conference Proceedings, p. 1607–1621.
- Grieve, R.A.F., and Cintala, M., 1997, Planetary differences in impact melting: Advances in Space Research, v. 20, p. 1551–1560.

- Grieve, R.A.F., Dence, M.R., and Robertson, P.B., 1977, Cratering processes-As interpreted from the occurrence of impact melts: Impact and explosion cratering: Planetary and terrestrial implications, v. 1, p. 791–814.
- Grieve, R.A.F., Stoffler, D., and Deutsch, A., 1991, The Sudbury Structure - controversial or misunderstood? *Journal of Geophysical Research-Planets*, v. 96, p. 22753–22764.
- Gueguen, B., Rouxel, O., Ponzevera, E., Bekker, A., and Fouquet, Y., 2013, Nickel isotope variations in terrestrial silicate rocks and geological reference materials measured by MC-ICP-MS: *Geostandards and Geoanalytical Research*, v. 37, p. 297–317.
- He, Y., Wu, H., Ke, S., Liu, S.-A., and Wang, Q., 2017, Iron isotopic compositions of adakitic and non-adakitic granitic magmas: Magma compositional control and subtle residual garnet effect: *Geochimica et Cosmochimica Acta*, v. 203, p. 89–102.
- Hecht, L., Wittek, A., Riller, U., Mohr, T., Schmitt, R.T., and Grieve, R.A.F., 2008, Differentiation and emplacement of the Worthington Offset Dike of the Sudbury impact structure, Ontario: *Meteoritics & Planetary Science*, v. 43, p. 1659–1679.
- Heimann, A., Beard, B.L., and Johnson, C.M., 2008, The role of volatile exsolution and sub-solidus fluid/rock interactions in producing high $^{56}\text{Fe}/^{54}\text{Fe}$ ratios in siliceous igneous rocks: *Geochimica et Cosmochimica Acta*, v. 72, p. 4379–4396.
- Hiebert, R.S., Bekker, A., Wing, B.A., and Rouxel, O.J., 2013, The role of paragneiss assimilation in the origin of the Voisey's Bay Ni-Cu sulfide deposit, Labrador: Multiple S and Fe isotope evidence: *Economic Geology*, v. 108, p. 1459–1469.
- Hofmann, A., Bekker, A., Dirks, P., Gueguen, B., Rumble, D., and Rouxel, O.J., 2014, Comparing orthomagmatic and hydrothermal mineralization models for komatiite-hosted nickel deposits in Zimbabwe using multiple-sulfur, iron, and nickel isotope data: *Mineralium Deposita*, v. 49, p. 75–100.

- Horn, I., von Blanckenburg, F., Schoenberg, R., Steinhoefel, G., and Markl, G., 2006, In situ iron isotope ratio determination using UV-femtosecond laser ablation with application to hydrothermal ore formation processes: *Geochimica et Cosmochimica Acta*, v. 70, p. 3677–3688.
- Kehata, K.I., and Irata, T.H., 2013, Evaluation of UV-fs-LA-MC-ICP-MS for Precise in situ Copper Isotopic Microanalysis of Cubanite: *Analytical Sciences*, v. 29, p. 1213–1217.
- Kenkmann, T., Collins, G.S., and Kunnemann, K., 2013, The modification stage of crater formation, in Osinski G.R. and Pierazzo E. eds., *Impact Cratering: Processes and Products*, John Wiley & Sons, p. 60.
- Klimesch, L.M., Hecht, L., and Riller, U., 2015, Emplacement, Differentiation and Mineralisation of the Trill Offset Dike, Sudbury, Canada.: *Economic Geology*,.
- Krogh, T.E., McNutt, R.H., and Davis, G.L., 1982, Two high precision U–Pb zircon ages for the Sudbury Nickel Irruptive: *Canadian Journal of Earth Sciences*, v. 19, p. 723–728.
- Larson, P.B., Maher, K., Ramos, F.C., Chang, Z., Gaspar, M., and Meinert, L.D., 2003, Copper isotope ratios in magmatic and hydrothermal ore-forming environments: *Chemical Geology*, v. 201, p. 337–350.
- Lazar, C., Young, E.D., and Manning, C.E., 2012, Experimental determination of equilibrium nickel isotope fractionation between metal and silicate from 500??C to 950??C: *Geochimica et Cosmochimica Acta*, v. 86, p. 276–295.
- Li, W., Jackson, S.E., Pearson, N.J., and Graham, S., 2010, Copper isotopic zonation in the Northparkes porphyry Cu-Au deposit, SE Australia: *Geochimica et Cosmochimica Acta*, v. 74, p. 4078–4096.
- Lightfoot, P.C., 2016, *Nickel Sulfide Ores and Impact Melts: Origin of the Sudbury Igneous Complex*: Elsevier.

- Lightfoot, P.C., and Farrow, C.E.G., 2002, Geology, Geochemistry, and Mineralogy of the Worthington offset dike: A genetic model for offset dike mineralization in the Sudbury Igneous Complex: *Economic Geology*, v. 97, p. 1419–1446.
- Lightfoot, P.C., Keays, R.R., and Doherty, W., 2001, Chemical Evolution and Origin of Nickel Sulfide Mineralization in the Sudbury Igneous Complex, Ontario, Canada: *Economic Geology*, v. 96, p. 1855–1875.
- Lightfoot, P.G., Keays, R.R., Morrison, G.G., Bite, A., and Farrell, K.P., 1997, Geochemical relationships in the Sudbury Igneous Complex: Origin of the main mass and offset dikes: *Economic Geology*, v. 92, p. 289–307.
- Liu, S.-A., Li, D., Li, S., Teng, F.-Z., Ke, S., He, Y., and Lu, Y., 2014, High-precision copper and iron isotope analysis of igneous rock standards by MC-ICP-MS: *J. Anal. At. Spectrom.*, v. 29, p. 122–133.
- Maher, K.C., and Larson, P.B., 2007, Variation in Copper Isotope Ratios and Controls on Fractionation in Hypogene Skarn Mineralization at Corocochuayco and Tintaya , Perú: *Economic Geology*, v. 102, p. 225–237.
- Malitch, K.N., Latypov, R.M., Badanina, I.Y., and Sluzhenikin, S.F., 2014, Insights into ore genesis of Ni-Cu-PGE sulfide deposits of the Noril'sk Province (Russia): Evidence from copper and sulfur isotopes: *Lithos*, v. 204, p. 172–187.
- Maréchal, C.N., and Sheppard, S.M.F., 2002, Isotopic fractionation of Cu and Zn between chloride and nitrate solutions and malachite or smithsonite at 30 degrees and 50 degrees C, in *Geochimica et Cosmochimica Acta*, p. A484--A484.
- Markl, G., von Blanckenburg, F., and Wagner, T., 2006, Iron isotope fractionation during hydrothermal ore deposition and alteration: *Geochimica et Cosmochimica Acta*, v. 70, p. 3011–3030..
- Markl, G., Lahaye, Y., and Schwinn, G., 2006, Copper isotopes as monitors of redox processes in hydrothermal mineralization: *Geochimica et Cosmochimica Acta*, v. 70, p. 4215–4228.

- Mathur, R., Ruiz, J., Casselman, M.J., Megaw, P., and van Egmond, R., 2012, Use of Cu isotopes to distinguish primary and secondary Cu mineralization in the Cañariaco Norte porphyry copper deposit, Northern Peru: *Mineralium Deposita*, v. 47, p. 755–762.
- Mathur, R., Ruiz, J., Titley, S., Liermann, L., Buss, H., and Brantley, S., 2005, Cu isotopic fractionation in the supergene environment with and without bacteria: *Geochimica et Cosmochimica Acta*, v. 69, p. 5233–5246.
- Mathur, R., Titley, S., Barra, F., Brantley, S., Wilson, M., Phillips, A., Munizaga, F., MaksaeV, V., Vervoort, J., and Hart, G., 2009, Exploration potential of Cu isotope fractionation in porphyry copper deposits: *Journal of Geochemical Exploration*, v. 102, p. 1–6.
- Melosh, H.J., 1989, *Impact cratering: A geologic process: Research supported by NASA*. New York, Oxford University Press (Oxford Monographs on Geology and Geophysics, No. 11), 1989, 253 p., v. 11.
- Melosh, H.J., and Ivanov, B.A., 1999, Impact Crater Collapse: *Annual Review of Earth and Planetary Sciences*, v. 27, p. 385–415.
- Morris, A., and Pay, R., 1981, Genesis of the Foy (?) Offset and Its Sulfide Ores : The Paleomagnetic Evidence from a Study in Hess Township , Sudbury , Ontario: *Economic Geology*, v. 76, p. 1895–1905.
- Moynier, F., Koeberl, C., Beck, P., Jourdan, F., and Telouk, P., 2010, Isotopic fractionation of Cu in tektites: *Geochimica et Cosmochimica Acta*, v. 74, p. 799–807.
- Moynier, F., Vance, D., Fujii, T., and Savage, P., 2017, The Isotope Geochemistry of Zinc and Copper: *Reviews in Mineralogy and Geochemistry*, v. 82, p. 543–600.
- Murphy, A.J., and Spray, J.G., 2002, Geology, mineralization, and emplacement of the Whistle-Parkin offset dike, Sudbury: *Economic Geology*, v. 97, p. 1399–1418.

- Oberbeck, V.R., 1975, The role of ballistic erosion and sedimentation in lunar stratigraphy: *Reviews of Geophysics*, v. 13, p. 337–362.
- Osinski, G.R., and Pierazzo, E., 2013, Chapter 1: Impact Cratering : Processes and Products: John Wiley & Sons, 1-20 p.
- Osterman, M., Schürer, U., and Deutsch, A., 1996, Impact melt dikes in the Sudbury multi-ring basin (Canada): Implications from uranium-lead geochronology on the Foy Offset Dike: *Meteoritics and Planetary Science*, v. 31, p. 494–501.
- Othman, D. Ben, Luck, J.M., Bodinier, J.L., Arndt, N.T., and Albarede, F., 2006, Cu--Zn isotopic variations in the Earth's mantle: *Geochimica et Cosmochimica Acta*, v. 70, p. A46.
- Pilles, E., Osinski, G.R., Grieve, R.A.F., Smith, D., and Bailey, J., 2017, Chemical variations and genetic relationships between the Hess and the Foy Offset Dikes at the Sudbury Impact Structure: *Meteoritics & Planetary Science*, v. 52., p. 2,647-2,671.
- Poitrasson, F., and Freydier, R., 2005, Heavy iron isotope composition of granites determined by high resolution MC-ICP-MS: *Chemical Geology*, v. 222, p. 132–147.
- Polyakov, V. B., & Soultanov, D. M. (2011). New data on equilibrium iron isotope fractionation among sulfides: Constraints on mechanisms of sulfide formation in hydrothermal and igneous systems. *Geochimica et Cosmochimica Acta*, 75(7), 1957–1974.
- Pope, K.O., Kieffer, S.W., and Ames, D.E., 2004, Empirical and theoretical comparisons of the Chicxulub and Sudbury impact structures: *Meteoritics and Planetary Science*, v. 39, p. 97–116.
- Raharimahefa, T., Lafrance, B., and Tinkham, D.K., 2014, New structural, metamorphic, and U–Pb geochronological constraints on the Blezardian Orogeny and Yavapai

- Orogeny in the Southern Province, Sudbury, Canada: *Canadian Journal of Earth Sciences*, v. 51, p. 750–774.
- Ripley, E.M., Dong, S., Li, C., and Wasylenki, L.E., 2015, Cu isotope variations between conduit and sheet-style Ni–Cu–PGE sulfide mineralization in the Midcontinent Rift System, North America: *Chemical Geology*, v. 414, p. 59–68.
- Rivers, T., 1997, Lithotectonic elements of the Grenville Province: review and tectonic implications: *Precambrian Research*, v. 86, p. 117–154.
- Rouxel, O., Fouquet, Y., & Ludden, J. N. (2004). Subsurface processes at the lucky strike hydrothermal field, Mid-Atlantic ridge: Evidence from sulfur, selenium, and iron isotopes. *Geochimica et Cosmochimica Acta*, 68(10), 2295–2311.
- Rouxel, O., Shanks, W. C., Bach, W., & Edwards, K. J. (2008). Integrated Fe- and S-isotope study of seafloor hydrothermal vents at East Pacific Rise 9-10°N. *Chemical Geology*, 252(3–4), 214–227.
- Savage, P.S., Moynier, F., Chen, H., Shofner, G., Siebert, J., Badro, J., and Puchtel, I.S., 2015, Copper isotope evidence for large-scale sulphide fractionation during Earth's differentiation: *Geochemical Perspectives Letters*, p. 53–64.
- Van Schmus, W.R., 1993, Transcontinental Proterozoic provinces: *Geological Society of America*, v. *Geology of*, p. 171–334.
- Schuessler, J.A., Schoenberg, R., Behrens, H., and Blanckenburg, F. von, 2007, The experimental calibration of the iron isotope fractionation factor between pyrrhotite and peralkaline rhyolitic melt: *Geochimica et Cosmochimica Acta*, v. 71, p. 417–433.
- Schuessler, J.A., Schoenberg, R., and Sigmarsson, O., 2009, Iron and lithium isotope systematics of the Hekla volcano, Iceland — Evidence for Fe isotope fractionation during magma differentiation: *Chemical Geology*, v. 258, p. 78–91.

- Schulz, K.J., and Cannon, W.F., 2007, The Penokean orogeny in the Lake Superior region: *Precambrian Research*, v. 157, p. 4–25.
- Sherman, D.M., 2013, Equilibrium isotopic fractionation of copper during oxidation / reduction , aqueous complexation and ore-forming processes : Predictions from hybrid density functional theory: *Geochimica et Cosmochimica Acta*, v. 118, p. 85–97.
- Sossi, P.A., Foden, J.D., and Halverson, G.P., 2012, Redox-controlled iron isotope fractionation during magmatic differentiation : an example from the Red Hill intrusion, S . Tasmania: ,
- Spray, J.G., Butler, H.R., and Thompson, L.M., 2004, Tectonic influences on the morphometry of the Sudbury impact structure: Implications for terrestrial cratering and modeling: *Meteoritics & Planetary Science*, v. 39, p. 287–301.
- Spudis, P.D., Martin, D.J.P., and Kramer, G., 2014, Geology and composition of the orientale basin impact melt sheet: *Journal of Geophysical Research E: Planets*, v. 119, p. 19–29.
- Steele, R.C.J., Elliott, T., Coath, C.D., and Regelous, M., 2011, Confirmation of mass-independent Ni isotopic variability in iron meteorites: *Geochimica et Cosmochimica Acta*, v. 75, p. 7906–7925.
- Syverson, D.D., Luhmann, A.J., Tan, C., Borrok, D.M., Ding, K., and Seyfried, W.E., 2017, Fe isotope fractionation between chalcopyrite and dissolved Fe during hydrothermal recrystallization: An experimental study at 350°C and 500bars: *Geochimica et Cosmochimica Acta*, v. 200, p. 87–109.
- Tanimizu, M., and Hirata, T., 2006, Determination of natural isotopic variation in nickel using inductively coupled plasma mass spectrometry: *Journal of Analytical Atomic Spectrometry*, v. 21, p. 1423, doi: 10.1039/b609543g.

- Teng, F.-Z., Dauphas, N., and Helz, R.T., 2008, Iron Isotope Fractionation During Magmatic Differentiation in Kilauea Iki Lava Lake: *Science*, v. 320, p. 1620–1622.
- Teng, F.-Z., Dauphas, N., and Watkins, J.M., 2017, Non-Traditional Stable Isotopes: Retrospective and Prospective: *Reviews in Mineralogy and Geochemistry*, v. 82, p. 1–26.
- Therriault, A.M., Fowler, A.D., and Grieve, R.A.F., 2002, The Sudbury Igneous Complex: A differentiated impact melt sheet: *Economic Geology*, v. 97, p. 1521–1540.
- Tuchscherer, M., and Spray, J., 2002, Geology, mineralization, and emplacement of the Foy Offset Dike, Sudbury impact structure: *Economic Geology*, v. 97, p. 1377–1397.
- Urey, H.C., 1947, The Thermodynamic Properties of Isotopic Substances: *Journal of the Chemical Society*, v. 53, p. 562–581.
- Vaughan, W.M., and Head, J.W., 2014, Impact melt differentiation in the South Pole-Aitken basin: Some observations and speculations: *Planetary and Space Science*, v. 91, p. 101–106.
- Vaughan, W.M., Head, J.W., Wilson, L., and Hess, P.C., 2013, Geology and petrology of enormous volumes of impact melt on the Moon: A case study of the Orientale basin impact melt sea: *Icarus*, v. 223, p. 749–765.
- Wang, Y., Zhu, X. kun, and Cheng, Y., 2015, Fe isotope behaviours during sulfide-dominated skarn-type mineralisation: *Journal of Asian Earth Sciences*, v. 103, p. 374–392.
- Wawryk, C.M., and Foden, J.D., 2015, Fe-isotope fractionation in magmatic-hydrothermal mineral deposits: A case study from the Renison Sn-W deposit, Tasmania: *Geochimica et Cosmochimica Acta*, v. 150, p. 285–298.

- Wood, C.R., and Spray, J.G., 1998, Origin and emplacement of offset dykes in the Sudbury impact structure: Constraints from Hess: *Meteoritics & Planetary Science*, v. 33, p. 337–347.
- Zambardi, T., Lundstrom, C.C., Li, X., and Mccurry, M., 2014, Fe and Si isotope variations at Cedar Butte volcano ; insight into magmatic differentiation: *Earth and Planetary Science Letters*, v. 405, p. 169–179.
- Zhu, D., Bao, H., and Liu, Y., 2015, Non-traditional stable isotope behaviors in immiscible silica-melts in a mafic magma chamber: *Nature Publishing Group*, p. 1–10.
- Zhu, X.K., Guo, Y., Williams, R.J.P., O’Nions, R.K., Matthews, a., Belshaw, N.S., Canters, G.W., de Waal, E.C., Weser, U., Burgess, B.K., and Salvato, B., 2002, Mass fractionation processes of transition metal isotopes: *Earth and Planetary Science Letters*, v. 200, p. 47–62, doi.
- Zhu, B., Zhang, H.F., Zhao, X.M., and He, Y.S., 2016, Iron isotope fractionation during skarn-type alteration: Implications for metal source in the Han-Xing iron skarn deposit: *Ore Geology Reviews*, v. 74, p. 139–150.
- Zieg, M.J., and Marsh, B.D., 2005, The Sudbury Igneous Complex: Viscous emulsion differentiation of a superheated impact melt sheet: *Bulletin of the Geological Society of America*, v. 117, p. 1427–1450.

Chapter 2

2 Chemical Extraction and Measurement of Stable Fe, Cu, and Ni isotopes

2.1 Introduction

Recent advancements in the field of stable isotope geochemistry have pushed the boundaries of materials and elements that can be isotopically analyzed. In this chapter the methods for extracting and purifying Fe, Cu, and Ni from rock samples and the measurement of stable Fe, Cu, and Ni isotopic ratios using Multi Collector Inductively Coupled Plasma Mass Spectrometry (MC-ICP-MS) are described. The objective of this chapter is to explain and evaluate methods used for extracting and purifying Fe, Ni, and Cu from geologic materials, and the measurement of their isotopic ratios.

For this study, Cu isotope ratios were measured as $^{65}\text{Cu}/^{63}\text{Cu}$, and are reported as $\delta^{65}\text{Cu}$ (NIST SRM 976) per mil (‰). Fe isotope ratios were measured as $^{56}\text{Fe}/^{54}\text{Fe}$, and are reported as $\delta^{56}\text{Fe}$ (IRMM-014) per mil (‰). Ni isotope ratios were measured as $^{60}\text{Ni}/^{58}\text{Ni}$, and are reported as $\delta^{60}\text{Ni}$ (NIST SRM 986) per mil (‰).

2.2 Evaluation of Analytical Methods

Prior to isotopic analysis samples were dissolved and run through ion exchange column chromatography to purify sample aliquots of Cu, Fe, and Ni from the rock and mineral sample matrices. All dissolutions and chemistry methods were performed using Savillex PFA Teflon beakers, purified water, distilled acids, and high-purity reagents. Nitric and hydrochloric acids used in dissolutions and column chemistry were distilled in-house in Savillex® sub-boiling distillation stills, and water used was 18.2 mΩ resistivity grade (using a Millipore®, USA Advantage 10 and QPOD Element purification systems). Acetone, acetic acid, and hydrofluoric acids were purchased at ultra trace metal grades (ppt level). All geochemical procedures were performed at the GEOMETRIC lab at the University of Western Ontario. For concentration measurements, a Thermo Scientific iCAP Q Inductively Coupled Plasma Mass Spectrometer (ICP-MS) with a helium collision cell, was used to measure the abundance of major, minor, and trace elements.

The iCAP Q was calibrated using serially diluted elemental standards, and was used to measure the composition of samples, calibrate ion-exchange columns, and ensure the purity and yield of sample cuts. High-precision isotopic measurements were performed using multi-collector (MC-) ICPMS instruments at the Trent University Water Quality Centre, and SESAME laboratory at Indiana University.

2.2.1 Sample Dissolution

Prior to ion exchange chromatography purification, samples were dissolved according to their dominant matrix. Crushed and powdered samples were weighed out into pre-cleaned Savillex® PFA Teflon beakers. Beakers were cleaned in a 50% HNO₃ bath, rinsed with MQ water, dried, and fluxed individually in 6M HCl. Silicate samples were dissolved in HNO₃ and HF for two days followed by treatment in perchloric acid (HClO₄) to break down fluoride phases formed during HNO₃ and HF digestion. A solution of 30% hydrogen peroxide (H₂O₂) was also added to reduce Cr prior to column chemistry. Sulfide samples were dissolved in aqua regia at a 1:3 molar ratio of HNO₃ and HCl in PFA Teflon beakers, and were placed on a hotplate overnight at 120°C. After dissolution, samples were brought up in 6M HCl, and centrifuged to remove refractory phases such as zircons in the silicate samples and quartz in the sulfide samples. These phases were found to represent less <<1% of the dissolved sample, and do not contain large amounts of Fe, Ni, and Cu and thus do not affect our whole-rock measurements. An aliquot of the dissolved material was taken for analysis by quadrupole ICPMS to measure elemental abundances before measuring out aliquots for column chemistry.

2.2.2 Cu and Fe Purification and Measurement

Column chemistry for Cu purification is based off Maréchal et al. (1999) and modifications by Chapman et al. (2006). Acid washed Bio-Rad® AG MP-1M (100-200 mesh) resin was used along with acid washed Bio-Rad® polypropylene columns (2ml resin bed and 10ml reservoir). Prior to loading the sample aliquot, column and resin were washed and conditioned with 6M HCl. Samples were loaded with 1ml of 7M HCl; then the matrix was eluted with 8 ml of 7M HCl; Cu was finally eluted with 25 ml of 7M HCl. After the elution of Cu, Fe was then eluted off the column with 20mL of 2M HCl. For

silicate samples, the Cu elution step was repeated to remove additional matrix elements. Cu and Fe recovery for both sulfide and silicate matrices were tested and found to be $100 \pm 5\%$ (Fig. 2-1). Column yields was measured by running solutions of known concentration through the column and measuring the amount of eluted Cu and Fe by ICP-MS. Fractionation on the column was evaluated using georeference standards, the results of which are reported in the next sections. After column separation, samples were dried overnight and taken up in 2% by volume HNO₃. Total procedural blanks for both Cu and Fe were measured to be less than ~6 ng which is <1% compared to the total amount of Cu and Fe processed in the samples. Column blanks were ~0.04 ng for Cu and ~0.3 ng for Fe.

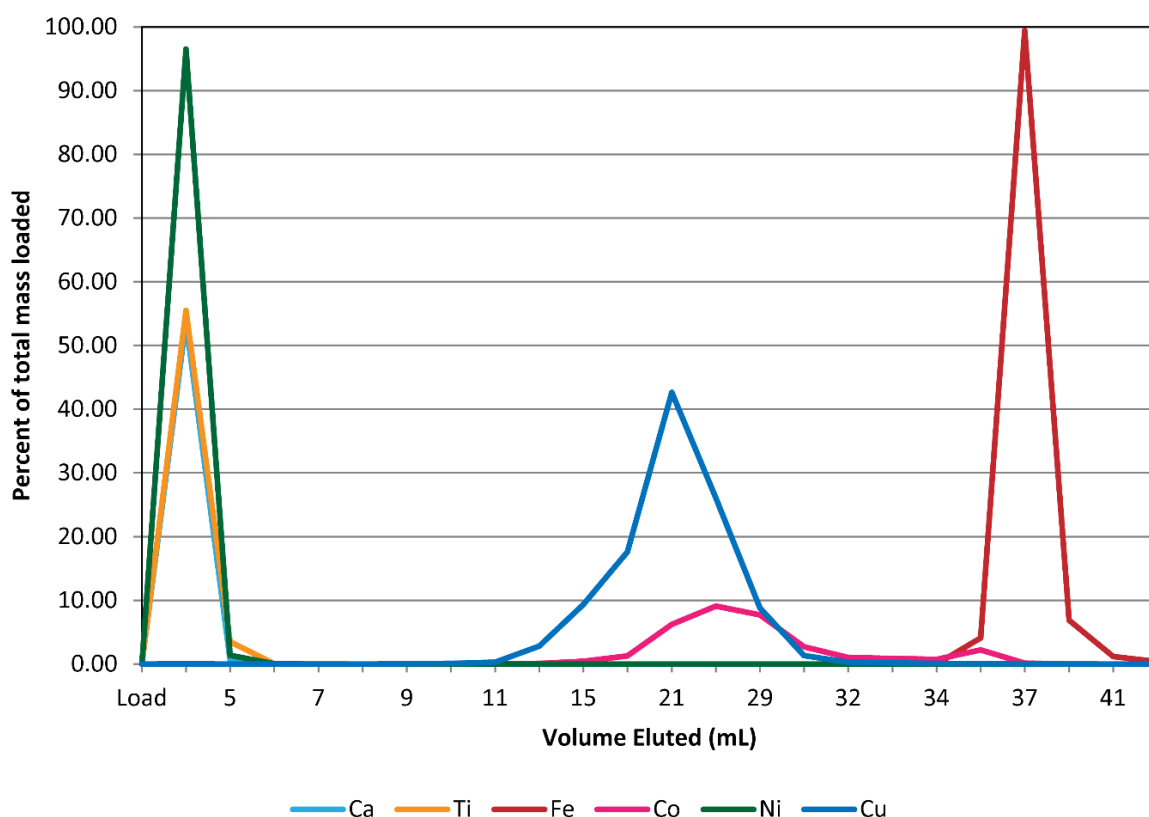


Figure 2-1: Elution Curve for SUDPAC 017, a sulfide containing QD sample from the intersection of the Foy and Hess offsets.

2.2.3 Cu Mass Spectrometry

Cu isotope ratios were measured using a Nu Instrument Plasma II or a Thermo Neptune multi-collector inductively coupled plasma mass spectrometer (MC-ICP-MS) at the Trent University Water Quality Centre. Sample introduction was achieved using a CETAC Aridus II (NuPlasma II) or ApexQ (Neptune) desolvating nebulizer and PFA nebulizer to enhance the ion yield transferred to the mass spectrometer. ^{65}Cu was measured on H4 and ^{63}Cu was measured on L2 Faraday cups respectively. Standard sample bracketing was used to monitor and correct for instrumental mass bias, with samples and standards run as one block of 25 measurements, with 40s wash-out with 2% nitric acid and 40s transfer time in between. NIST SRM 976 with defines zero per mil $\delta^{65}\text{Cu}$ (Eq. 1-3 & 1-4) was used as the standard bracketing material; Cu isotope ratios are reported as $\delta^{65}\text{Cu}$ (NIST SRM 976) per mil (‰). Each standard sample bracket was performed three times, sample error is reported as twice the standard deviation of the bracketed measurements; average error for $\delta^{65}\text{Cu}$ was 0.05‰ (2SD). The georeference standards SU-1 (sulfide ore from Sudbury) and BIR-1 (Icelandic basalt) were analyzed to evaluate column separation procedures. Triplicate analyses of SU-1 on the Nu Plasma II and Neptune resulted in an average value of $-0.07 \pm 0.08\text{‰}$; previously reported values are $-0.02 \pm 0.08\text{‰}$ (2SE) (Chapman et al., 2006) and $-0.09 \pm 0.09\text{‰}$ (2SD) (Ripley et al., 2015). A single analysis of BIR-1 gave a value of $0.05 \pm 0.16\text{‰}$ over three bracketed measurements; the recommended value of BIR-1 is $0.02 \pm 0.06\text{‰}$ (2SE) (Moynier et al., 2017). Duplicate and triplicate analyses over multiple sessions indicate an uncertainty of $\sim 0.11\text{‰}$ (2SD). This is different from the average error, which is the average error from each block of 3 sample-standard brackets. This uncertainty is higher than the average error, and likely the result of analytical conditions not being perfectly identical between sessions.

Measurements were conducted with different sample/standard concentrations to determine if a difference in standard concentration creates a significant difference in measured $\delta^{65}\text{Cu}$ values. Results from the experiments show that at half and twice sample concentration relative to standard concentration produce no significant difference in $\delta^{65}\text{Cu}$ values (Fig. 2-2A). Co is known to be non-completely removed from sample aliquots during column chemistry (Fig. 2-1). Experiments were thus performed by doping

a known Cu ICPMS solution with Co (which is monoisotopic ^{59}Co) along with trace amounts of common matrix elements to determine whether Co produced a significant matrix effect on $\delta^{65}\text{Cu}$ values measured. Results from the experiment show that no significant difference is noted by the presence of Co at concentrations up to twice that of Cu (Fig. 2-2B).

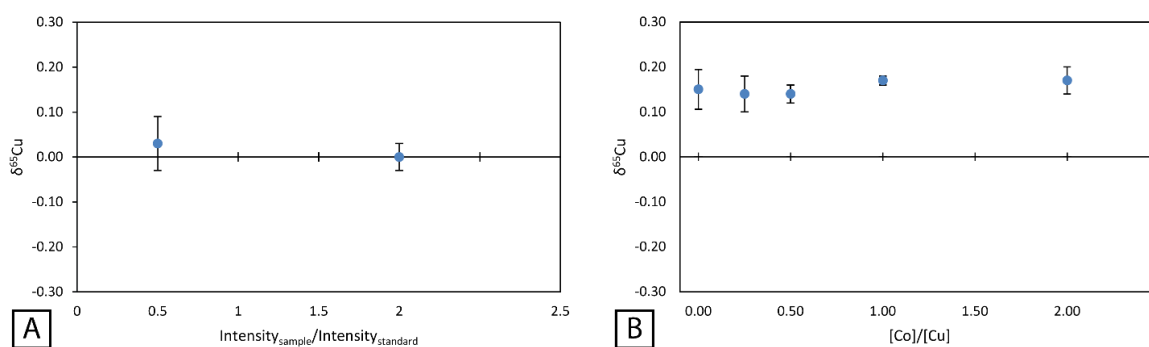


Figure 2-2: A) $\delta^{65}\text{Cu}$ of ICP Cu solution at twice concentration and half concentration relative to the bracketing standard. B) $\delta^{65}\text{Cu}$ of ICP Cu solution doped with common matrix elements K (28%), Mg (7%), Co (65%), 50ppb Zn and variable amounts of Cu. A shift can be seen from 0‰ (A) to ~0.15‰ (B) $\delta^{65}\text{Cu}$ likely due to the presence of Zn. Zn doping was tested as an internal standard, but failed to yield reproducible standard values.

2.2.4 Fe Mass Spectrometry

Fe isotope ratios were measured using a Thermo Neptune MC-ICP-MS at the Trent University Water Quality Centre. Sample introduction was achieved using an ApexQ desolvating nebulizer and PFA nebulizer. The standard sample bracketing method was used to monitor and correct for instrumental mass bias, with samples and standards run as one block of 25 measurements integrated over 10s. Each standard sample bracket was performed three times, with a wash step in-between. IRMM-014 defines 0 per mil (‰) $\delta^{56}\text{Fe}$ (Eq. 1-3 & 1-4), and was used as the standard bracketing material; Fe isotope ratios are reported as $\delta^{56}\text{Fe}_{(\text{IRMM-014})}$ in per mil unit (‰). Sample error is reported as twice the standard deviation (2SD) of the repeated bracketed measurements; on average, the error for $\delta^{56}\text{Fe}$ was 0.05‰ (2SD). BCR-2 and BIR-1 georeference standards were measured to ensure a sufficient removal of matrix elements, and that the column procedure was not

fractionating Fe on the column. Analyses of BCR-2 gave a result of $0.14 \pm 0.03\%$ and analyses of BIR-1 gave a result of $0.03 \pm 0.06\%$; recommended values from Craddock and Dauphas (2010) are $0.09 \pm 0.01\%$ and $0.05 \pm 0.02\%$ for BCR-2 and BIR-1 respectively. Recommended values from Craddock and Dauphas (2010), are reported as an error-weighted mean of independent replicates. Error for these recommended values was reported as a 95% confidence interval. Duplicate and triplicate analyses over multiple sessions indicate uncertainty of $\sim 0.12\%$. This is different from the average error, which is the average error from each block of 3 sample-standard brackets. This uncertainty is higher than the average error, and likely the result of analytical conditions not being perfectly identical between sessions.

2.2.5 Ni Purification

Ni was purified was achieved utilizing a double column and double spike method modified after Wasylenki et al. (2015). Bio-Rad® polypropylene columns (2ml resin bed and 10ml reservoir) were filled with 2 mL of acid-cleaned AG50W-X8 cation exchange resin (200-400 mesh). Prior to column chemistry, samples were brought up in a mixture of 20% volume 10M HCl (first) then 80% volume of acetone was added before column chemistry. Prior to adding acetone, samples were spiked with a ^{62}Ni and ^{61}Ni double spike at a spike-to-sample ratio of 64:36, this resulted in 4 μg of spike for every 2 μg of sample. For the first column, columns were initially washed with 6M HCl and conditioned with a 4 mL mixture of 80% acetone and 20% 10M HCl, mixed by volume right prior to loading. Samples were then loaded with a mixture of 200 μL of 10M HCl and 800 μL of high-purity acetone for 6 μg of Ni (2 μg Ni from the sample and 4 μg of Ni from the double spike). Next, 7 mL of a mixture of 80% acetone and 20% 10M HCl mixture were used to elute matrix elements including Fe, Mn, and Cr. Ni was then eluted off the column using 4 mL of 6M HCl, collected, and dried in preparation for the second column step. The second column is identical to the first, except that the solution used during elution steps is an 85% acetic acid and 15% 10M HCl volumetric mixture. Fresh acid-cleaned resin was used in both columns, with resin changed in-between sample passes. Prior to loading, columns are washed with 6M HCl, MQ water, and then conditioned with 4 mL of the 85% acetic acid-15% 10M HCl mixture. Collected Ni cuts

from the first column are brought up in a mixture of 150 μL 10M HCl and 850 μL acetic acid, which is used to load samples onto the column. After loading, 15 mL of the acetic-HCl mixture is used to elute Ni, while Mg, Ca, Al, and Ti are retained on the column. Ni cuts are then dried down and brought up in 2% by volume HNO_3 for analysis. While samples were double spiked prior to column chemistry to help correct for fractionation during column chemistry and mass spectrometry, yields were determined to be >95%. Some high-matrix silicate samples required an additional pass on the second column to remove additional Mg, Na and Ca. Total procedure blanks were measured to be less than ~5ng which remains $\ll 1\%$ of the minimum Ni contents processed per sample and thus negligible. Column blanks were ~0.5ng Ni

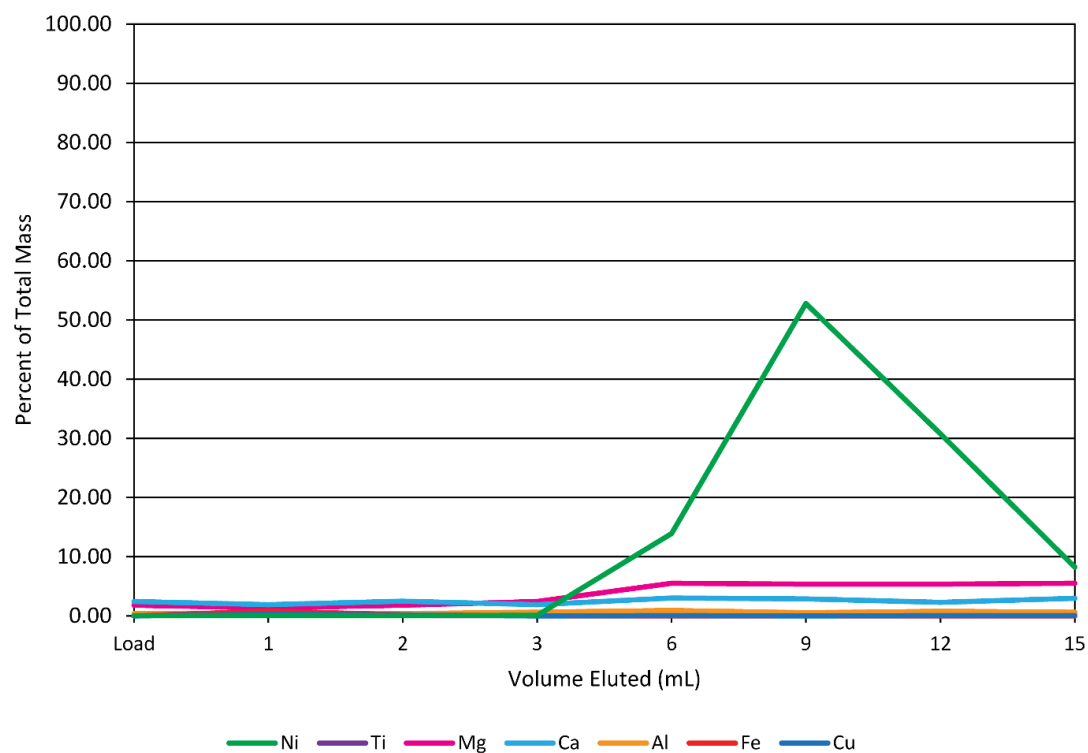
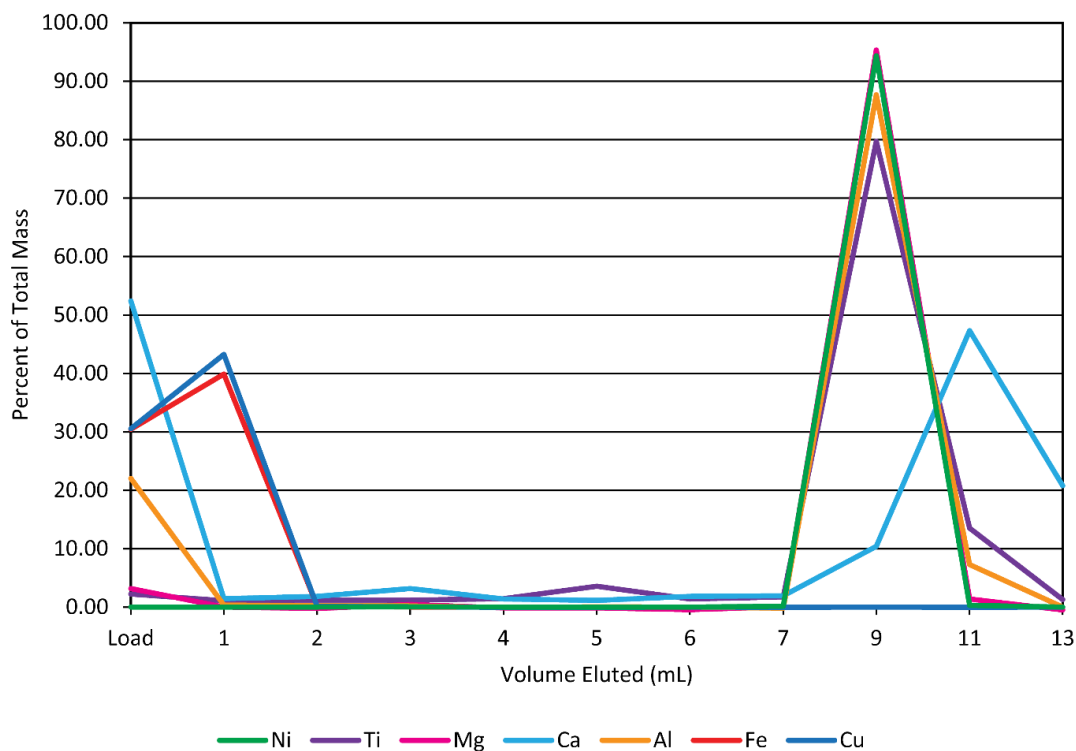


Figure 2-3: Elution curves for the first column of the Ni separation protocol separating metals such as Fe and Cu (top), and the second column protocol separating Ni from cations such as Ca, Al, Ti, and Mg (bottom).

2.2.6 Ni Mass Spectrometry

Ni isotopic analyses were conducted at the SESAME Laboratory at Indiana University using a Nu Plasma II MC-ICP-MS. Sample introduction was achieved using an Aridus II desolvating nebulizer. The stable isotopes of Ni (^{62}Ni , ^{61}Ni , ^{60}Ni , and ^{58}Ni) were measured on the following Faraday Cups, H4, H2, Axial, and L4 respectively. To correct the isobaric interference (interference of the same mass) of ^{58}Fe on ^{58}Ni , ^{57}Fe was measured on L5. Standard sample bracketing was used to monitor and correct for instrument mass bias. NIST SRM 986 defines zero per mil $\delta^{60}\text{Ni}$ (Eq. 1-3 & 1-4), and was used as the standard bracketing material; Ni isotope ratios are reported as $\delta^{60}\text{Ni}$ (NIST SRM 986) per mil (‰). Each standard sample bracket was performed three times, sample error is reported as twice the standard deviation (2SD) of the bracketed measurements; average 2SD error for $\delta^{60}\text{Ni}$ was 0.09‰ on each block of three sample-standard brackets. Both samples and bracketing standard were spiked with a ^{61}Ni and ^{62}Ni double spike which was used to correct for instrument-induced mass bias and column isotopic fractionation using double-spike equations according to methods described by (Wasylenki et al., 2015). To ensure a sufficient removal of matrix elements, and that the column procedure was not fractionating Ni, the georeferenced standard BIR-1 was processed and measured four times during one session. A value of $0.12 \pm 0.09\%$ (2SD) was obtained which is in agreement with previously published values of $0.12 \pm 0.04\%$ (2SE) (Gueguen et al., 2013) and $0.19 \pm 0.07\%$ (2SD) (Chernonozhkin et al., 2015).

2.2.7 Double Spiking

Double spiking is an analytical technique used to correct for instrumental mass fractionation which has been in use for a long period of time (Dodson, 1963). Fundamentally, spiking is the addition of a known composition to a substance of unknown composition, to then calculate the composition of the unknown. Double spiking is a technique where a known amount of two isotopes is added to an unknown sample as a “spike”. The double spike technique can be used with any isotopic system which contains four isotopes. This makes it an ideally suited technique to correct for instrumental mass fractionation of many non-traditional stable isotopes (e.g. Cr, Fe, Ni, Zn, Se, and Hg). It is important to note that the spike must be pure in its isotopic

composition or very well known to minimize error from its subtraction from the measured sample composition. Knowing the composition of the spike, the composition of an unknown is obtained by inverting the measurements of the spiked sample (mixture). For the case of a double spike, the inversion is solving three simultaneous non-linear equations.

For the Ni double spike used in this study, the optimal composition of the double spike and spike sample ratio was modeled by Wasylenki et al. (2015) using the code of Rudge et al. (2009). The optimal spike composition was determined to be ~41% ^{61}Ni and ~54% ^{62}Ni with the optimal ratio of the spike-to-sample being 64:36. The double spike correction used is from Wasylenki et al. (2015).

2.3 Conclusions

The methods for extracting and purifying Fe, Ni, and Cu from geologic materials and measuring their isotopic composition were evaluated in this chapter. The ion-exchange column chemistry protocols had their yields tested to ensure that recovery was greater than 95%. Incomplete recovery of a sample from an ion-exchange column can result in large isotopic fractionations to that sample. Ion-exchange column yields were tested by loading a solution of known concentration onto the ion-exchange column and measuring the concentration of metal collected during the elution step. Yields for Fe, Ni, and Cu were determined to be >95%.

Additional tests were also performed to evaluate column chemistry procedures and to ensure accurate measurement of isotopic ratios by Multi Collector Inductively Coupled Plasma Mass Spectroscopy (MC-ICP-MS). Georeference standards of known isotopic composition were passed through the ion-exchange column procedures and measured by MC-ICP-MS methods. These standards were then compared to their known values to ensure a lack of isotopic fractionation during column chemistry, and that the isotopic ratios measured by MC-ICP-MS were accurate. Georeference standards SU-1 and BIR-1 were analyzed for Cu, BCR-2 and BIR-1 were analyzed for Fe, and BIR-1 was analyzed for Ni. All georeference standards measured reported values which were in agreement with previously published values.

To conclude, methods for extracting and purifying Fe, Ni, and Cu from geologic materials and measuring their isotopic composition have been evaluated, and are effective in measuring the Fe, Ni, and Cu stable isotopic compositions of geologic materials. For future work, evaluating methods that can extract and purify Ni and Cu from low concentration samples would greatly expand the number of samples which could be analyzed.

2.4 References

- Chapman, J., Mason, T., Weiss, D., Coles, B., and Wilkinson, J., 2006, Chemical separation and isotopic variations of Cu and Zn from five geological reference materials: *Geostand Geoanal Res*, v. 30, p. 5–16.
- Chernonozhkin, S.M., Goderis, S., Lobo, L., Claeys, P., and Vanhaecke, F., 2015, Development of an isolation procedure and MC-ICP-MS measurement protocol for the study of stable isotope ratio variations of nickel: *J. Anal. At. Spectrom.*, v. 30, p. 1518–1530.
- Craddock, P.R., and Dauphas, N., 2010, Iron Isotopic Compositions of Geological Reference Materials and Chondrites: v. 35, p. 101–123.
- Dodson, M.H., 1963, A theoretical study of the use of internal standards for precise isotopic analysis by the surface ionization technique: Part I - General first-order algebraic solutions: *Journal of Scientific Instruments*, v. 40, p. 289.
- Gueguen, B., Rouxel, O., Ponzevera, E., Bekker, A., and Fouquet, Y., 2013, Nickel isotope variations in terrestrial silicate rocks and geological reference materials measured by MC-ICP-MS: *Geostandards and Geoanalytical Research*, v. 37, p. 297–317.
- Maréchal, C.N., Télouk, P., and Albarède, F., 1999, Precise analysis of copper and zinc isotopic compositions by plasma-source mass spectrometry: *Chemical Geology*, v. 156, p. 251–273.

- Moynier, F., Vance, D., Fujii, T., and Savage, P., 2017, The Isotope Geochemistry of Zinc and Copper: Reviews in Mineralogy and Geochemistry, v. 82, p. 543–600.
- Ripley, E.M., Dong, S., Li, C., and Wasylenki, L.E., 2015, Cu isotope variations between conduit and sheet-style Ni–Cu–PGE sulfide mineralization in the Midcontinent Rift System, North America: Chemical Geology, v. 414, p. 59–68..
- Rudge, J.F., Reynolds, B.C., and Bourdon, B., 2009, The double spike toolbox: Chemical Geology, v. 265, p. 420–431.
- Wasylenki, L.E., Howe, H.D., Spivak-Birndorf, L.J., and Bish, D.L., 2015, Ni isotope fractionation during sorption to ferrihydrite: Implications for Ni in banded iron formations: Chemical Geology, v. 400, p. 56–64.

Chapter 3

3 Stable Cu, Fe, and Ni Isotopic Systematics of the Sudbury Offset Dikes and Associated Rocks

3.1 Introduction

Impact cratering is a process ubiquitous throughout the solid bodies of the solar system; possibly a key process to the origin of life on Earth, and in the formation of economically valuable geologic deposits (Grieve, 1991, 1994; Reimold et al., 2005; Osinski and Pierazzo, 2013). Large scale impacts events that formed large diameter (>100 km) impact craters were a common event during the early history of the solid objects in the solar system. These impact events have also been suggested to play an important role in the development of evolved magma compositions that may have aided the development of plate tectonics here on Earth (Taylor and McLennan, 1995; Grieve and Cintala, 1997; O'Neill et al., 2017). Unlike endogenic melting, impact melting is formed by pressure-volume work, making the large volumes of molten rock produced during these events unique. Due to the difficulties in accessing lunar impact basins and the low number of identified peak-ring and multi-ring impact basins on the Earth, however, relatively little is known about igneous processes that occur in craters of these magnitudes.

The Sudbury Igneous Complex (SIC) is the eroded and deformed remains of the Sudbury impact structure that formed ~1.85 Ga (Dietz, 1964; Grieve, 1994; Golightly, 1994; Davis, 2008). While important questions have been answered at Sudbury as a result of the presence of the second largest concentration Ni-Cu-PGE sulfide ore on Earth and over a century of mining and exploration (Coleman, 1905; Lightfoot, 2016). How the SIC formed as a differentiated impact melt sheet, and specifics about how and where sulfide mineralization formed; these are questions which if better answered, will greatly improve mineral exploration models at Sudbury. Additionally, igneous processes such as igneous differentiation are poorly understood at large impact melt sheets. Obtaining better answers to these questions at Sudbury will greatly increase understanding of impact cratering processes. To go further, such knowledge will benefit exploration for space-based resources, such as those found in impact craters on asteroids, and the Moon.

To these ends, the Offset Dikes of the SIC potentially offer important insight into the history of the SIC. The Offset Dikes are possibly the best representation of the initial composition of the Sudbury impact melt sheet as they are thought to have been emplaced early in the cooling history of the SIC (Lightfoot et al., 1997; Wood and Spray, 1998; Murphy and Spray, 2002; Tuchscherer and Spray, 2002; Hecht et al., 2008). By comparing them to other members of the SIC as a compositional starting point, insight can be gained into processes which occurred within the Sudbury impact melt sheet as it cooled.

Fe, Ni, and Cu isotopes offer a powerful tool as they are effected by magma differentiation and sulfide segregation, two processes of importance at Sudbury. Critically, they are also yet to be systemically measured at the SIC. Thus, the objectives of the analysis of Cu, Fe, and Ni isotopes from the Offset Dikes, SIC, and associated rocks are:

- Evaluate the origin(s) and source(s) of the Offset Dikes within the SIC and the sulfides they contain.
- Examine what the Fe, Ni, and Cu isotopic composition of the Offset Dikes, SIC, and target rocks can tell us about the evolution and differentiation of the SIC as the impact melt sheet of a large diameter impact crater.

3.2 Geologic Background

The Sudbury Igneous Complex (SIC) is the surviving material of the impact melt sheet generated by the large hypervelocity impact that made the Sudbury impact structure (Grieve, 1994). This large impact event occurred ~1.85 Ga during the Penokean Orogeny (Grieve et al., 1991; Ames et al., 2008). The crater and impact melt sheet were subsequently modified by the Penokean (1.89-1.83 Ga) (Schulz and Cannon, 2007), Yavapai (1.744-1.704 Ga) (Raharimahefa et al., 2014), Mazatzal/ Labradorian (1.7-1.6 Ga) (Van Schmus, 1993; Rivers, 1997), and Grenville (1.235-0.945 Ga) Orogenies (Bethune and Ty, 1997). In addition to the generation of an impact melt sheet, the impact event shocked, brecciated, and altered the target rocks. Collectively, these are termed the

footwall rocks. The Sudbury footwall consists of the Archean Cartier Granitoids and Levack Gneiss Complex in the north and the Paleoproterozoic metasedimentary and metavolcanic Huronian Supergroup in the northeast and south (Fig. 3-1) (Ames et al., 2008). Associated with the SIC and related to the Sudbury impact are the pseudotachylitic Sudbury Breccia, which occurs in the footwall, and the Onaping Formation, which overlies the SIC (Grieve, 1994; Thompson and Spray, 1994; Spray and Thompson, 1995; Thompson and Spray, 1996; Grieve et al., 2010; O'Callaghan et al., 2016).

Stratigraphically, the “Main Mass” of the SIC can be divided into four main units, from top to bottom, Upper Contact Unit, Granophyre, Quartz Gabbro, Norite, and Sublayer (Dickin et al., 1996; Lightfoot, Keays, et al., 1997a; Anders et al., 2015). The Upper Contact Unit, previously referred to as the Basal Onaping Intrusion, is interpreted to represent the roof rocks of the impact melt sheet (Anders et al., 2015). The Granophyre, Quartz Gabbro, and Norite were generated from the differentiation of the Sudbury melt sheet, while the Sublayer was generated from the heating and assimilation of target material by the superheated (~2000 °C or greater) Sudbury melt sheet (Dickin et al., 1996; Lightfoot, Keays, et al., 1997b; Zieg and Marsh, 2005). Several mechanisms have been proposed for the differentiation of the Sudbury melt sheet of the Sudbury impact melt sheet into the present-day Main Mass. Simple fractional crystallization of the melt was initially proposed by Naldrett et al. (1970). Crystal-liquid differentiation whereby cumulus minerals settled and accumulated at the base of the melt sheet to create the Norite and Quartz Gabbro units. (Lightfoot et al., 1997a). Crystallization of a density stratified melt, thereby forming the Norite and Granophyre units (Golightly, 1994; Lightfoot et al., 2001a; Farrow and Lightfoot, 2002; Keays and Lightfoot, 2004). Differentiation of a viscous emulsion where initially two immiscible melts formed in the melt sheet; these melts then coalesced and separated due to immiscibility into two melts forming the Norite and Granophyre (Zieg and Marsh, 2005).

The Offset Dikes are a series of concentric, radial, and discontinuous dikes generated from melt derived from the SIC (Lightfoot et al., 1997), comparable to the granophyre dikes seen at the Vredefort impact structure in South Africa (Dietz, 1961). The name is

derived from offsets of the dikes on the metre to kilometre scale perpendicular to strike. Lithologically (Fig. 3-2), the Offset Dikes range in composition from quartz monzodioritic, granodioritic, to tonalitic (Wood and Spray, 1998a; Lightfoot et al., 2001b). Historically the Offset Dikes have been referred to as quartz diorite, and for consistency will be referred to as quartz diorite. Within the Offset Dikes the quartz diorite is mainly divided into two different lithologies, an inclusion-rich quartz diorite phase (IQD), and an inclusion-poor quartz diorite phase (QD). Inclusions found within the IQD range from Footwall material of the Levack Gneiss Complex, Cartier Granitoid, Huroinian Supergroup, and ultramafic clasts. Clasts of crystallized QD have also been observed within the IQD. Several mechanisms have been proposed for the emplacement of the Offset Dikes. Flow differentiation whereby inclusions were moved inward resulting in IQD at the core of the dikes and QD outward along the margins (Cochrane 1984; Grant and Bite 1984; Prevec et al. 2000). Or that the QD and IQD were emplaced by multiple injections of material (Rickard and Watkinson 2001; Lightfoot and Farrow 2002; Murphy and Spray 2002; Scott and Benn 2002; Hecht et al. 2008)

The Offset Dikes are considered to have been derived from the undifferentiated impact melt sheet of the Sudbury Impact structure (Lightfoot et al., 1997a). U-Pb zircon ages from the Hess Offset Dike of 1849.1 ± 0.9 Ma (Bleeker et al., 2014), Copper Cliff Offset Dike of 1849.8 ± 2 Ma (Corfu and Lightfoot, 1996), and zircon and baddelyite ages from Foy of $1852 \pm 4/-3$ Ma (Osterman et al., 1996) are identical with the 1.85 Ga age of the impact (Davis, 2008). These geochronology analyses have established the timing of Offset Dike emplacement as being approximately coeval with the impact event. Additional geochemical analyses of elemental abundances support Offset Dike were emplacement shortly after impact (Tuchscherer and Spray, 2002). There is however disagreement as to when specifically they were emplaced. Arguments have been made for emplacement during the modification stage (Wood and Spray, 1998b; Tuchscherer and Spray, 2002), during the excavation stage of impact (Murphy and Spray, 2002), and between 1-10 Ky post-impact (Hecht et al., 2008) have been proposed. There is additional debate about the emplacement mechanisms of the Offset Dikes; whether multiple injections of material (Morris and Pay, 1981; Murphy and Spray, 2002; Klimesch et al., 2015) or a single injection of material (Pilles et al., 2017).

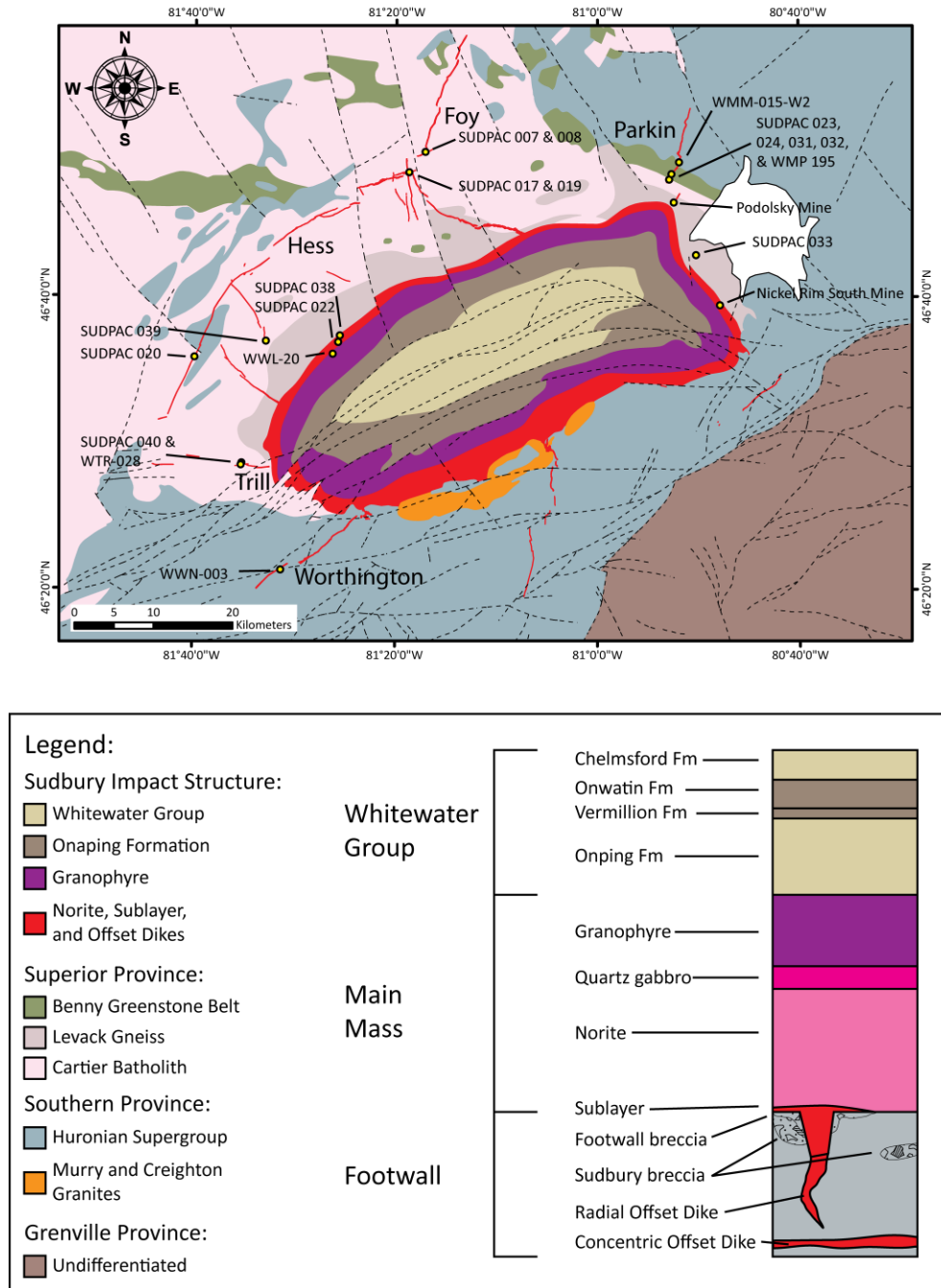


Figure 3-1: Geologic map of the Sudbury Igneous Complex and surrounding Superior Province and Huronian footwall rocks along with the post-impact Whitewater Group. From OGS bedrock regional 1:250,000 scale and internal Wallbridge Mining Company Limited maps. Sample numbers and locations are displayed as yellow dots. Also displayed is a schematic cross section of the rock units associated with the Sudbury impact structure after Ames et al. (2008).

3.3 Samples

Of the eighteen known Offset Dikes, samples were collected from five: Foy, Hess, Parkin, Trill, and Worthington (Fig. 3-1). The Offset Dikes of the North Range were the focus of sampling efforts, to avoid the more complex geological relationships of the South Range. Samples from the North Range were not metamorphosed to the same degree as the South Range, and are more likely to contain the primary signature of the Offset Dikes. Samples of IQD (Figs. 3-2 A,B) and QD (Figs. 3-2 C,D) were collected from each of the Offset Dikes listed above, along with massive sulfide mineralization hosted within the QD and IQD. In collaboration with Wallbridge Mining Company Limited, samples from the Foy, Hess, Parkin, and Trill offset Dikes were collected from outcrops on the company's property. Samples from Worthington, Parkin, and Trill were collected from drill core provided by Wallbridge.

In addition to Offset Dike samples, samples were also collected of the SIC and footwall rocks. Samples of the Sublayer, Quartz Gabbro, and Granophyre samples were collected from drill core; additional Sublayer, Norite, and Granophyre samples were collected from publically accessible outcrop. Footwall rocks sampled include Granite from the Cartier Batholith, Archean mafic gneiss from the Frost Lake ultramafic body, Matachewan Basaltic Dike, and Huronian metavolcanic material that had been incorporated into the Parkin Offset Dike. Footwall rocks were sampled in order to constrain the various reservoirs of Cu and Ni that could have mixed with SIC derived melts. Samples of massive sulfide mineralization were collected from the Parkin and Trill Offsets, and Podolsky and Nickel Rim South mines. Deposit styles that were sampled include massive sulfide mineralization in the Offset Dikes and footwall-hosted mineralization. Massive sulfide samples included three samples from the Podolsky Mine (SUD P1, P2, and P3) and a sample from the Nickel Rim South Mine (Ni Rim South).

Surficial outcrop weathering is a concern with isotope systems such as O. Therefore, with one known and noted exception (SUDPAC 030) samples were selected which displayed minimal oxidation and weathering. Additionally, when examined under thin section sulfides samples, and sulfides within mineralized QD and IQD samples showed very little alteration.

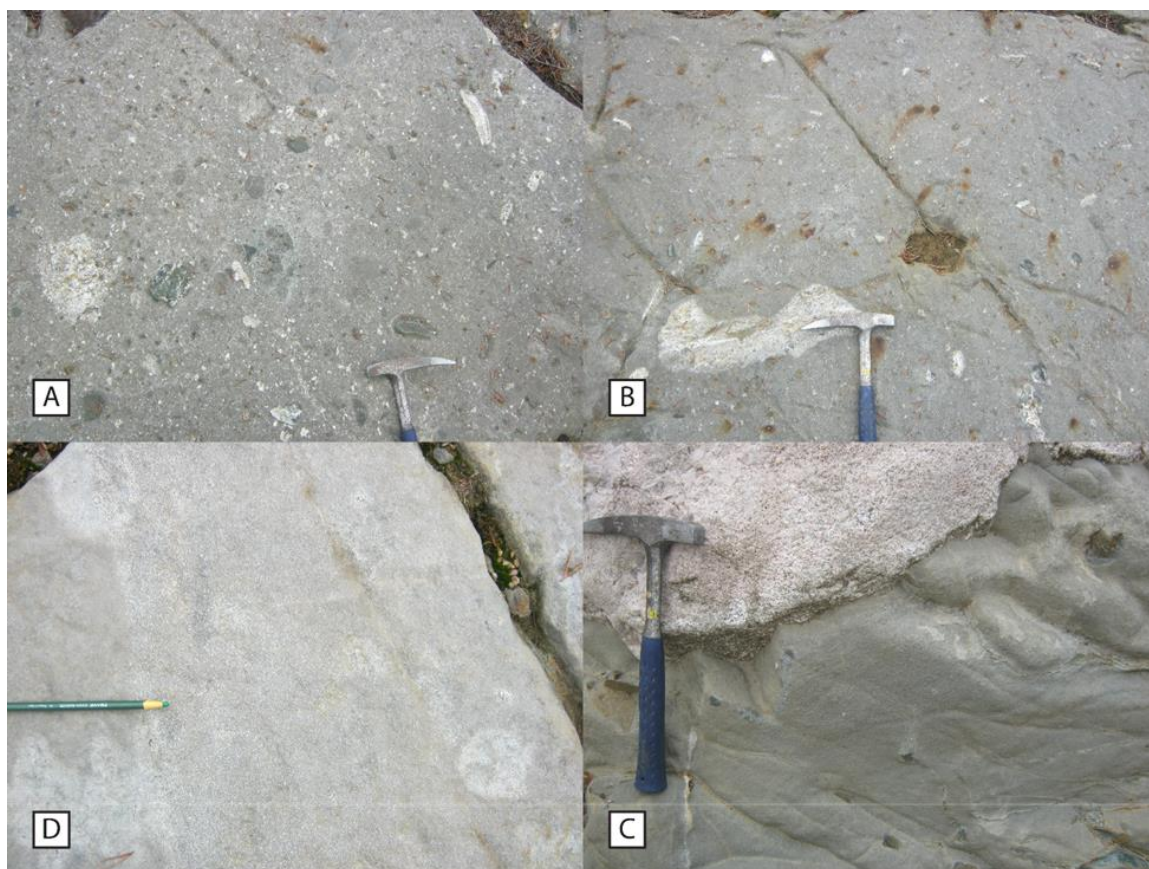


Figure 3-2: A) Outcrop of IQD from the Foy Offset containing clasts of felsic and mafic gneiss hammer for scale. B) Outcrop of IQD from the Foy Offset containing felsic and mafic gneiss along with disseminated blebs of sulfide mineralization hammer for scale. C) Outcrop of QD from the Hess Offset in contact with granite of the Cartier Batholith hammer for scale. D) Outcrop of QD from the Foy Offset with grease pencil for scale. Outcrops shown in A, B, and D are from a section of the Foy Offset north of the intersection between the Foy and Hess Offset Dikes. Outcrop shown in C is from the western section of the Hess Offset Dike where SUDPAC 020 was collected.

Cu, Fe, and Ni isotopes were selected as their isotopic compositions have been shown to vary with geological processes due to their multiple redox states or chemical bonding environment in materials even during high temperature processes (Teng et al., 2008; Dauphas et al., 2014; Dauphas et al., 2017 Elliott and Steele, 2017; Moynier et al., 2017).

A key goal of this study is the evaluation of sulfide petrogenesis and any magmatic and/or hydrothermal alteration afterwards. As these elements are also highly compatible in sulfide minerals, processes such as sulfide segregation within a melt; hydrothermal mobilization and alteration (Graham et al., 2004; Maher and Larson, 2007; Li et al., 2010; Mathur et al., 2012); and metal sourcing (Graham et al., 2004; Malitch et al., 2014; Ripley et al., 2015) within magmatic systems should be able to be recognized and evaluated. Additionally, redox processes and sulfide segregation also affect the isotopic ratios of silicates as heavier isotopes prefer the stronger bonds of higher redox states (Teng et al., 2008; Dauphas et al., 2014; Foden et al., 2015). For example, a systematic difference has been noted between silicate and sulfide isotopic ratios, thought to be the result of fractionation driven by the separation of sulfide from silicate melt (Zhu et al., 2002; Williams et al., 2006; Shahar et al., 2008; Williams and Archer, 2011; Zhao et al., 2017). While many of these processes happen in concert with one another, Hofmann et al. (2014) demonstrated that it is possible to peer-through multiple events by evaluating multiple isotopic system, and coupling these analyses with petrographic analyses. For further details see Chapter 1.1.

3.4 Analytical Methods

The geochemical and isotopic analyses performed by this study required that samples be dissolved prior to analyses and elemental extraction and purification procedures. To facilitate this, collected samples were crushed and powdered prior to sample dissolution. Nitric and hydrochloric acids used were prepared in PFA sub-boiling distillation stills. Other reagents such as hydrofluoric acid, hydrogen peroxide, perchloric acid, acetic acid or acetone were purchased at ultra-trace metal level grade (ppt levels for Ni, Cu and Fe). MQ water used for acid preparation and column chemistry was 18.2 m Ω grade (Millipore®, USA). All geochemical procedures were performed at the GEOMETRIC lab at the University of Western Ontario. Elemental concentration analyses were conducted using a Thermo Scientific iCAP Q Inductively Coupled Plasma Mass Spectrometer (ICP-MS) equipped with helium collision cell. Hand samples of the sampled lithologies were crushed, powdered, and weighed out into pre-cleaned Savillex® PFA Teflon beakers. Silicate samples were dissolved in HNO₃ and HF for two days at

120°C followed by treatment in HClO₄. Massive sulfide samples were dissolved in aqua regia at a 1:3 molar ratio of HNO₃ and HCl also at 120°C. After dissolution, samples were brought up in 6M HCl, and centrifuged; silicate samples were treated with H₂O₂ along with the 6M HCl. Beakers were cleaned in a 50% HNO₃ bath, rinsed with MQ water, dried, and fluxed individually in 6M HCl.

For elemental purification, three protocols of ion exchange column chemistries were used, one for the separation of Fe and Cu and two for the separation of Ni (detailed in Chapter 2). The Fe and Cu chemistry (Table 3-1) was based on the column separation procedure outlined by Chapman et al. (2006), modified from Maréchal et al. (1999). The Ni chemistry (Table 3-2) was based on the method described by Wasylenki et al. (2015). In summary, Cu and Fe were separated using MP-1a anion resin in 7M and 2M HCl respectively (Fig. 2-1). Ni was separated using AG50W-X8 resin across two columns. The first step procedure was used to separate Fe from matrix elements using acetone and HCl, while the second column separates cations such as Mg and Na using acetic acid and HCl (Fig. 2-3). See Tables 3-1 and 3-2 for detailed protocols. Total analytical blanks were for Cu, Fe and Ni respectively which was negligible (<<1%) compared to the total amounts of metals processed.

3.4.1 Mass Spectroscopy

Cu isotope ratios were measured using a Nu Instrument Plasma II and Thermo Neptune multi-collector inductively coupled plasma mass spectrometer (MC-ICP-MS) at the Trent University Water Quality Centre. Sample introduction was achieved using a CETAC Aridus II (NuPlasma II) or ApexQ (Neptune) desolvating nebulizer and PFA nebulizer. Standard sample bracketing was used to monitor and correct for instrumental mass bias, with samples and standards run as one block of 25 measurements, with 40s wash-out with 2% nitric acid and 40s transfer time in between. ⁶⁵Cu was measured on H4 and ⁶³Cu was measured on L2 Faraday cups at a typical intensity of ~5-15v for 50-100 ppb Cu in solution. Samples were diluted to match the concentration of the standard within 10-15%. Each standard sample bracket was performed three times, sample error is reported as twice the standard deviation of the bracketed measurements; average error for δ⁶⁵Cu was 0.05‰. NIST SRM 976 with defines zero per mill δ⁶⁵Cu (Eq. 1-3 & 1-4) was used as the

standard bracketing material; Cu isotope ratios are reported as $\delta^{65}\text{Cu}$ (NIST SRM 976) per mil (‰). The georeference standards SU-1 and BIR-1 were analyzed to evaluate column separation procedures. Triplicate analyses of SU-1 on the Nu Plasma II and Neptune resulted in an average value of $-0.07 \pm 0.08\text{‰}$; previously reported values are $-0.02 \pm 0.08\text{‰}$ (2SE) (Chapman et al., 2006) and $-0.09 \pm 0.09\text{‰}$ (2SD) (Ripley et al., 2015). A single analysis of BIR-1 gave a value of $0.05 \pm 0.16\text{‰}$; the recommended value of BIR is $0.02 \pm 0.06\text{‰}$ (2SD) (Moynier et al., 2017).

Fe isotope ratios were measured using a Thermo Neptune MC-ICP-MS at the Trent University Water Quality Centre. Sample introduction was achieved using an ApexQ desolvating nebulizer and PFA nebulizer. Standard sample bracketing was used to monitor and correct for instrument mass bias. Sample and standard solution were analyzed at a concentration of 150-200ppb corresponding to an intensity of $\sim 15\text{-}20\text{V}$ on the ^{56}Fe cup. Samples were diluted to match the concentration of the standard within 10-15%. Each standard sample bracket was performed three times, sample error is reported as twice the standard deviation of the bracketed measurements; average error for $\delta^{56}\text{Fe}$ was 0.05‰ . IRMM-014 defines zero per mill $\delta^{56}\text{Fe}$ (Eq. 1-3 & 1-4), and was used as the standard bracketing material; Fe isotope ratios are reported as $\delta^{56}\text{Fe}$ (IRMM-014) per mil (‰). The georeference standards BCR-2 and BIR-1 were measured to ensure a sufficient removal of matrix elements, and that the column procedure was not fractionating isotopes on the column. Analyses of BCR-2 gave a result of $0.14 \pm 0.03\text{‰}$ and analyses of BIR-1 gave a result of $0.03 \pm 0.06\text{‰}$; recommended values from Craddock and Dauphas (2010) are $0.09 \pm 0.01\text{‰}$ and $0.05 \pm 0.02\text{‰}$ for BCR-2 and BIR-1 respectively. Error given for both measurements represent 95% confidence intervals. Duplicate and triplicate analyses indicate uncertainty of $\sim 0.12\text{‰}$.

Ni isotopic analyses were conducted at the SESAME Laboratory at Indiana University using a Nu Plasma II MC-ICP-MS. Sample introduction was achieved using an Aridus II desolvating nebulizer. Standard sample bracketing was used to monitor and correct for instrument mass bias. Sample and standard solution were analyzed at a concentration of 300ppb corresponding to a total intensity of $\sim 5\text{V}$ for ^{58}Ni and ^{60}Ni . Samples were diluted to match the concentration of the standard within 10-15%. Each standard sample bracket

was performed three times, sample error is reported as twice the standard deviation of the bracketed measurements; average error for $\delta^{60}\text{Ni}$ was 0.09‰. NIST SRM 986 defines zero per mill $\delta^{60}\text{Ni}$ (Eq. 1-3 & 1-4), and was used as the standard bracketing material; Ni isotope ratios are reported as $\delta^{60}\text{Ni}$ (NIST SRM 986) per mil (‰). Both samples and bracketing standard were spiked with a ^{61}Ni and ^{62}Ni double spike which was used to correct for instrument-induced mass bias and column isotopic fractionation using double-spike equations according to methods described by Wasylenki et al., 2014. To ensure a sufficient removal of matrix elements, and that the column procedure was not fractionating Ni, the georeferenced standard BIR-1 was processed and measured. A value of $0.12 \pm 0.09\text{‰}$ was obtained which is in agreement with previously published values of $0.12 \pm 0.04\text{‰}$ (2SE) (Gueguen et al., 2013) and $0.19 \pm 0.07\text{‰}$ (2SD) (Chernonozhkin et al., 2015).

Elution Step	Cu and Fe Separation
1) Column Conditioning	6 mL 7M HCl
2) Sample Loading	1 mL 7M HCl
3) Matrix Elution	8 mL 7M HCl
4) Cu Elution	25 mL 7M HCl
5) Fe Elution	20 mL 2M HCl

Table 3-1: Column chemistry procedure for the separation of Cu and Fe from sample matrices on 2ml of AG-MP1 100-200 mesh in Biorad® poly-prep columns.

Elution Step	First Column	Second Column
1) Column Conditioning	Mixture of 3.2mL acetone and 0.8mL 10M HCl	mixture of 3.4mL acetic acid and 0.6mL 10M HCl
2) Sample Loading	Mixture of 0.8mL acetone and 0.2mL 10M HCl	Mixture of 0.8mL acetic acid and 0.2mL 10M HCl

3) Matrix Elution	Mixture of 4.8mL acetone and 1.2mL 10M HCl	N/A
4) Ni Elution	6mL 6M HCl	Mixture of 12.75mL acetic acid and 2.25 10M HCl

Table 3-2: Column chemistry procedure for the separation of Ni from sample matrices on 2ml of AG50W-X8, 200-400 mesh in Biorad® poly-prep columns.

3.4.2 Optical and Electron Microscopy Methods

Optical and electron microscopy analysis of thin sections and pucks was conducted at the Earth and Planetary Materials Analysis (EPMA) laboratory at the University of Western Ontario. Optical microscopy was conducted on polished one inch epoxy rounds and thin sections in both reflected and transmitted light using a Nikon Eclipse LV100 POL. Energy dispersive x-ray spectroscopy (EDS) and wave length dispersive x-ray spectroscopy (WDS) measurements were conducted using the JEOL JXA-8530F field emission electron microprobe. Samples were polished one inch epoxy rounds and thin sections which had been carbon coated. Measurements consisted of single point spectra used to identify mineral phases, and compositional maps to identify the spatial distribution of specific elements and phases. Beam conditions during analyses were 15kV accelerating voltage and 100-200nA beam current for WDS and EDS analyses. For composition maps, pixel spacing ranged from 4-6µm depending on the scale of the analysis. A suite of minerals of known composition were used as standards for WDS analysis.

3.5 Results

Results of optical and electron microscopy analyses are given below. In addition, Fe, Cu, and Ni isotopic measurements of Sudbury Offset Dikes and associated rocks and ores are given in tables below. Additional geochemical analyses of elemental abundances are reported in Appendix A and B.

3.5.1 Petrographic, EDS, and WDS Data

Thin sections and epoxy pucks were analyzed by optical and electron microscopes to identify sulfide phases and textures within samples prepared for isotopic analysis.

From these analyses, textures, accessory phases, and sulfide mineral assemblages were identified within the samples analyzed. Two different sulfide mineral assemblages were observed within the Offset Dikes. Within the QD and the IQD, sulfides are present as disseminated blebs of sulfide dominated by pyrite with associated chalcopyrite, pentlandite, and magnetite. These disseminated blebs typically make up no more than 10% of a QD or IQD sample. The massive sulfide ores hosted within the Offset Dikes contain pyrite, chalcopyrite, pentlandite, pyrrhotite, and magnetite.

Several textures were observed optically. Pentlandite lamellae were observed within pyrite and pyrrhotite where present (Figs. 3-5A,B). Within the QD and IQD, pyrite occurs as large subhedral grains while chalcopyrite and pentlandite occur as anhedral grains surrounding the pyrite grains (Fig. 3-3D). Mineralization consisting solely of chalcopyrite is also observed. Magnetite occurs predominantly as rounded blebs within both the QD, IQD, and massive sulfide ore bodies (Figs. 3-3)

Using EDS and WDS measurements compositional textures were observed, and accessory phases identified. Accessory PGM phases were identified using EDS measurements, and predominantly occurred as PGE bismuth tellurides with some exceptions (e.g., sperrylite [PtAs₂]). Other accessory phases identified in the massive sulfides include galena, sphalerite, and native Sn. One sample from the Trill Offset (WTR-028) included Fluorite and several carbonate phases, including the REE bearing carbonate bastnäsite ([REE]CO₃F). WDS analyses revealed oscillatory zonation of Co within pyrites in one sample from the Trill Offset (WTR-028) (Fig. 3-4), and Co enrichment in pyrite in another sample from the Trill Offset (SUD 040) (Fig. 3-5C). This is in contrast to disseminated blebby sulfides analyzed from QD collected from the intersection of the Foy and Hess Offsets (SUD 017) (Figs. 3-5A,B).

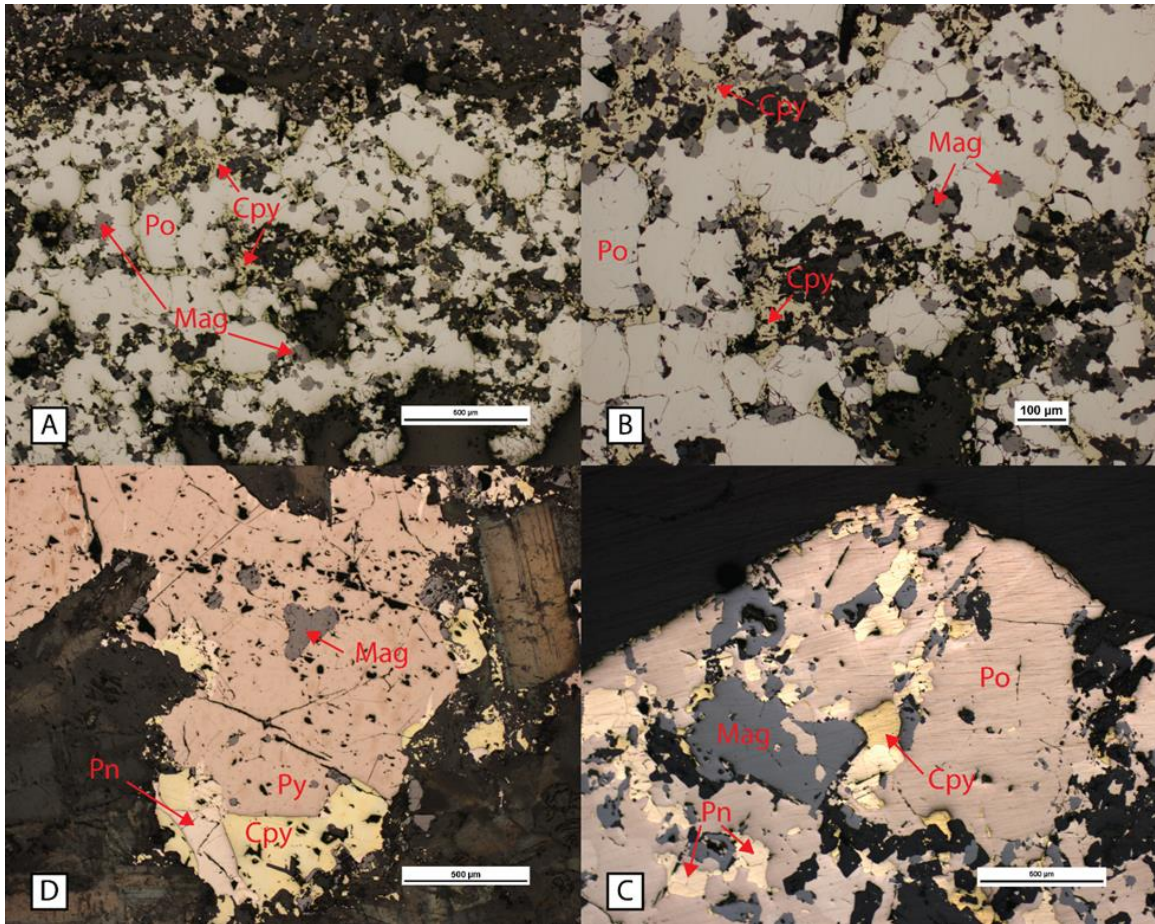


Figure 3-3: Photomicrographs showing the two styles of sulfide mineralization seen within the Offset Dikes. A,B, and C) massive sulfide mineralization consisting of pyrrhotite, pyrite, chalcopyrite, pentlandite, and magnetite from the Trill Offset (SUD 040 [A,B]) and Parkin Offset (WMM-015-W2 [C]). D) disseminated blebby sulfide mineralization from the intersection of the Foy and Hess Offsets (SUD 017).

Abbreviations are as follows: Cpy – chalcopyrite, Mag – magnetite, Pn – pentlandite, Po – pyrrhotite, and Py – pyrite.

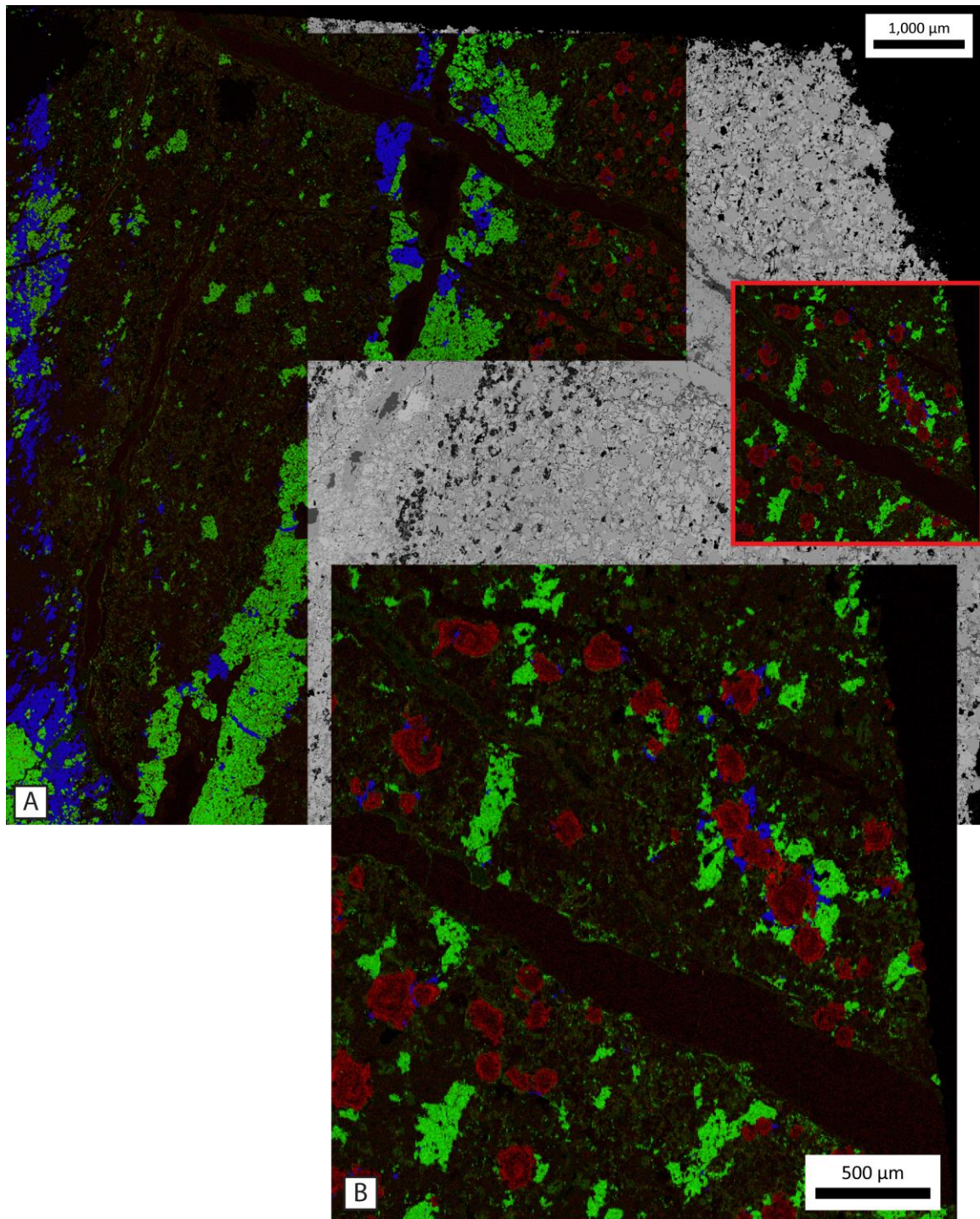


Figure 3-4: A) Composition maps of CoNiCu (RGB) of massive sulfide ore from the Trill Offset (WTR-028). Enlarged area highlighted in red. B) Enlargement displaying oscillatory zonation of Co within pyrite grains in red.

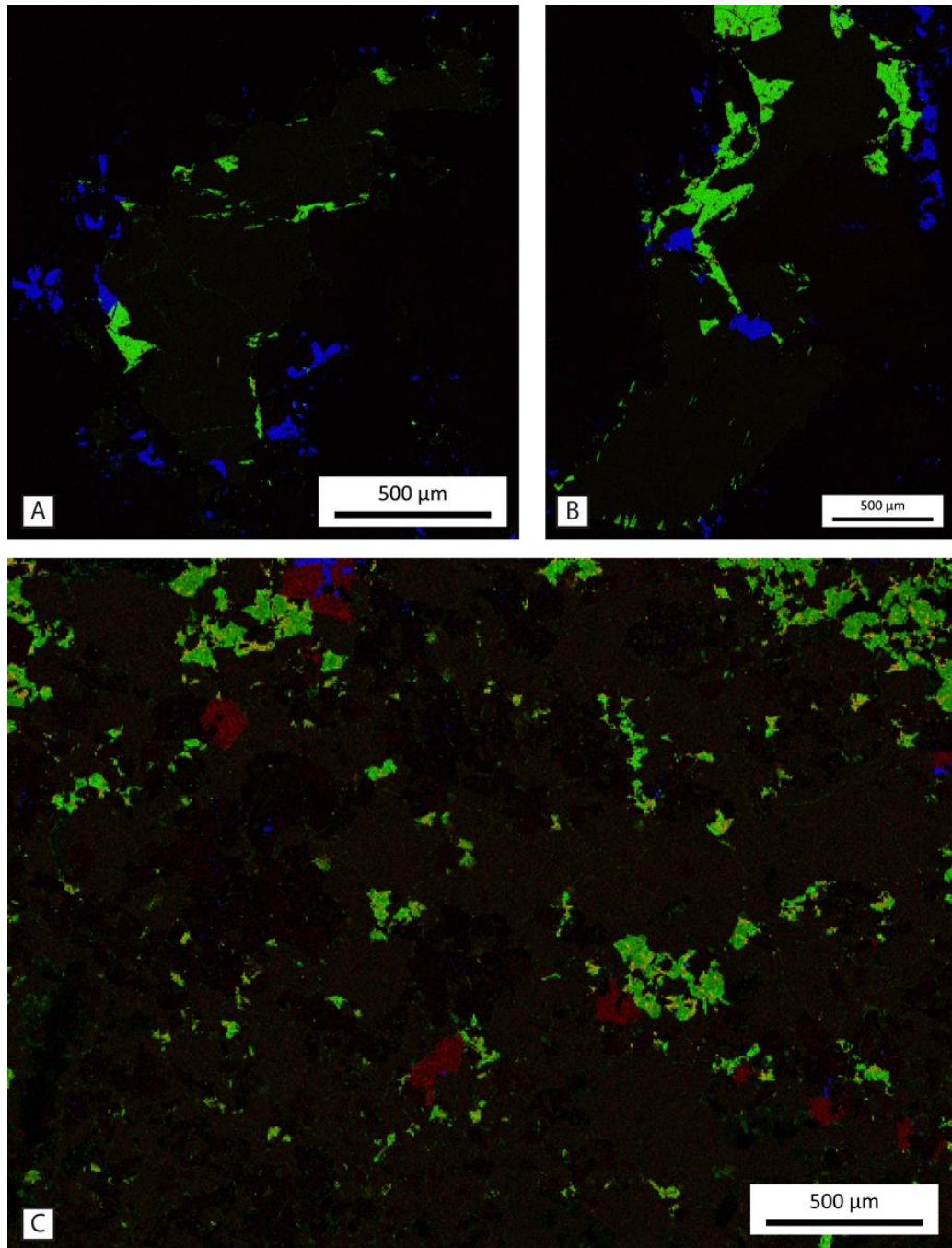


Figure 3-5: A,B) Composition map of CoNiCu (RGB) of a bleb of disseminated sulfide from sample SUD 017 displaying a lack of Co zonation or enrichment. Optical photomicrograph of the sample shown in Fig. 3-5D. C) Composition map of CoNiCu (RGB) of massive sulfide ore from the Trill Offset (SUD 040). Co enrichment is displayed within the pyrites in red. Optical photomicrograph of the sample shown in Fig. 3-5A,B.

3.5.2 Isotopic Results

The results from the measurement of Fe, Cu, and Ni isotopes are given in Tables 3-3, 3-4, and 3-5. Cu isotopic values display the greatest amount of variability with a range of values measured from $-0.97 \pm 0.03\text{‰}$ to $1.05 \pm 0.15\text{‰}$ $\delta^{65}\text{Cu}$; Fe displays a range from $-0.16 \pm 0.03\text{‰}$ to $0.45 \pm 0.02\text{‰}$ $\delta^{56}\text{Fe}$; and Ni displays a range from $0.41 \pm 0.06\text{‰}$ to $-1.69 \pm 0.07\text{‰}$ $\delta^{60}\text{Ni}$.

The QD, IQD, Main Mass (with the exception of the Sublayer), and target rocks all display a self-consistent Cu, and Ni isotopic composition (0.18 to -0.23‰), while Fe values form a tighter range (0.06 to -0.04‰). Some exceptions are the only silicate samples that display significant variation in Cu and Ni values are a sample of the Sublayer (WWL-20 1299m), and SUD 032, a sample of IQD from the Parkin Offset Dike (Tables 3-3 and 4). A simple linear regression and t-test of the correlation of the Fe, Ni, and Cu elemental abundance of a sample against their respective $\delta^{56}\text{Fe}$, $\delta^{60}\text{Ni}$, and $\delta^{65}\text{Cu}$ ratio was performed to evaluate the influence of elemental abundance on the measured isotopic ratios (Table 3-6). While moderately significant p-values are obtained with regard to Fe and Cu within the sulfide samples, the R^2 show only a moderate correlation. Coupled with a low sample size ($n=7$ in both cases), there appears to be little significant correlation between the amount of sulfide within the silicate samples and the isotopic ratios measured. In contrast to the silicate samples, eight samples of massive sulfide, however, display large variations in $\delta^{56}\text{Fe}$, $\delta^{60}\text{Ni}$, and $\delta^{65}\text{Cu}$, in contrast to the silicate QD, IQD, Main Mass, and country rocks (Fig. 3-6). Massive sulfide samples display a total variation of approximately 2‰ $\delta^{65}\text{Cu}$, approximately 0.3‰ $\delta^{60}\text{Ni}$, and approximately 0.5‰ $\delta^{56}\text{Fe}$. Large variations are also seen in measured values from massive sulfide ores within the same offset dike as seen in samples from the Trill and Parkin Offsets. Plots of the $\delta^{56}\text{Fe}$ and $\delta^{60}\text{Ni}$ compositions of the samples against their $\delta^{65}\text{Cu}$ ratio were also generated (Fig 3-7). A simple linear regression was performed on all points of the $\delta^{60}\text{Ni}$ vs $\delta^{65}\text{Cu}$ (excepting outliers WWL-20-1299 and SUDPAC 032), the resulting line is termed the Sudbury Fractionation Line (SFL). WWL-20-1299 was excluded due to significant alteration seen within the thin section. Due to its anomalous isotopic composition, it appears this alteration has changed its isotopic composition.

Sample Name	Lithology	Location	$\delta^{65}\text{Cu}$ (‰)	2SD	Cu Wt. %	Number of Analyses
<i>Offset Dikes</i>						
SUD PAC 007	QD	Foy Offset	0.11	0.03	0.007491	1
SUD PAC 008	IQD	Foy Offset	0.05	0.03	0.007136	1
SUD PAC 017	QD	Foy/Hess Intersection	0.12	0.07	0.217505	1
SUD PAC 019	IQD	Foy/Hess Intersection	n.a	n.a.	0.004536	n.a.
SUD PAC 020	QD	Hess Offset	-0.05	0.08	0.007849	1
SUD PAC 023	QD	Parkin Offset	0.17	0.09	0.009702	1
SUD PAC 024	IQD	Parkin Offset	0.00	0.01	0.091287	1
SUD PAC 031	Mafic meta-volcanic	Parkin Offset	-0.06	0.04	0.013152	1
SUD PAC 032	IQD	Parkin Offset	0.95	0.15	0.068127	1
WMP-195 60m	IQD	Parkin Offset	-0.10	0.04	0.822315	1
WWN-003 280m	QD	Worthington Offset	0.01	0.01	0.016270	1
WWN-003 287m	IQD	Worthington Offset	-0.05	0.01	0.008666	1
<i>Sulfide Ores</i>						
SUD PAC 030	Massive Sulfide	Parkin Offset	-0.97	0.03	0.73	2
SUD PAC 040	Massive Sulfide	Trill Offset	-0.79	0.05	0.64	2
Ni Rim	Massive Sulfide	Nickel Rim South Mine	1.05	0.00	52.47	2
SUD PAC P1	Massive Sulfide	Podolsky Mine	-0.51	0.03	0.09	2
SUD PAC P2	Massive Sulfide	Podolsky Mine	0.67	0.01	35.91	2
SUD PAC P3	Massive Sulfide	Podolsky Mine	-0.08	0.03	30.08	2
WMM-015-W2 1477m	Massive Sulfide	Parkin Offset	-0.31	0.09	0.72	2
WTR-028 29m	Massive Sulfide	Trill Offset	-0.24	0.01	1.53	2
<i>SIC Main Mass</i>						
WWL-20 101.5m	Granophyre	Windy Lake Core	0.03	0.01	0.001676	1
SUD PAC 022	Felsic Norite	Rt. 144 Road Cut	0.10	0.26	0.001722	1
SUD PAC 038	Sublayer	Onaping Dump	0.22	0.02	0.021687	1
WWL-20 1299m	Sublayer	Windy Lake Core	-0.92	0.01	0.008957	1
<i>Target Rocks</i>						
SUD PAC 033	Pyroxenite	Frost Lake	0.00	0.03	0.008611	1
SUD PAC 039	Matachawan Basalt	Cascaden Township	0.11	0.06	0.026336	1

Table 3-3: Table of $\delta^{65}\text{Cu}$ values, Cu concentrations, and number of analyses of Offset Dikes, Sulfide Ores, SIC Main Mass, and Target Rocks from the Sudbury impact structure.

Sample Name	Lithology	Location	$\delta^{56}\text{Fe}$ (‰)	2SD	Fe Wt. %	Number of Analyses
<i>Offset Dikes</i>						
SUD PAC 007	QD	Foy Offset	0.01	0.06	5.21	1
SUD PAC 008	IQD	Foy Offset	-0.01	0.03	4.90	1
SUD PAC 017	QD	Foy/Hess Intersection	-0.02	0.05	7.77	1
SUD PAC 019	IQD	Foy/Hess Intersection	0.05	0.06	5.42	1
SUD PAC 020	QD	Hess Offset	-0.04	0.06	5.34	1
SUD PAC 023	QD	Parkin Offset	n.a.	n.a.	4.40	n.a.
SUD PAC 024	IQD	Parkin Offset	0.07	0.03	6.35	1
SUD PAC 031	Mafic meta-volcanic	Parkin Offset	n.a.	n.a.	9.47	n.a.
SUD PAC 032	IQD	Parkin Offset	n.a.	n.a.	2.66	n.a.
WMP-195 60m	IQD	Parkin Offset	n.a.	n.a.	8.41	n.a.
WWN-003 280m	QD	Worthington Offset	0.03	0.03	6.11	1
WWN-003 287m	IQD	Worthington Offset	0.06	0.04	5.56	1
<i>Sulfide Ores</i>						
SUD PAC 030	Massive Sulfide	Parkin Offset	n.a.	n.a.	37.06	n.a.
SUD PAC 040	Massive Sulfide	Trill Offset	-0.16	0.03	49.42	1
Ni Rim	Massive Sulfide	Nickel Rim South Mine	0.01	0.03	47.97	1
SUD PAC P1	Massive Sulfide	Podolsky Mine	-0.10	0.06	52.65	1
SUD PAC P2	Massive Sulfide	Podolsky Mine	0.41	0.03	27.19	1
SUD PAC P3	Massive Sulfide	Podolsky Mine	0.45	0.02	24.95	1
WMM-015-W2 1477m	Massive Sulfide	Parkin Offset	0.10	0.05	46.19	1
WTR-028 29m	Massive Sulfide	Trill Offset	0.23	0.06	38.59	1
<i>SIC Main Mass</i>						
WWL-20 101.5m	Granophyre	Windy Lake Core	n.a.	n.a.	6.02	n.a.
SUD PAC 022	Felsic Norite	Rt. 144 Road Cut	0.01	0.08	4.92	1
SUD PAC 038	Sublayer	Onaping Dump	n.a.	n.a.	9.15	n.a.
WWL-20 1299m	Sublayer	Windy Lake Core	n.a.	n.a.	5.36	n.a.
<i>Target Rocks</i>						
SUD PAC 033	Pyroxenite	Frost Lake	n.a.	n.a.	8.51	n.a.
SUD PAC 039	Matachawan Basalt	Cascaden Township	n.a.	n.a.	11.08	n.a.

Table 3-4: Table of $\delta^{54}\text{Fe}$ values, Fe concentrations, and number of analyses of Offset Dikes, Sulfide Ores, SIC Main Mass, and Target Rocks from the Sudbury impact structure.

Sample Name	Lithology	Location	$\delta^{60}\text{Ni}$ (‰)	2SD	Ni Wt. %	Number of Analyses
<i>Offset Dikes</i>						
SUD PAC 007	QD	Foy Offset	-0.14	0.25	0.006902	1
SUD PAC 008	IQD	Foy Offset	0.11	0.11	0.011967	1
SUD PAC 017	QD	Foy/Hess Intersection	0.17	0.08	0.186395	1
SUD PAC 019	IQD	Foy/Hess Intersection	-0.25	0.18	0.007267	1
SUD PAC 020	QD	Hess Offset	0.11	0.10	0.010918	1
SUD PAC 023	QD	Parkin Offset	n.a.	n.a.	0.006388	n.a.
SUD PAC 024	IQD	Parkin Offset	0.15	0.01	0.064863	1
SUD PAC 031	Mafic meta-volcanic	Parkin Offset	n.a.	n.a.	0.007399	n.a.
SUD PAC 032	IQD	Parkin Offset	0.18	0.05	0.019786	1
WMP-195 60m	IQD	Parkin Offset	0.03	0.06	0.100360	1
WWN-003 280m	QD	Worthington Offset	n.a.	n.a.	0.011586	n.a.
WWN-003 287m	IQD	Worthington Offset	-0.23	0.07	0.019837	1
<i>Sulfide Ores</i>						
SUD PAC 030	Massive Sulfide	Parkin Offset	n.a.	n.a.	3.90	n.a.
SUD PAC 040	Massive Sulfide	Trill Offset	-0.39	0.08	4.32	1
Ni Rim	Massive Sulfide	Nickel Rim South Mine	n.a.	n.a.	1.22	n.a.
SUD PAC P1	Massive Sulfide	Podolsky Mine	n.a.	n.a.	5.55	n.a.
SUD PAC P2	Massive Sulfide	Podolsky Mine	n.a.	n.a.	0.05	n.a.
SUD PAC P3	Massive Sulfide	Podolsky Mine	n.a.	n.a.	0.08	n.a.
WMM-015-W2 1477m	Massive Sulfide	Parkin Offset	-0.15	0.05	4.99	1
WTR-028 29m	Massive Sulfide	Trill Offset	-0.06	0.04	4.42	1
<i>SIC Main Mass</i>						
WWL-20 101.5m	Granophyre	Windy Lake Core	n.a.	n.a.	0.002261	n.a.
SUD PAC 022	Felsic Norite	Rt. 144 Road Cut	n.a.	n.a.	0.001427	n.a.
SUD PAC 038	Sublayer	Onaping Dump	0.41	0.06	0.051476	1
WWL-20 1299m	Sublayer	Windy Lake Core	-1.69	0.07	0.011081	1
<i>Target Rocks</i>						
SUD PAC 033	Pyroxenite	Frost Lake	n.a.	n.a.	0.038470	n.a.
SUD PAC 039	Matachawan Basalt	Cascaden Township	n.a.	n.a.	0.006054	n.a.

Table 3-5: Table of $\delta^{60}\text{Ni}$ values, Ni concentrations, and number of analyses of Offset Dikes, Sulfide Ores, SIC Main Mass, and Target Rocks from the Sudbury impact structure.

Element	Lithology	R ²	P-value	Number of Samples
Fe	Sulfides	0.731	0.014	7
	Silicates	1.54×10^{-3}	0.920	9
	All Samples	1.14×10^{-5}	0.990	16
Ni	Sulfides	0.151	0.75	3
	Silicate	0.129	0.31	10
	All Samples	4.87×10^{-3}	0.81	14
Cu	Sulfides	0.680	0.022	7
	Silicates	1.54×10^{-3}	0.881	17
	All Samples	0.07	0.211	24

Table 3-6: Table of R² and P-values obtained from performing a simple linear regression of the listed elements abundance against the isotopic ratio of a given sample (e.g. $\delta^{54}\text{Fe}$ against Fe elemental abundance). The given P-values indicate that the only statistically significant results are the moderate correlations between the concentration of Fe and Cu within the sulfides and their corresponding isotopic compositions. All simple linear regressions performed in ioGAS.

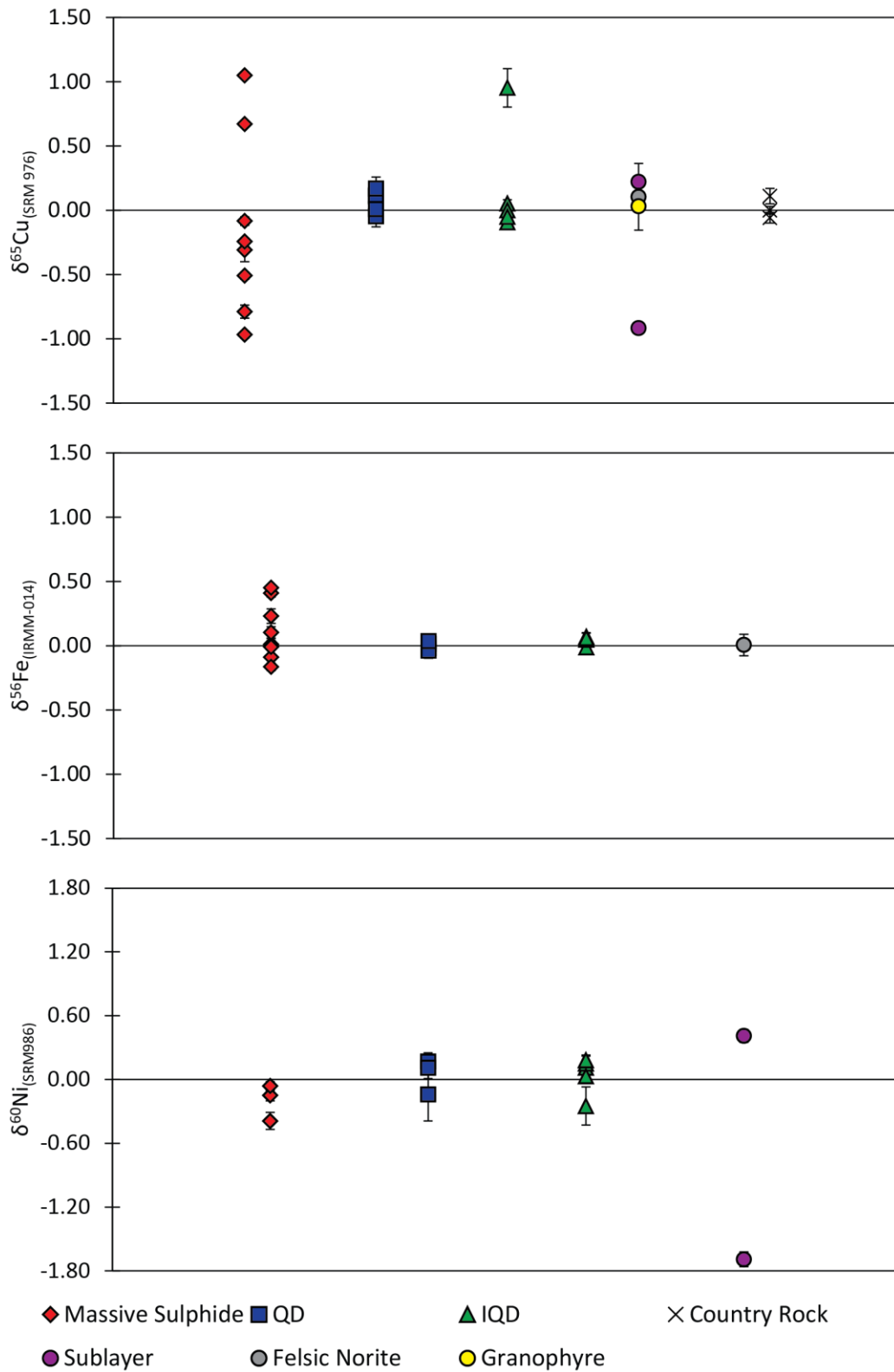


Figure 3-6: Graphs displaying the distribution of $\delta^{65}\text{Cu}$, $\delta^{56}\text{Fe}$, and $\delta^{60}\text{Ni}$ values measured for each lithology sampled. Error bars given as 2SD.

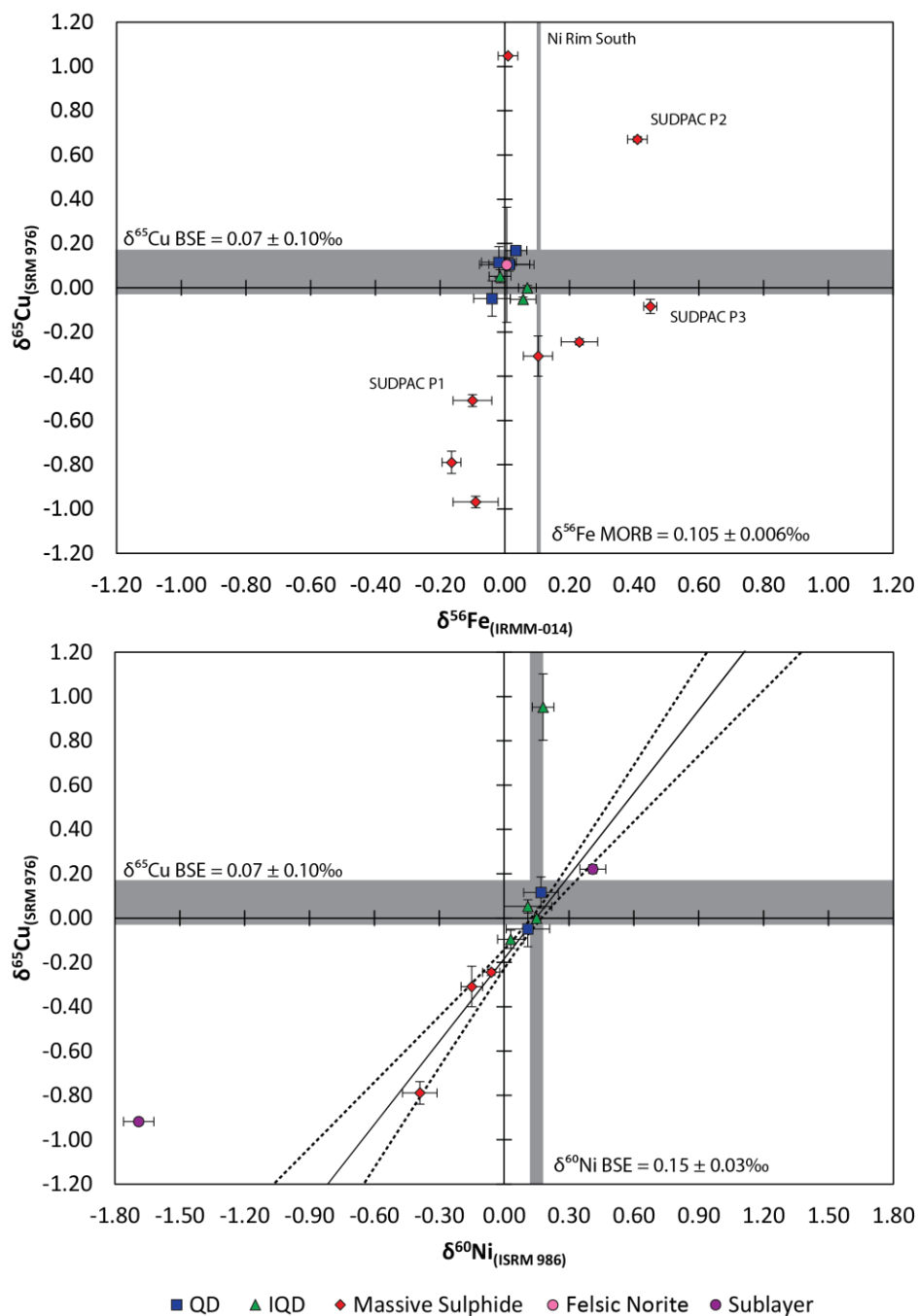


Figure 3-7: Plot of $\delta^{65}\text{Cu}$ values against $\delta^{56}\text{Fe}$ values (top) and $\delta^{65}\text{Cu}$ values against $\delta^{60}\text{Ni}$ values (bottom) measured for each sample along with basic sample description with some specific samples labelled. Gray bars correspond to Bulk Silicate Earth (BSE) values for $\delta^{65}\text{Cu}$ and $\delta^{60}\text{Ni}$, and MORB values for $\delta^{56}\text{Fe}$. The black line is a linear regression of Sublayer, QD, IQD, and massive sulfide isotopic compositions, and defined as $\delta^{65}\text{Cu} = 1.24 * \delta^{60}\text{Ni} - 0.19$ with an R^2 of 0.93. Dashed lines represent a 95% confidence envelope.

3.6 Discussion

3.6.1 Isotopic Variations in Offset Dikes, Main Mass, and Country Rocks

The $\delta^{65}\text{Cu}$ signature of a majority of the Offset Dike, Main Mass, and Country rock samples is very similar to that of the Bulk Silicate Earth (BSE) value of $\delta^{65}\text{Cu}_{\text{BSE}} = 0.07 \pm 0.10\text{‰}$ (Savage et al., 2015) (Fig. 3-7). While the $\delta^{56}\text{Fe}$ signature of the Offset Dikes (i.e., IQD and QD) is much closer to zero, similar to the BSE composition estimated from chondrites and terrestrial peridotites at $\delta^{56}\text{Fe} = 0.025 \pm 0.025\%$ (Dauphas et al., 2009; Craddock and Dauphas, 2010; Craddock et al., 2013), but below the $\delta^{56}\text{Fe}$ for MORBs ($\delta^{56}\text{Fe}_{\text{MORB}} = 0.105 \pm 0.006\text{‰}$) (Teng et al., 2013) and average continental crust value of $\delta^{57}\text{Fe} = 0.10 \pm 0.03\text{‰}$ (Poitrasson et al., 2006). The $\delta^{60}\text{Ni}$ signature of the QD and IQD samples show a similarity to BSE values ($\delta^{60}\text{Ni}_{\text{BSE}} = 0.15 \pm 0.03\text{‰}$) (Cameron et al., 2009; Gueguen et al., 2013; Chernonozhkin et al., 2015), while the Sublayer displays significant fractionation relative to the BSE (Fig. 3-7). Estimating the initial isotopic composition of the Sudbury impact melt sheet is difficult due to the variety of lithologies melted by the impact process. Significant contribution from the impactor to the composition of the melt sheet is not likely, due to the relatively small volume of the impactor relative to the melt sheet. Previous work has ruled out any mantle contribution to the Sudbury melt sheet (Dickin et al., 1996; Morgan et al., 2002). Lightfoot et al. (1997) found that a maximum of 20% mantle contribution could be incorporated into the SIC; however, this contribution is not required to explain the geochemistry of the SIC (Lightfoot et al., 2001b). The SIC has generally been accepted to be a crustal melt (Darling et al., 2010), with no strong evidence to support a mantle input. Indeed, mixing between Superior Province gneisses and Huronian Supergroup sequences with the addition of mafic material from the Nipissing was suggested to explain the geochemical and Pb, Sr-Nd, and Os isotopic variations within the SIC (Darling et al., 2010). The data presented here show the SIC as having a Cu and Ni composition similar to that of the Bulk Silicate Earth (BSE) (Fig. 3-4). The Fe compositions measured however, are lighter than values previously measured for MORBs and continental crust; closer to peridotite values (Fig. 3-4).

A comparison of the felsic norite and granophyre units of the Main Mass to the Offset Dikes shows that the two display similar values (Fig 3-6). It is notable that the QD and IQD samples cluster together, this implies that there is little variability inter- or intra-dike, between QD and IQD, or North Range vs. South Range (Fig 3-6). Additionally, despite a variation in sulfide content of ~5-15%, the similar values shown by the QD and IQD (Fig 3-6) shows that the sulfide content does not significantly alter the isotopic composition of a sample (Table 3-6). A comparison of barren QD and IQD and samples containing disseminated sulfide mineralization display similar values, as all the QD and IQD samples cluster together. To determine whether the isotopically analyzed Cu is hosted within sulfides or silicates, Cu abundance measured by ICP-MS was compared against the estimated abundance of Cu in a sample based on hand sample and petrographic analyses. Assuming that ~10% of the sample mass of SUDPAC 017 (a QD sample with disseminated sulfide blebs) is made up of sulfide based on hand sample observation, and that ~10% of the sulfide is chalcopyrite based on thin section analysis at ~33.3 wt.% Cu gives a result of ~3 mg/g Cu in the sample. This is greater than the 2.175 mg/g of Cu measured in the sample by ICP-MS, but likely within error of the hand samples and petrographic based chalcopyrite abundance estimates. This basic analysis suggests that a large majority of the Cu measured in QD and IQD samples can be accounted for by the chalcopyrite present in the sample. This implies that the Cu and Ni compositions measured from bulk samples of QD and IQD both containing disseminated sulfides are representative of the sulfide phases rather than silicate phases such as micas. Since the QD and IQD samples show $\delta^{65}\text{Cu}$ and $\delta^{60}\text{Ni}$ values quite similar to BSE values, it might be safely concluded that the sulfides within the QD and IQD display values similar to the Bulk Silicate Earth.

Measurements of $\delta^{65}\text{Cu}$ from Matachawan basalt, pyroxenite from the Frost Lake ultramafic zone, and a clast of mafic meta-volcanic entrained in the Parkin Offset (Table 3-3) provided values of the country rock of the SIC. The measured values display a narrow range from $0.11 \pm 0.06\text{‰}$ $\delta^{65}\text{Cu}$ to $-0.06 \pm 0.04\text{‰}$ $\delta^{65}\text{Cu}$. This range of values falls within $\delta^{65}\text{Cu}_{\text{BSE}} = 0.07 \pm 0.10\text{‰}$ (Savage et al., 2015), and the range of values displayed by SIC samples (Fig. 3-6).

Of additional interest, is the lack of Fe fractionation displayed between samples of QD, IQD, and a sample of felsic norite. Fe isotopes are known to show significant fractionation during fractional crystallization driven by redox processes or fluid exsolution (Teng et al., 2008; Telus et al., 2012; Dauphas et al., 2014). The fact that there is little difference between the Fe isotopic compositions of the QD, IQD, and felsic norite would seem to imply a lack of a high degree of fractional crystallization between these two units. However, this interpretation is subject to caution, as only one sample of felsic norite was analyzed and further sampling may reveal a different result.

3.6.2 Isotopic Variations in Massive Sulfide Mineralization

The isotopic signatures of the sulfide mineralization displays a wide range of $\delta^{65}\text{Cu}$, $\delta^{56}\text{Fe}$, and $\delta^{60}\text{Ni}$ values $-0.97 \pm 0.03\text{‰}$ to $1.05 \pm 0.00\text{‰}$ $\delta^{65}\text{Cu}$; $-0.16 \pm 0.03\text{‰}$ to $0.45 \pm 0.02\text{‰}$ $\delta^{56}\text{Fe}$; and $-0.06 \pm 0.04\text{‰}$ to $-0.39 \pm 0.08\text{‰}$ $\delta^{60}\text{Ni}$ (Fig. 3-6). This is expected, as sulfides commonly record a larger range in values than silicates due to the different processes which affect their isotopic compositions (Dauphas et al., 2017; Moynier et al., 2017; Elliott and Steele, 2017). For further details, see Chapter 1.1. The sulfide samples range in petrologic type from the chalcopyrite dominated footwall-style mineralization of the Nickel Rim South Mine to the Offset Dike-hosted massive sulfide ores. Samples from the Nickel Rim South and Podolsky Mines are not Offset Dike-host sulfide mineralization and are therefore useful in providing a comparison between Offset Dike-hosted and non-Offset Dike-hosted mineralization. They show that there is little relation between the footwall-style ores seen at Nickel Rim South, and the Offset hosted massive sulfides due to their large difference in $\delta^{65}\text{Cu}$ and $\delta^{56}\text{Fe}$ values (Fig. 3-7). Massive sulfide mineralization hosted within the Offset Dikes displays $\delta^{65}\text{Cu}$, $\delta^{56}\text{Fe}$, and $\delta^{60}\text{Ni}$ values which are fractionated relative to QD and IQD values. These results suggest that the massive sulfide hosted within the Offset Dikes are different from the QD and IQD of the Offset Dikes. Based on $\delta^{65}\text{Cu}$ and $\delta^{60}\text{Ni}$ values, a regression line can be defined with the equation $\delta^{65}\text{Cu} = 1.24 * \delta^{60}\text{Ni} - 0.19$ (Fig. 3-7) with the massive sulfides, QD, IQD, and Sublayer all falling along this line. Two points were not included in the linear regression from which this line was created, WWL-20-1299 and SUDPAC 032, these two samples are considered outliers. WWL-20-1299, a sample of the Sublayer displays significant

alteration which likely causes it to display a differing isotopic value. While SUDPAC 032 likely contains sulfides formed through different magmatic or possibly hydrothermal processes than the other QD and IQD samples. However, the low number of samples displaying this isotopic signature make it difficult to identify what specifically its origin is. This line is significant in that it allows for the evaluation of the origin of the sulfide mineralization within the Offset Dikes, as discussed in the next section.

Petrographic analysis of the samples analyzed in this study support the observation of a difference between the offset-hosted massive sulfides and disseminated sulfides made using their isotopic compositions. QD and IQD observed show a sulfide mineral assemblage consisting of pyrite, chalcopyrite, and pentlandite (Fig. 3-3D). While the offset hosted massive sulfides contain additional pyrrhotite (Figs. 3-3A-C). There is also a lack of Co enrichment or zonation observed in QD pyrites, while offset-hosted massive sulfides display Co enrichment or zonation within pyrite (Figs. 3-4 & 3-5). Co zonation within pyrite has been previously recognized at other sulfide deposits at Sudbury; the presence of Co zoning along with zonation of Iridium Platinum Group Elements (IPGE), Pt, and As are thought to be a result of pyrite growth from Monosulfide Solid Solution (MSS) (Craig and Solberg, 1999; Naldrett et al., 1999; Dare et al., 2011). Pyrites that do not display zonation of Co, IPGE, and As are believed to have had their zonation removed by deuteric fluids (Craig and Solberg, 1999; Dare et al., 2011). These observations were noted at the McCreedy East Deposit, which mainly consists of contact style ores with rarer footwall ores (Dare et al., 2011). These deposits are different from offset dike style deposits due to the fact that the pyrrhotite-rich MSS has fractionated from the Cu-rich fluid that later forms chalcopyrite. The model of Dare et al. (2011) would imply that pyrites which display zonation are pyrites which record the initial isotopic composition from their sulfide liquid evolution, while pyrites that are depleted in Co have had their isotopic composition altered by the later fluids that has removed their initial zonation.

However, the massive sulfides, QD, IQD, and Sublayer all fall along a Cu and Ni fractionation line (Fig. 3-7), implying that only a common fractionation process affected the Cu and Ni isotopic composition of the samples. As discussed further in the next

section, this fractionation line (Fig. 3-7) displays a magmatic signature based on the enrichment of $\delta^{65}\text{Cu}$ and $\delta^{60}\text{Ni}$ in the Sublayer, and depletion of $\delta^{65}\text{Cu}$ and $\delta^{60}\text{Ni}$ in the massive sulfides indicative of metal extraction during sulfide segregation (Savage et al., 2015; Zhao et al., 2017). That the QD and IQD also fall on this line (Fig. 3-7) strongly suggests a magmatic origin for the disseminated sulfides, and no significant hydrothermal alteration. A significant hydrothermal over print would likely display itself as a much larger range in isotopic ratios (i.e. a range of $\pm 5\%$), similar to what sample WWL-20-1299 displays. Therefore, the isotopic data collected does not support a hydrothermal origin or significant hydrothermal alteration with respect to the massive and disseminated sulfides within the Offset Dikes.

Based on the mineral assemblages and isotopic compositions observed, a reasonable argument can be made that the offset dikes contain two different types of sulfide mineralization. One being a pyrite, chalcopyrite, and pentlandite assemblage that exhibits an isotopic signature with little fractionation from $\delta^{65}\text{Cu}_{\text{BSE}} = 0.07 \pm 0.10\%$ (Savage et al., 2015) and $\delta^{60}\text{Ni}_{\text{BSE}} = 0.15 \pm 0.03\%$ (Cameron et al., 2009; Gueguen et al., 2013; Chernonozhkin et al., 2015) (Figs. 3-3 & 3-7). The second type consists of pyrite, chalcopyrite, pentlandite, pyrrhotite, and magnetite; and shows a greater fractionation of its isotopic composition relative to BSE values (Figs. 3-3 & 3-7). Some possibilities for creating this difference are:

- These petrographic and isotopic differences represent two different sulfide liquids. As discussed further in the next chapter, sulfide liquid from the SIC could have formed the Offset Dike hosted massive sulfides. While disseminated sulfides within the QD and IQD were formed within the Offset Dikes themselves.
- The offset hosted massive sulfides and disseminated sulfides are genetically the same, however a post-emplacement event remobilized the sulfides and concentrated them into the larger massive sulfide bodies and in the process caused an isotopic fractionation.

3.6.3 Origin of Sulfide Mineralization within the Offset Dikes

Analyses of Fe, Ni, and Cu stable isotopes coupled with petrographic and X-ray microanalysis has enabled a fresh evaluation of the origin of sulfide mineralization within the Offset Dikes and Offset Dikes themselves. The $\delta^{65}\text{Cu}$, $\delta^{60}\text{Ni}$, and $\delta^{56}\text{Fe}$ values measured from the QD and IQD of several Offset Dikes, along with those of the Felsic Norite suggest that isotopically, all Offset Dikes measured here are identical. When plotting $\delta^{60}\text{Ni}$ versus $\delta^{65}\text{Cu}$, a correlation between the isotopic compositions for Cu and Ni is observed indicative of fractionation process. The slope of the line (1.24) differs from what would be expected due to mass fractionation processes (i.e. a slope of 0.9). However, the low number of sulfide data points, and error associated with each measurement likely added to uncertainty when calculating the slope of the line. The QD and IQD show a similarity to BSE values (Fig. 3-4), while massive sulfide ores from the Offset Dikes and a sample from the Sublayer show fractionations relative to the QD and IQD values. The heavy values shown by the Sublayer sample are likely a result of sulfide segregation leaving behind an isotopically heavy residue (Savage et al., 2015; Zhao et al., 2017). In contrast, we suggest that the massive sulfides hosted by the offsets are likely derived from the Main Mass of the SIC, with their isotopically light signature indicative of early sulfide segregation similar to that seen at the Tulaergen magmatic Ni–Cu deposit in NW China (Zhao et al., 2017). Further to this point, the QD, IQD, massive sulfides, and Sublayer all fall along a Cu–Ni fractionation line. This, along with the lack of fractionation seen in the QD and IQD relative to both BSE and Felsic Norite values implies that the metals found in the offset dike-hosted massive sulfides were not locally derived from the Offset Dikes. This is in contrast to the disseminated sulfides within the QD and IQD which do not display fractionation relative to the Felsic Norite and BSE values for Cu and Ni (Fig. 3-7). A possible explanation for the isotopic composition of QD and IQD, is that their sulfides were derived from the Offset Dikes in a closed system, whereby no fractionation would be observed.

If these interpretations are correct, it would also imply that each Offset Dike was emplaced as a single injection of material. If the Offset Dikes were emplaced over multiple episodes of injection, it would be expected that these multiple injections would

display differing isotopic compositions. However, due to the common isotopic composition of the QD, IQD, geographically different dikes; one event, a single injection of material is more likely. The preservation of a metal extraction signature seen in the massive sulfides and Sublayer also implies that there is no hydrothermal overprint seen in these samples. The fact that the QD and IQD also fall along this fractionation line, thought to be defined by igneous processes, implies that the disseminated and massive sulfides within the Offset Dikes do not record a significant hydrothermal history of alteration or emplacement. Additionally, these measurements might indicate that the Offset Dikes were derived from a homogenous isotopic reservoir of Fe, Ni, and Cu. While these measurements come from geographically distinct areas of the SIC, more data points from the South Range (e.g. Copper Cliff) would help in drawing this conclusion.

3.7 Conclusions

- For the first time, Cu, Fe, and Ni stable isotopic ratios of Offset Dikes, SIC units, and country rocks at Sudbury have been systematically measured. As much as possible, Cu, Fe, and Ni were extracted from the same sample aliquot to avoid heterogeneities intrinsic to sampling methods. Previous studies have not examined Sudbury, or used all three isotopes in concert with one another.
- Based on a small number of samples from geographically distinct locations, the initial isotopic reservoir of the impact melt sheet appears to have been homogenous.
- Little fractionation is observed within silicate samples analyzed. This is consistent with previous observations that igneous processes within silicate rocks at high temperature create little fractionation within Cu, and Ni isotopic systems (Moynier et al., 2017). Fe can show significant fractionation during fractional crystallization driven by redox processes or fluid ex-solution (Teng et al., 2008; Telus et al., 2012; Dauphas et al., 2014). The lack of significant Fe isotopic fractionation that we find in our sample suite suggests that during crater formation and dike emplacement there was little fractional crystallization of magmas nor fluid activity as a mechanism for an open system.

- Sulfides within the Offset Dikes are magmatic in origin, with no significant hydrothermal overprint shown. The massive sulfide mineralization hosted within the Offset Dikes display different isotopic compositions than the QD and IQD which contain disseminated blebby sulfides. This is based on the fact that both the massive sulfides, QD, IQD, and importantly Sublayer all fall along a single Cu-Ni fractionation line, and that this fractionation line is likely defined by the magmatic process of sulfide segregation (Savage et al., 2015; Zhao et al., 2017).
- Using the $\delta^{65}\text{Cu}$ and $\delta^{60}\text{Ni}$ values measured by this study, a SIC fractionation line (SFL) can be created (Fig. 3-7). From this line it can be concluded that each dike was emplaced in one injection event as all points cluster together on the fractionation line. The location of the Sublayer high on the SFL shows that it served as a source of metals for sulfide mineralization within the SIC. Finally, the presence of the offset-hosted massive sulfide mineralization lower on the SFL is likely the result of genetic differences between the offset-hosted massive sulfide mineralization, and disseminated sulfides within the QD and IQD. This suggests that the blebby disseminated sulfides in the QD and IQD were crystallized out along with the QD in a closed system. While the massive sulfide ores were crystallized from monosulfide solid solution (MSS) generated from the Sudbury impact melt sheet. Due to liquid immiscibility it was separated from the silicate melt of the Sudbury impact melt sheet, and transported into the silicate magma of the QD.

3.8 References

- Ames, D.E., Davidson, A., and Wodicka, N., 2008, Geology of the giant Sudbury polymetallic mining camp, Ontario, Canada: *Economic Geology*, v. 103, p. 1057–1077.
- Anders, D.A., Osinski, G.R., Grieve, R.A.F., and Brillinger, D.T.M., 2015, The Basal Onaping Intrusion in the North Range: Roof rocks of the Sudbury Igneous Complex: *Meteoritics & Planetary Science*, v. 50, p. 1577–1594.

- Bethune, K.R., and Ty, A., 1997, Metamorphism of the Sudbury diabase dyke-swarm: From Protolith to two-pyroxene-garnet coronite: *Canadian Mineralogist*, v. 35, p. 1191–1220.
- Bleeker, W., Kamo, S.L., Ames, D.E., and Smith, D., 2014, New U-Pb ages for some key events in the Sudbury area, including the Creighton Granite and Joe Lake metagabbro, in *Geological Association of Canada - Mineralogical Association of Canada Annual Meeting, Program with Abstracts*, p. 33.
- Cameron, V., Vance, D., Archer, C., and House, C.H., 2009, A biomarker based on the stable isotopes of nickel: *Proceedings of the National Academy of Sciences*, v. 106, p. 10944–10948.
- Chapman, J., Mason, T., Weiss, D., Coles, B., and Wilkinson, J., 2006, Chemical separation and isotopic variations of Cu and Zn from five geological reference materials: *Geostand Geoanal Res*, v. 30, p. 5–16.
- Chernonozhkin, S.M., Goderis, S., Lobo, L., Claeys, P., and Vanhaecke, F., 2015, Development of an isolation procedure and MC-ICP-MS measurement protocol for the study of stable isotope ratio variations of nickel: *J. Anal. At. Spectrom.*, v. 30, p. 1518–1530.
- Cochrane L. B. 1984. Ore deposits of the Copper Cliff offset, in Pye, E.G., Naldrett, A.J., and Giblin, P.E. eds., *The Geology and Ore Deposits of the Sudbury Structure*, Toronto, Ministry of Natural Resources, p. 275–300.
- Coleman, A.P., 1905, *The Sudbury nickel region: Ontario Department of Mines Annual Report* v. 14, p. 1–188.
- Corfu, F., and Lightfoot, P.C., 1996, U-Pb Geochronology of the Sublayer Environment, Sudbury Igneous Complex, Ontario: *Economic Geology*, v. 91, p. 1263–1269.
- Craddock, P.R., and Dauphas, N., 2010, Iron Isotopic Compositions of Geological Reference Materials and Chondrites: v. 35, p. 101–123.

- Craddock, P.R., Warren, J.M., and Dauphas, N., 2013, Abyssal peridotites reveal the near-chondritic Fe isotopic composition of the Earth: *Earth and Planetary Science Letters*, v. 365, p. 63–76.
- Craig, J.R., and Solberg, T.N., 1999, Compositional zoning in ore minerals at the Craig mine, Sudbury, Ontario, Canada: *Canadian Mineralogist*, v. 37, p. 1163–1176.
- Dare, S. a S., Barnes, S.J., Prichard, H.M., and Fisher, P.C., 2011, Chalcophile and platinum-group element (PGE) concentrations in the sulfide minerals from the McCreedy East deposit, Sudbury, Canada, and the origin of PGE in pyrite: *Mineralium Deposita*, v. 46, p. 381–407.
- Darling, J.R., Hawkesworth, C.J., Storey, C.D., and Lightfoot, P.C., 2010, Shallow impact: Isotopic insights into crustal contributions to the Sudbury impact melt sheet: *Geochimica et Cosmochimica Acta*, v. 74, p. 5680–5696.
- Dauphas, N., Craddock, P.R., Asimow, P.D., Bennett, V.C., Nutman, A.P., and Ohnenstetter, D., 2009, Iron isotopes may reveal the redox conditions of mantle melting from Archean to Present: *Earth and Planetary Science Letters*, v. 288, p. 255–267.
- Dauphas, N., John, S.G., and Rouxel, O., 2017, Iron Isotope Systematics: Reviews in *Mineralogy and Geochemistry*, v. 82, p. 415–510.
- Dauphas, N., Roskosz, M., Alp, E.E., Neuville, D.R., Hu, M.Y., Sio, C.K., Tissot, F.L.H., Zhao, J., Tissandier, L., Médard, E., and Cordier, C., 2014, Magma redox and structural controls on iron isotope variations in Earth ' s mantle and crust: v. 398, p. 127–140.
- Davis, D.W., 2008, Sub-million-year age resolution of Precambrian igneous events by thermal extraction-thermal ionization mass spectrometer Pb dating of zircon: Application to crystallization of the Sudbury impact melt sheet: *Geology*, v. 36, p. 383–386.

- Dickin, A.P., Artan, M.A., and Crocket, J.H., 1996, Isotopic evidence for distinct crustal sources of North and South Range ores, Sudbury Igneous Complex: *Geochimica et Cosmochimica Acta*, v. 60, p. 1605–1613.
- Dietz, R.S., 1964, Sudbury Structure as an Astrobleme: *The Journal of Geology*, v. 72, p. 412–434.
- Dietz, R.S., 1961, Vredefort Ring Structure : Meteorite Impact Scar ? *The Journal of Geology*, v. 69, p. 499–516.
- Elliott, T., and Steele, R.C.J., 2017, The Isotope Geochemistry of Ni: Reviews in *Mineralogy and Geochemistry*, v. 82, p. 511–542.
- Farrow, C.E.G., and Lightfoot, P.C., 2002, Sudbury PGE revisited: Towards an integrated model: *CIM Special Volume*, v. 54, p. 273–297.
- Foden, J., Sossi, P.A., and Wawryk, C.M., 2015, Lithos Fe isotopes and the contrasting petrogenesis of A-, I- and S-type granite: *Lithos*, v. 212–215, p. 32–44.
- Golightly, J.P., 1994, The Sudbury Igneous Complex as an impact melt; evolution and ore genesis: *Proceedings of the Sudbury-Noril'sk Sym*, p. 105–117.
- Graham, S., Pearson, N., Jackson, S., Griffin, W., and O'Reilly, S.Y., 2004, Tracing Cu and Fe from source to porphyry: In situ determination of Cu and Fe isotope ratios in sulfides from the Grasberg Cu-Au deposit: *Chemical Geology*, v. 207, p. 147–169.
- Grant, R.W., and Bite, A., 1984, Sudbury quartz diorite offset dikes, in Pye, E.G., Naldrett, A.J., and Giblin, P.E. eds., *The Geology and Ore Deposits of the Sudbury Structure*, Toronto, Ministry of Natural Resources, p. 275–300.
- Grieve, R.A.F., 1994, An Impact Model of the Sudbury Structure: *Proceedings of the Sudbury-Noril'sk Symposium*, p. 119–132.

- Grieve, R.A.F., 1991, Terrestrial Impact: The record in the rocks: Meteoritics & Planetary Science, v. 26, p. 175–194.
- Grieve, R.A.F., Ames, D.E., Morgan, J. V., and Artemieva, N., 2010, The evolution of the Onaping Formation at the Sudbury impact structure: Meteoritics and Planetary Science, v. 45, p. 759–782.
- Grieve, R.A.F., and Cintala, M., 1997, Planetary differences in impact melting: Advances in Space Research, v. 20, p. 1551–1560.
- Grieve, R.A.F., Stoffler, D., and Deutsch, A., 1991, The Sudbury Structure - controversial or misunderstood? Journal of Geophysical Research-Planets, v. 96, p. 22,753–22,764.
- Gueguen, B., Rouxel, O., Ponzevera, E., Bekker, A., and Fouquet, Y., 2013, Nickel isotope variations in terrestrial silicate rocks and geological reference materials measured by MC-ICP-MS: Geostandards and Geoanalytical Research, v. 37, p. 297–317.
- Hecht, L., Wittek, A., Riller, U., Mohr, T., Schmitt, R.T., and Grieve, R.A.F., 2008, Differentiation and emplacement of the Worthington Offset Dike of the Sudbury impact structure, Ontario: Meteoritics & Planetary Science, v. 43, p. 1659–1679.
- Hofmann, A., Bekker, A., Dirks, P., Gueguen, B., Rumble, D., and Rouxel, O.J., 2014, Comparing orthomagmatic and hydrothermal mineralization models for komatiite-hosted nickel deposits in Zimbabwe using multiple-sulfur, iron, and nickel isotope data: Mineralium Deposita, v. 49, p. 75–100.
- Keays, R.R., and Lightfoot, P.C., 2004, Formation of Ni-Cu-Platinum Group Element sulfide mineralization in the Sudbury Impact Melt Sheet: Mineralogy and Petrology, v. 82, p. 217–258.
- Klimesch, L.M., Hecht, L., and Riller, U., 2015, Emplacement, Differentiation and Mineralization of the Trill Offset Dike, Sudbury, Canada.: Economic Geology,.

- Li, W., Jackson, S.E., Pearson, N.J., and Graham, S., 2010, Copper isotopic zonation in the North parkes porphyry Cu-Au deposit, SE Australia: *Geochimica et Cosmochimica Acta*, v. 74, p. 4078–4096.
- Lightfoot, P.C., 2016, *Nickel Sulfide Ores and Impact Melts: Origin of the Sudbury Igneous Complex*: Elsevier.
- Lightfoot, P.C., and Farrow, C.E.G., 2002, Geology, Geochemistry, and Mineralogy of the Worthington Offset Dike: A Genetic Model for Offset Dike Mineralization in the Sudbury Igneous Complex: *Economic Geology*, v. 97, p. 1419–1446.
- Lightfoot, P.C., Keays, R.R., and Doherty, W., 2001a, Chemical Evolution and Origin of Nickel Sulfide Mineralization in the Sudbury Igneous Complex, Ontario, Canada: *Economic Geology*, v. 96, p. 1855–1875.
- Lightfoot, P.C., Keays, R.R., and Doherty, W., 2001b, Chemical Evolution and Origin of Nickel Sulfide Mineralization in the Sudbury Igneous Complex, Ontario, Canada: *Economic Geology*, v. 96, p. 1855–1875.
- Lightfoot, P.G., Keays, R.R., Morrison, G.G., Bite, A., and Farrell, K.P., 1997a, Geochemical relationships in the Sudbury Igneous Complex: Origin of the main mass and offset dikes: *Economic Geology*, v. 92, p. 289–307.
- Lightfoot, P.G., Keays, R.R., Morrison, G.G., Bite, A., and Farrell, K.P., 1997b, Geologic and geochemical relationships between the contact sublayer, inclusions, and the main mass of the sudbury igneous complex: A Case study of the whistle mine embayment: *Economic Geology*, v. 92, p. 647–673.
- Lightfoot, P.C., Morrison, G.G., Bite, A., and Farrell, P., 1997, Geochemical Relationships in the Sudbury Igneous Complex: Origin of the Main Mass and Offset Dikes: *Economic Geology*, v. 92, p. 289–307.
- Maher, K.C., and Larson, P.B., 2007, Variation in Copper Isotope Ratios and Controls on Fractionation in Hypogene Skarn Mineralization at Coroccohuayco and Tintaya , Perú: *Economic Geology*, v. 102, p. 225–237.

- Malitch, K.N., Latypov, R.M., Badanina, I.Y., and Sluzhenikin, S.F., 2014, Insights into ore genesis of Ni-Cu-PGE sulfide deposits of the Noril'sk Province (Russia): Evidence from copper and sulfur isotopes: *Lithos*, v. 204, p. 172–187.
- Maréchal, C.N., Télouk, P., and Albarède, F., 1999, Precise analysis of copper and zinc isotopic compositions by plasma-source mass spectrometry: *Chemical Geology*, v. 156, p. 251–273.
- Mathur, R., Ruiz, J., Casselman, M.J., Megaw, P., and van Egmond, R., 2012, Use of Cu isotopes to distinguish primary and secondary Cu mineralization in the Cañariaco Norte porphyry copper deposit, Northern Peru: *Mineralium Deposita*, v. 47, p. 755–762.
- Morgan, J.W., Walker, R.J., Horan, M.F., Beary, E.S., and Naldrett, A.J., 2002, 190Pt – 186 Os and 187Re – 187 Os systematics of the Sudbury Igneous Complex , Ontario: *Geochimica et Cosmochimica Acta*, v. 66, p. 273–290.
- Morris, A., and Pay, R., 1981, Genesis of the Foy (?) Offset and Its Sulfide Ores : The Paleomagnetic Evidence from a Study in Hess Township , Sudbury , Ontario: *Economic Geology*, v. 76, p. 1895–1905.
- Moynier, F., Vance, D., Fujii, T., and Savage, P., 2017, The Isotope Geochemistry of Zinc and Copper: *Reviews in Mineralogy and Geochemistry*, v. 82, p. 543–600.
- Murphy, A.J., and Spray, J.G., 2002, Geology, mineralization, and emplacement of the Whistle-Parkin offset dike, Sudbury: *Economic Geology*, v. 97, p. 1399–1418.
- Naldrett, A.J., Asif, M., Schandl, E., Searcy, T., Morrison, G.G., Binney, W.P., and Moore, C., 1999, Platinum-Group Elements in the Sudbury Ores: Significance with Respect to the Origin of Different Ore Zones and to the Exploration for Footwall Orebodies: , p. 185–210.
- Naldrett, A.J., Bray, J.G., Gasparri, E.L., Podolsky, T., and Rucklidge, J.D., 1970, Cryptic variation and the petrology of the Sudbury Nickel Irruption: *Economic Geology*, v. 65, p. 122–155.

- O'Callaghan, J.W., Osinski, G.R., Lightfoot, P.C., Linnen, R.L., and Weirich, J.R., 2016, Reconstructing the geochemical signature of Sudbury Breccia, Ontario, Canada: Implications for its formation and trace metal content: *Economic Geology*, v. 111, p. 1705–1729.
- O'Neill, C., Marchi, S., Zhang, S., and Bottke, W., 2017, Impact-driven subduction on the Hadean Earth: *Nature Geoscience*, v. 10.
- Osinski, G.R., and Pierazzo, E., 2013, Chapter 1: Impact Cratering : Processes and Products: John Wiley & Sons, 1-20 p.
- Osterman, M., Schürer, U., and Deutsch, A., 1996, Impact melt dikes in the Sudbury multi-ring basin (Canada): Implications from uranium-lead geochronology on the Foy Offset Dike: *Meteoritics and Planetary Science*, v. 31, p. 494–501.
- Pilles, E., Osinski, G.R., Grieve, R.A.F., Smith, D., and Bailey, J., 2017, Chemical variations and genetic relationships between the Hess and the Foy Offset Dikes at the Sudbury Impact Structure: *Meteoritics & Planetary Science*, v. 52., p. 2,647-2,671.
- Prevec S. A., Lightfoot P. C., and Keays R. R. 2000. Evolution of the sublayer of the Sudbury Igneous Complex: Geochemical, Sm–Nd isotopic and petrologic evidence. *Lithos* v.51, p.271–292.
- Raharimahefa, T., Lafrance, B., and Tinkham, D.K., 2014, New structural, metamorphic, and U–Pb geochronological constraints on the Blezardian Orogeny and Yavapai Orogeny in the Southern Province, Sudbury, Canada: *Canadian Journal of Earth Sciences*, v. 51, p. 750–774.
- Reimold, W.U., Koeberl, C., Gibson, R.L., and Dressler, B.O., 2005, Economic Mineral Deposits in Impact Structures: A Review, in Koeberl, C. and Henkel, H. eds., *Impact Tectonics*, Springer, p. 479.
- Rickard J. H. and Watkinson D. H. 2001. Cu-Ni-PGE mineralization within the Copper Cliff Offset Dike, Copper Cliff North mine, Sudbury, Ontario: Evidence for

- multiple stages of emplacement. *Exploration and Mining Geology* v. 1–2, p.111–124.
- Ripley, E.M., Dong, S., Li, C., and Wasylenki, L.E., 2015, Cu isotope variations between conduit and sheet-style Ni–Cu–PGE sulfide mineralization in the Midcontinent Rift System, North America: *Chemical Geology*, v. 414, p. 59–68.
- Rivers, T., 1997, Lithotectonic elements of the Grenville Province: review and tectonic implications: *Precambrian Research*, v. 86, p. 117–154.
- Savage, P.S., Moynier, F., Chen, H., Shofner, G., Siebert, J., Badro, J., and Puchtel, I.S., 2015, Copper isotope evidence for large-scale sulphide fractionation during Earth's differentiation: *Geochemical Perspectives Letters*, p. 53–64.
- Scott R. G. and Benn K. 2002. Emplacement of sulfide deposits in the Copper Cliff Offset Dyke during collapse of the Sudbury crater rim: Evidence from magnetic fabric studies. *Economic Geology* v.97, p.1447–1458.
- Van Schmus, W.R., 1993, Transcontinental Proterozoic provinces: *Geological Society of America*, v. *Geology of*, p. 171–334.
- Schulz, K.J., and Cannon, W.F., 2007, The Penokean orogeny in the Lake Superior region: *Precambrian Research*, v. 157, p. 4–25.
- Shahar, A., Young, E.D., and Manning, C.E., 2008, Equilibrium high-temperature Fe isotope fractionation between fayalite and magnetite: An experimental calibration: *Earth and Planetary Science Letters*, v. 268, p. 330–338.
- Spray, J.G., and Thompson, L.M., 1995, Friction melt distribution in a multi-ring impact basin: *Nature*, v. 373, p. 130–132.
- Taylor, S., and McLennan, S., 1995, The geochemical evolution of the continental crust: *Reviews of Geophysics*, v. 33, p. 241–265.

- Telus, M., Dauphas, N., Moynier, F., Tissot, F.L.H., Teng, F.-Z., Nabelek, P.I., Craddock, P.R., and Groat, L.A., 2012, Iron, zinc, magnesium and uranium isotopic fractionation during continental crust differentiation: The tale from migmatites, granitoids, and pegmatites: *Geochimica et Cosmochimica Acta*, v. 97, p. 247–265.
- Teng, F.-Z., Dauphas, N., and Helz, R.T., 2008a, Iron Isotope Fractionation During Magmatic Differentiation in Kilauea Iki Lava Lake: *Science*, v. 320, p. 1620–1622.
- Teng, F.-Z., Dauphas, N., and Helz, R.T., 2008b, Iron Isotope Fractionation During Magmatic Differentiation in Kilauea Iki Lava Lake: *Science*, v. 320, p. 1620–1622.
- Teng, F.Z., Dauphas, N., Huang, S., and Marty, B., 2013, Iron isotopic systematics of oceanic basalts: *Geochimica et Cosmochimica Acta*, v. 107, p. 12–26.
- Thompson, L.M., and Spray, J.G., 1996, Pseudotachylyte petrogenesis: constraints from the Sudbury impact structure: *Contributions to Mineralogy and Petrology*, v. 125, p. 359–374.
- Thompson, L.M., and Spray, J.G., 1994, Pseudotachylytic rock distribution and genesis within the Sudbury impact structure, in Dressler, B.O., Greive, R.A.F., and Sharpton, V.L. eds., *Large Meteorite Impacts and Planetary Evolution*, Geological Society of America Special Paper 293, p. 275–288.
- Tuchscherer, M., and Spray, J., 2002, Geology, mineralization, and emplacement of the Foy Offset Dike, Sudbury impact structure: *Economic Geology*, v. 97, p. 1377–1397.
- Wasylenki, L.E., Howe, H.D., Spivak-Birndorf, L.J., and Bish, D.L., 2015, Ni isotope fractionation during sorption to ferrihydrite: Implications for Ni in banded iron formations: *Chemical Geology*, v. 400, p. 56–64.

- Wasylenki, L.E., Swihart, J.W., and Romaniello, S.J., 2014, Cadmium isotope fractionation during adsorption to Mn oxyhydroxide at low and high ionic strength: *Geochimica et Cosmochimica Acta*, v. 140, p. 212–226.
- Williams, H.M., and Archer, C., 2011, Copper stable isotopes as tracers of metal-sulphide segregation and fractional crystallisation processes on iron meteorite parent bodies: *Geochimica et Cosmochimica Acta*, v. 75, p. 3166–3178.
- Williams, H.M., Markowski, A., Quitté, G., Halliday, A.N., Teutsch, N., and Levasseur, S., 2006, Fe isotope fractionation in iron meteorites: New insights into metal-sulphide segregation and planetary accretion: *Earth and Planetary Science Letters*, v. 250, p. 486–500.
- Wood, C.R., and Spray, J.G., 1998a, Origin and emplacement of offset dykes in the Sudbury impact structure: Constraints from Hess: *Meteoritics & Planetary Science*, v. 33, p. 337–347.
- Wood, C.R., and Spray, J.G., 1998b, Origin and Emplacement of Offset Dykes in the Sudbury impact structure: Constraints from Hess: *Meteoritics & Planetary Science*, v. 33, p. 337–347.
- Zhao, Y., Xue, C., Liu, S., Symons, D.T.A., Zhao, X., Yang, Y., and Ke, J., 2017, Copper isotope fractionation during sulfide-magma differentiation in the Tulaergen magmatic Ni – Cu deposit, NW China: *Lithos*, v. 286–287, p. 206–215.
- Zhu, X.K., Guo, Y., Williams, R.J.P., O’Nions, R.K., Matthews, a., Belshaw, N.S., Canters, G.W., de Waal, E.C., Weser, U., Burgess, B.K., and Salvato, B., 2002, Mass fractionation processes of transition metal isotopes: *Earth and Planetary Science Letters*, v. 200, p. 47–62.
- Zieg, M.J., and Marsh, B.D., 2005, The Sudbury Igneous Complex: Viscous emulsion differentiation of a superheated impact melt sheet: *Bulletin of the Geological Society of America*, v. 117, p. 1427–1450.

Chapter 4

4 Conclusions and Future work

For the first time a systematic study of Cu, Fe, and Ni stable isotopic ratios of Offset Dikes, SIC units, and country rocks at Sudbury has been conducted. From these measurement several important conclusions were drawn pertaining to the Origin of the Offset Dikes, their sulfide mineralization, and the magmatic evolution of the Sudbury Igneous Complex (SIC). Of perhaps greater importance to future workers however, is the integrated nature of the measurement of these three isotopic systems.

4.1 Fe, Ni, and Cu Method Improvements

As noted earlier this is the first time a systematic study of Cu, Fe, and Ni stable isotopic ratios had been conducted. While previous studies have measured stable Cu, Fe, and Ni isotopes (Dauphas et al., 2017; Elliott and Steele, 2017; Moynier et al., 2017) (See Chapter 1.1 for further details); few studies have measured all three systems from the same aliquot as presented herein. The ability to obtain measurements of $\delta^{56}\text{Fe}$, $\delta^{60}\text{Ni}$, and $\delta^{65}\text{Cu}$ from the same aliquot allowed for the plotting of these data against each other and the recognition of a fractionation line. Despite the success of these measurements, there does exist room for improvements to the extraction and purification of Fe, Ni, and Cu from geologic media:

- In order to obtain the Fe, Ni, and Cu used for isotopic analyses, two separation procedures were employed with three different column chemistries in total. An analysis of the elution curves presented in Chapter 2 (Figs. 2-1 & 2-3) show that it might be possible to consolidate the separation of Fe, Ni, and Cu into a single protocol using 2 column chemistries. Ni elutes with the matrix early during the Cu and Fe column at near >95% recovery (Fig. 2-1). Collecting this Ni, separated Fe, Cu, and Co; then passing it on the second column used during Ni chemistry to remove additional cations (i.e., Mg, Ca, and Ti) might allow a two-column protocol to separate Fe, Ni, and Cu.
- One challenge of analyzing Ni and Cu in particular, is that some felsic lithologies contain such low concentrations of Ni and Cu that it is not practical to analyze these

samples. While multiple columns could be used to extract multiple aliquots which are recombined for analysis, this also increases the chance for column derived error. Some of these felsic lithologies such as the Granophyre of the SIC are important components of the Sudbury impact melt sheet. The ability to analyze their Fe, Ni, and Cu isotopic composition would prove valuable for deciphering the magma evolution of the SIC. Using larger columns with a higher resin capacity or an additional step to remove major elements would allow a larger mass of sample to be loaded, enabling easier extraction of Cu and Ni from samples with low Cu and Ni concentrations such as the Granophyre.

These two modifications to the column chemistry used would help improve sample throughput, and broaden the scope of samples which could be analyzed.

4.2 Significance

From the data collected several important conclusions have been drawn about the Offset Dikes, their sulfide mineralization, and the magmatic evolution of the SIC:

- Sulfides within the Offset Dikes appear to be magmatic in origin, with the disseminated sulfides and massive sulfide bodies hosted within the Offsets Dikes being genetically different. Blebby disseminated sulfides in the QD and IQD were crystallized out along with the QD. While the massive sulfide ores were crystallized from monosulfide solid solution (MSS) generated from the Sudbury impact melt sheet. Due to liquid immiscibility it was separated from the silicate melt of the Sudbury impact melt sheet, and transported into the silicate magma of the QD.
- The QD and IQD share a common Fe, Cu, and Ni composition across multiple Offsets, suggestive that each Offset received a single injection of material which formed the QD and IQD. If the Offset Dikes represent the initial composition of the Sudbury melt sheet, this implies that the initial isotopic reservoir of the impact melt sheet was homogenous.
- The lack of significant Fe isotopic fractionation observed also suggests that during crater formation and dike emplacement there was little fractional crystallization of

magmas, nor fluid activity as a mechanism for an open system (Teng et al., 2008; Telus et al., 2012; Dauphas et al., 2014). However, this could be a result of a small sample size.

These findings are important both for further resource exploration at Sudbury, and understanding to evolution of the SIC magmatically. In exploration terms, it would suggest that within the Offset Dikes, the characteristics of the disseminated blebby sulfides are of a lower order of importance as an exploration finding. With regard to the SIC, if the impact melt sheet initially had a homogenous Fe, Cu, and Ni composition this observation would lend support to the crystal-liquid differentiation of the SIC proposed by Lightfoot et al. (2001) and Therriault et al. (2002).

4.3 Recommendations for future measurement

Future measurements can be divided into two categories. First, further measurements of the SIC. While this study covered a large geographic area, several Offset Dikes which have a long history of exploration and study (e.g., Copper Cliff) were not measured by this study. In addition, there are many deposits not measured by this study which if measured would aid both further exploration at Sudbury, and attempts to better understand the magmatic evolution of the SIC. While this study measured members of the Main Mass, a systemic measurement of isotopic values both vertically through the Main Mass and horizontally across its entire width would prove useful for identifying the magmatic processes which differentiated the Main Mass. A modified column chemistry protocol would be required to execute this however, as most units of the Main Mass contain very low amounts of Cu and Ni. A large cation column as a first step would likely be required.

Second, experiments to constrain the fractionation factors of Fe, Cu, and Ni isotopes during processes relevant to magmatic sulfide systems (i.e., sulfide segregation). While some experiments have been conducted involving sulfides (Ehrlich et al., 2004; Shahar et al., 2008; Savage et al., 2015; Shahar et al., 2017; Syverson et al., 2017), there is a lack of experimental data of high-temperature magmatic processes (e.g., 800-1000 °C). Critically, exact fractionation factors between silicate and sulfide liquid during sulfide segregation remains unknown. Experimentally derived fractionation factors would allow

future workers to identify the exact conditions (e.g., temperature) under which these processes took place at in nature.

These experimental measurements, connected with sample based observations would allow for

4.4 References

Dauphas, N., John, S.G., and Rouxel, O., 2017, Iron Isotope Systematics: Reviews in Mineralogy and Geochemistry, v. 82, p. 415–510.

Dauphas, N., Roskosz, M., Alp, E.E., Neuville, D.R., Hu, M.Y., Sio, C.K., Tissot, F.L.H., Zhao, J., Tissandier, L., Médard, E., and Cordier, C., 2014, Magma redox and structural controls on iron isotope variations in Earth ' s mantle and crust: v. 398, p. 127–140.

Ehrlich, S., Butler, I., Halicz, L., Rickard, D., Oldroyd, A., and Matthews, A., 2004, Experimental study of the copper isotope fractionation between aqueous Cu(II) and covellite, CuS: Chemical Geology, v. 209, p. 259–269.

Elliott, T., and Steele, R.C.J., 2017, The Isotope Geochemistry of Ni: Reviews in Mineralogy and Geochemistry, v. 82, p. 511–542.

Lightfoot, P.C., Keays, R.R., and Doherty, W., 2001, Chemical Evolution and Origin of Nickel Sulfide Mineralization in the Sudbury Igneous Complex, Ontario, Canada: Economic Geology, v. 96, p. 1855–1875.

Moynier, F., Vance, D., Fujii, T., and Savage, P., 2017, The Isotope Geochemistry of Zinc and Copper: Reviews in Mineralogy and Geochemistry, v. 82, p. 543–600.

Savage, P.S., Moynier, F., Chen, H., Shofner, G., Siebert, J., Badro, J., and Puchtel, I.S., 2015, Copper isotope evidence for large-scale sulphide fractionation during Earth's differentiation: Geochemical Perspectives Letters, p. 53–64.

- Shahar, A., Elardo, S.M., and Macris, C.A., 2017, Equilibrium Fractionation of Non-traditional Stable Isotopes: an Experimental Perspective: *Reviews in Mineralogy and Geochemistry*, v. 82, p. 65–83.
- Shahar, A., Young, E.D., and Manning, C.E., 2008, Equilibrium high-temperature Fe isotope fractionation between fayalite and magnetite: An experimental calibration: *Earth and Planetary Science Letters*, v. 268, p. 330–338.
- Syverson, D.D., Luhmann, A.J., Tan, C., Borrok, D.M., Ding, K., and Seyfried, W.E., 2017, Fe isotope fractionation between chalcopyrite and dissolved Fe during hydrothermal recrystallization: An experimental study at 350°C and 500bars: *Geochimica et Cosmochimica Acta*, v. 200, p. 87–109.
- Telus, M., Dauphas, N., Moynier, F., Tissot, F.L.H., Teng, F.-Z., Nabelek, P.I., Craddock, P.R., and Groat, L.A., 2012, Iron, zinc, magnesium and uranium isotopic fractionation during continental crust differentiation: The tale from migmatites, granitoids, and pegmatites: *Geochimica et Cosmochimica Acta*, v. 97, p. 247–265.
- Teng, F.-Z., Dauphas, N., and Helz, R.T., 2008, Iron Isotope Fractionation During Magmatic Differentiation in Kilauea Iki Lava Lake: *Science*, v. 320, p. 1620–1622.
- Therriault, A.M., Fowler, A.D., and Grieve, R.A.F., 2002, The Sudbury Igneous Complex: A differentiated impact melt sheet: *Economic Geology*, v. 97, p. 1521–1540.

Appendices

Appendix A: Silicate Geochemistry measured by ICP-MS, average error of 5-10%

Sample Name	SUD 007	SUD 008	SUD 010	SUD 017	SUD 019	SUD 020	SUD 022	SUD 023
Lithology	QD	IQD	Cartier Granite	QD	IQD	QD	Norite	QD
Location	Foy Offset	Foy Offset	Foy Offset	Foy/Hess Intersection	Foy/Hess Intersection	Hess Offset	Rt 144 road cut	Parkin Offset
Ca (wt. %)	0.53	0.36	0.14	0.52	0.49	0.59	0.66	0.33
Fe (wt. %)	5.21	4.90	0.83	7.77	5.42	5.34	4.92	4.40
Ti (wt. %)	0.27	0.40	0.06	0.37	0.35	0.33	0.27	0.40
Sc (ppm)	16.48	15.61	3.63	15.35	19.38	18.10	15.53	14.01
V (ppm)	126.52	124.44	8.75	125.71	160.27	137.61	104.19	111.45
Cr (ppm)	115.47	174.08	1.98	199.04	126.91	156.85	33.10	113.88
Mn (ppm)	828.53	571.36	198.92	870.17	713.24	916.36	815.30	596.13
Co (ppm)	24.20	25.78	3.10	101.39	24.00	25.68	28.25	7.45
Ni (ppm)	69.02	119.67	5.88	1,863.95	72.67	109.18	14.27	63.88
Cu (ppm)	74.91	71.36	8.49	2,175.05	45.36	78.49	17.22	97.02
Zn (ppm)	81.94	83.47	46.54	101.91	78.07	83.71	67.60	34.61
Ga (ppm)	19.26	22.62	19.13	18.03	21.14	18.44	19.27	17.50
Ge (ppm)	4.40	6.00	3.98	4.12	4.83	3.95	2.94	4.08
Rb (ppm)	71.39	89.16	17.76	48.75	61.63	63.08	38.88	43.53
Sr (ppm)	356.44	424.80	175.47	353.55	440.07	337.44	445.74	140.58
Y (ppm)	17.62	12.76	6.81	14.70	17.68	15.80	12.19	15.88
Zr (ppm)	152.90	162.53	142.44	140.88	159.85	138.84	91.76	147.11
Mo (ppm)	0.71	0.80	0.44	1.01	0.38	0.60	0.75	0.70
Cd (ppm)	0.10	0.06	0.15	0.75	0.04	0.07	0.08	0.06
Cs (ppm)	1.74	1.78	0.14	1.00	0.89	2.12	1.42	0.89
Ba (ppm)	614.74	753.34	192.29	611.68	730.85	704.29	452.02	297.00
La (ppm)	31.70	51.59	41.31	27.70	35.74	27.87	20.11	29.61
Ce (ppm)	65.40	101.72	78.22	56.80	71.24	56.87	41.00	61.29
Pr (ppm)	7.25	10.94	7.95	6.32	7.81	6.38	4.67	6.87
Nd (ppm)	27.68	40.22	25.62	24.02	29.51	24.35	17.98	26.27
Sm (ppm)	5.11	6.34	3.73	4.43	5.12	4.54	3.37	4.86
Eu (ppm)	1.29	1.52	0.56	1.16	1.45	1.09	1.07	0.92
Gd (ppm)	4.39	4.64	2.47	3.72	4.31	3.88	2.86	4.10
Tb (ppm)	0.61	0.54	0.25	0.51	0.58	0.54	0.40	0.56
Dy (ppm)	3.50	2.71	1.15	2.94	3.31	3.11	2.33	3.21
Ho (ppm)	0.68	0.51	0.21	0.57	0.67	0.61	0.46	0.62
Er (ppm)	1.98	1.44	0.60	1.66	1.97	1.75	1.36	1.75
Tm (ppm)	0.28	0.20	0.08	0.24	0.28	0.24	0.19	0.24
Yb (ppm)	1.83	1.33	0.60	1.54	1.86	1.61	1.29	1.59
Lu (ppm)	0.27	0.20	0.11	0.23	0.29	0.24	0.20	0.24
Hf (ppm)	3.90	4.23	4.00	3.47	3.94	3.54	2.35	3.74
W (ppb)	100.36	177.67	249.54	300.56	32.79	100.15	228.70	1,204.19
Tl (ppb)	482.32	779.78	81.67	456.33	435.42	457.15	244.68	170.12
Pb (ppm)	11.59	11.29	39.78	42.90	6.63	11.86	5.11	2.71
Th (ppm)	7.19	15.87	63.33	7.11	7.91	6.99	4.54	7.64
U (ppm)	1.56	0.84	8.34	1.40	0.72	1.58	0.96	1.48

Sample Name	SUD 023	SUD 024	SUD 026	SUD 031	SUD 032	SUD 033	SUD 037	SUD 038
Lithology	QD	IQD	QD	Entrained mafic clast	IQD	Pyroxenite	Granophyre	Sublayer
Location	Parkin Offset	Parkin Offset	Whistle Extension	Parkin Offset	Parkin Offset	Frost Lake Ultramafic	Guilleville Dump	Levack Dump
Ca (wt. %)	0.33	0.34	0.13	0.91	0.28	1.30	0.44	0.93
Fe (wt. %)	4.40	6.35	3.24	9.47	2.66	8.51	5.23	9.15
Ti (wt. %)	0.40	0.45	0.32	0.63	0.21	0.11	0.10	0.35
Sc (ppm)	14.01	16.29	12.77	35.55	8.08	n.a.	n.a.	27.75
V (ppm)	111.45	137.92	85.10	285.03	59.34	150.92	85.40	212.32
Cr (ppm)	113.88	140.45	122.23	89.20	131.16	1,076.92	7.51	1,615.61
Mn (ppm)	596.13	608.66	405.36	1,743.22	379.74	1,915.75	589.90	1,585.27
Co (ppm)	7.45	100.66	18.77	40.74	11.97	56.33	6.97	64.71
Ni (ppm)	63.88	648.63	35.81	73.99	197.86	384.70	4.16	514.76
Cu (ppm)	97.02	912.87	22.59	131.52	681.27	86.11	7.52	216.87
Zn (ppm)	34.61	53.59	63.56	119.54	71.93	134.17	45.39	159.47
Ga (ppm)	17.50	20.14	12.44	15.66	17.46	n.a.	n.a.	12.73
Ge (ppm)	4.08	4.47	2.74	2.57	2.70	n.a.	n.a.	2.74
Rb (ppm)	43.53	52.94	131.21	71.93	60.38	48.56	87.52	16.83
Sr (ppm)	140.58	202.82	76.66	341.48	482.74	58.91	302.39	88.74
Y (ppm)	15.88	17.75	12.53	22.54	5.54	10.65	35.47	12.79
Zr (ppm)	147.11	156.30	134.54	75.16	101.89	11.53	208.33	52.92
Mo (ppm)	0.70	1.14	4.30	0.71	0.95	0.27	0.11	0.48
Cd (ppm)	0.06	0.22	0.12	0.09	0.21	0.15	0.11	0.13
Cs (ppm)	0.89	0.90	0.48	2.95	0.63	n.a.	n.a.	0.93
Ba (ppm)	297.00	471.40	746.28	427.64	467.27	121.60	500.52	221.43
La (ppm)	29.61	31.63	18.42	8.79	19.86	7.18	43.58	9.44
Ce (ppm)	61.29	64.97	40.18	19.90	39.81	23.25	92.86	22.47
Pr (ppm)	6.87	7.35	4.61	2.60	4.42	3.48	9.83	3.02
Nd (ppm)	26.27	28.18	17.31	11.88	16.62	15.33	37.69	13.43
Sm (ppm)	4.86	5.21	3.30	3.17	2.90	3.77	7.30	3.11
Eu (ppm)	0.92	1.25	0.75	1.01	1.08	0.61	1.75	0.77
Gd (ppm)	4.10	4.39	2.78	3.71	2.13	3.18	6.83	2.96
Tb (ppm)	0.56	0.60	0.40	0.63	0.25	0.45	1.00	0.44
Dy (ppm)	3.21	3.45	2.31	4.19	1.22	2.40	6.03	2.67
Ho (ppm)	0.62	0.68	0.47	0.89	0.21	0.43	1.23	0.53
Er (ppm)	1.75	1.94	1.38	2.61	0.54	1.14	3.63	1.52
Tm (ppm)	0.24	0.27	0.20	0.38	0.07	0.15	0.51	0.22
Yb (ppm)	1.59	1.75	1.35	2.53	0.45	0.95	3.31	1.46
Lu (ppm)	0.24	0.25	0.21	0.38	0.07	0.13	0.48	0.23
Hf (ppm)	3.74	3.64	3.54	2.13	2.69	0.47	4.65	1.57
W (ppb)	1,204.19	891.54	1,783.81	228.25	70.68	n.a.	n.a.	186.58
Tl (ppb)	170.12	450.22	425.54	475.96	289.25	n.a.	n.a.	167.77
Pb (ppm)	2.71	22.89	17.34	8.80	27.40	6.81	3.44	3.67
Th (ppm)	7.64	7.18	8.05	1.21	5.09	0.21	10.51	2.04
U (ppm)	1.48	1.48	2.80	0.29	1.43	0.09	3.08	0.30

Sample Name	SUD 039	WMP-195 60m	WWL-20 101.5m	WWL-20 133m	WWL-20 1299m	WWN-003 280m	WWN-003 287m
Lithology	Matachawan Basalt	IQD	Granophyre	Quartz Gabbro	Sublayer	QD	IQD
Location	Cascaden Township	Parkin Offset	Windy Lake Core	Windy Lake Core	Windy Lake Core	Worthington Offset	Worthington Offset
Ca (wt. %)	0.82	0.38	0.36	0.69	0.44	0.53	0.47
Fe (wt. %)	11.08	8.41	6.02	9.24	5.36	6.11	5.56
Ti (wt. %)	1.62	0.29	0.95	1.74	0.16	0.43	0.52
Sc (ppm)	35.01	13.33	20.68	29.51	21.70	20.23	16.23
V (ppm)	274.60	104.11	158.93	467.05	181.05	157.33	136.91
Cr (ppm)	105.51	85.86	2.62	3.20	131.85	144.28	88.86
Mn (ppm)	1,669.28	1,026.54	936.22	1,223.99	957.18	898.19	717.31
Co (ppm)	41.17	44.60	23.61	44.75	27.06	35.11	28.03
Ni (ppm)	60.54	1,003.60	22.61	62.11	110.81	115.86	198.37
Cu (ppm)	263.36	8,223.15	16.76	218.45	89.57	162.70	86.66
Zn (ppm)	153.35	178.82	132.87	69.39	100.48	81.16	72.87
Ga (ppm)	23.10	18.08	28.84	20.99	19.23	19.65	19.57
Ge (ppm)	5.46	6.70	6.26	6.10	2.75	4.57	4.75
Rb (ppm)	154.61	70.25	175.65	60.95	33.02	96.18	77.59
Sr (ppm)	153.05	284.46	176.68	366.10	565.97	295.67	274.06
Y (ppm)	43.24	51.40	55.59	24.42	5.84	21.25	22.93
Zr (ppm)	265.14	284.22	1,020.41	126.74	36.85	140.24	155.53
Mo (ppm)	1.16	1.36	1.73	1.32	0.36	1.20	2.44
Cd (ppm)	0.14	1.86	0.16	0.07	0.10	0.05	0.04
Cs (ppm)	3.88	3.61	0.79	0.24	0.74	3.90	2.82
Ba (ppm)	538.09	557.96	624.61	549.21	631.67	485.68	538.09
La (ppm)	27.43	38.54	34.48	35.07	20.20	32.38	34.03
Ce (ppm)	60.40	91.37	77.16	76.77	40.26	65.53	70.94
Pr (ppm)	7.47	10.70	9.50	9.29	4.44	7.24	7.89
Nd (ppm)	32.06	42.63	39.95	38.85	16.40	27.63	30.00
Sm (ppm)	7.55	10.50	9.49	7.65	2.51	5.31	5.80
Eu (ppm)	2.15	1.44	1.62	1.99	1.40	1.35	1.44
Gd (ppm)	8.08	10.45	9.64	6.80	1.84	4.73	5.29
Tb (ppm)	1.30	1.79	1.50	0.91	0.21	0.69	0.78
Dy (ppm)	8.14	11.16	9.25	5.02	1.12	4.06	4.65
Ho (ppm)	1.68	2.19	1.92	0.96	0.23	0.82	0.93
Er (ppm)	4.86	6.08	5.69	2.61	0.72	2.34	2.70
Tm (ppm)	0.69	0.81	0.84	0.34	0.11	0.33	0.39
Yb (ppm)	4.58	4.82	5.69	2.14	0.84	2.14	2.56
Lu (ppm)	0.69	0.62	0.88	0.32	0.13	0.32	0.38
Hf (ppm)	6.09	7.60	26.29	3.30	1.18	3.58	4.18
W (ppb)	343.00	329.00	421.87	247.30	41.78	89.09	457.34
Tl (ppb)	1,209.32	1,128.61	714.39	336.33	196.76	657.90	584.29
Pb (ppm)	17.38	172.01	10.39	6.04	6.35	4.57	4.89
Th (ppm)	4.75	21.86	6.26	6.00	1.73	8.04	10.59
U (ppm)	1.13	4.11	3.11	1.39	0.13	1.91	2.52

Appendix B: Sulfide Geochemistry measured by ICP-MS, average error of 5-10%

Sample Name	SUD 030	SUD 040	Ni Rim	SUD P1	SUD P2	SUD P3	WMM-015-W2 1477m	WTR-028 29m
Lithology	Massive Sulfide	Massive Sulfide	Massive Sulfide	Massive Sulfide	Massive Sulfide	Massive Sulfide	Massive Sulfide	Massive Sulfide
Location	Parkin Offset	Trill Offset	Nickel Rim South Mine	Podolsky Mine	Podolsky Mine	Podolsky Mine	Parkin Offset	Trill Offset
Fe (wt. %)	37.06	49.42	47.97	52.65	27.19	24.95	46.19	38.59
Co (wt. %)	0.50	0.15	52.04	0.11	0.00	0.00	0.13	0.17
Ni (wt. %)	3.90	4.32	1.22	5.55	0.05	0.08	4.99	4.42
Cu (wt. %)	0.73	0.64	52.47	0.09	35.91	30.08	0.72	1.53
Ca (ppm)	72.34	256.49	64.91	33.15	74.53	233.29	459.17	230.90
Ti (ppm)	170.28	1026.91	4.33	121.95	50.68	221.81	1196.08	94.94
V (ppm)	7.24	40.81	0.21	37.98	2.07	5.31	235.50	56.85
Cr (ppm)	87.48	6.68	0.22	0.43	1.36	4.12	12.61	27.63
Mn (ppm)	106.32	417.95	25.51	146.73	42.66	70.49	260.31	44.13
Zn (ppm)	58.41	104.02	18.65	24.36	1043.20	498.89	59.96	39.00
Mo (ppm)	3.36	2.12	0.05	0.23	1.49	0.69	1.72	1.04
Ru (ppm)	2.25	n.a.	n.a.	n.a.	n.a.	n.a.	n.a.	0.23
Rh (ppm)	1.83	0.14	n.a.	0.01	0.03	0.02	0.10	0.79
Pd (ppm)	0.64	9.00	0.08	0.08	13.09	2.05	2.14	7.97
Ag (ppm)	2.85	39.35	1.98	0.51	33.58	69.46	35.20	25.59
Cd (ppm)	0.53	0.76	2.50	0.03	45.71	24.76	0.32	0.21
Sn (ppm)	0.94	6.43	n.a.	0.53	58.52	29.04	8.11	4.38
W (ppb)	n.a.	n.a.	0.45	15.62	258.97	68.82	n.a.	n.a.
Os (ppb)	126.48	2.60	15.46	18.82	18.15	31.04	77.37	59.64
Ir (ppb)	456.83	19.13	0.20	21.08	14.36	23.65	n.a.	142.08
Pt (ppm)	n.a.	2.12	0.04	n.a.	5.74	2.73	0.37	3.62
Au (ppm)	1.16	270.71	0.01	0.29	4.62	9.64	0.48	1.53

Curriculum Vitae

Name: Peter Christoffersen

Post-secondary Education and Degrees: St. Lawrence University
Canton, New York, USA
2009-2013 B.S. with Honors in Geology

University of Montana
Missoula, Montana, USA
2013-2014 M.Sc (Uncompleted)

University of Western Ontario
London, Ontario, Canada
2015-2017 M.Sc (Candidate)

Honours and Awards: Tobacco Root Geological Society Graduate Research Grant*
2014

Geological Society of America Graduate Research Grant*
2014

Mark Erickson Summer Research Fellowship
2012

* Awards declined because graduate study was not continued at the University of Montana

Related Work Experience Teaching Assistant
The University of Western Ontario
2015-2017

Teaching Assistant
University of Montana
2013-2014

Teaching Assistant
St. Lawrence University
2011-2013

Summer Research Assistant
NASA Johnson Space Center
2011